THE MECHANICS OF WINDING

LAMINATE WEBS AND THE PREDICTION OF

MACHINE DIRECTION CURL

By

SHENG PAN

Bachelor of Science in Process Equipment and Control
Beijing University of Chemical Technology
Beijing, China
2010

Master of Science in Machinery in
Chemical Industry Process
Beijing University of Chemical Technology
Beijing, China
2013

Submitted to the Faculty of the
Graduate College of the
Oklahoma State University
in partial fulfillment of
the requirements for
the Degree of
DOCTOR OF PHILOSOPHY
May, 2019

THE MECHANICS OF WINDING

LAMINATE WEBS AND THE PREDICTION OF

MACHINE DIRECTION CURL

Dissertation Approved:

Dr. Good, J. Keith

Dissertation Adviser

Dr. Reid, Karl N.

Dr. Azoug, Aurelie

Dr. Wang, Shuodao

Dr. Ley, M. Tyler

Name: SHENG PAN

Date of Degree: MAY, 2019

Title of Study: THE MECHANICS OF WINDING LAMINATE WEBS AND THE PREDICTION OF MACHINE DIRECTION CURL

Major Field: MECHANICAL ENGINEERING

Abstract: Winding models that describe the residual stresses due to winding single layer webs at the end of roll-to-roll manufacturing machines began development over 50 years ago. These models have been used to reduce or avoid defects that are due to winding. Many products that are wound can have considerable thickness. Laminates formed from webs are joined to form yet thicker composite webs where the properties of each layer provide unique functionality. The winding models developed previously have focused on determining membrane stresses in the tangential and axial directions and the radial pressure as a function of radius, web material properties and winder operating conditions. These models have considered the web to be a thin homogenous layer. While bending strains result from any web being wound at a radius of curvature into a roll, these bending stains are largest for the thicker homogeneous webs and laminates. Many webs are viscoelastic at some level. Creep will result from the bending strains. When the web material is unwound and cut into discrete samples some residual curvature will remain. This curvature, called curl, is the inability for the web to lie flat at no tension. Curl is an undesirable web defect that causes loss of productivity in a subsequent web process. The goal of this research is to develop tools by which process engineers can explore and mitigate curl in homogenous and laminated webs. Findings and conclusions: laminated winding models and predictive models for curl based upon viscoelastic material characterization were developed. Tests were performed to confirm the accuracy of these models.

TABLE OF CONTENTS

Chapter Page

Chapter Page

LIST OF TABLES

Table Page

Table Page

LIST OF FIGURES

Figure Page

Figure Page

Figure Page

NOMENCLATURE

A	Total Cross Sectional Area of the Web
A_e	Area of Element
B	Deformation Matrix
BR	Bending Recovery
C_1, C_2, C_3	Coefficients of a Polynomial Function
D	Bending Rigdity
DEN	Definition Value of D Matrix
E	Young's Modulus
E_0	Initial Young's Modulus at Time t=0
E_c	Core Stiffness
E_{MD1}, E_{MD2}	Machine Direction Young's Modulus for Layer 1 and 2
E_r, E_θ, E_z	Young's Modulus in Radial, Tangential, CMD Directions
E_{com}, E_{ten}	Relaxation Modulus in Compressive and Tensile State
$E_{w\theta}, E_{wz}, E_{wr}$	Web Material Young's Modulus in Tangential, Axial and Radial Directions
e	Base of the Natural Logarithm
F_e	Force Vector of Element
h	Thickness of Web
h_{avg}	Average Thickness of Web
h_i, h_j	Thickness of Web(i-th, j-th element)
I	Moment of Inertial
J_θ, J_r	Creep Function of Tangential, Radial Directions
$J_{\theta r}, J_{r\theta}$	Creep Function Couples Terms

K_1, K_2	Pfeiffer Material Parameters
K_e	Element Stiffness Matrix
M	Symmetric Matrix about Orthotropic Materials Behavior
M_b	Bending Moment
M_e	Element Mass Matrix
M_x^T, M_y^T, M_z^T	Components of the Equivalent Moment due to Temperature Change
N_x^T, N_y^T, N_z^T	Components of the Equivalent Force due to Temperature Change
N_i, N_j	Shape Function Values
NIT	Nip Induced Tension
n	Number of Sectors
P	Radial Pressure
R, r	Radius
R_i, R_o	Inner Radius and Outer Radius
R2R	Roll to Roll
$\bar{r}$	Center Radial Position for Current Configuration
r_{avg}	Average Radius of the Outer Lap
r_c	Radius of Core
r_i	Outer Radius of ith Element
r_0	Relaxation Radius
s	Radius of Outer Layer
T	Total Tension of the Web(units of load)
T_{layer1}, T_{layer2}	Lamination Tension in Layer 1 and 2
T_{cap}	Torque Capacity
T_i	Tangential Stress of the i^{th} sector((units of load))
T_w	Web winding Tension(units of stress)
T_{wi}	Winding Tension of Laminate i(units of load)
T_{wj}	Winding Tension of Laminate j(units of load)

TPE	Total Potential Energy
t	Real Time
u	Radial Deformation
W, w	Web Width
$\varepsilon_r, \varepsilon_\theta, \varepsilon_z$	Radial Strain, Tangential Strain, Axial Strain
σ	Stress
σ_0	Initial Tension
$\sigma_r, \sigma_\theta, \sigma_z$	Radial Stress, Tangential Stress, Axial Stress
ν	Poisson's Ratios
$\nu_{rz}, \nu_{r\theta}, \nu_{z\theta}, \nu_{zr},$ $\nu_{\theta r}, \nu_{\theta z}$	Out-of-Plane and in-plane Poisson's Ratios
ε	Strain
ε_0	Initial Strain
ε_{avg}	Average Strain in the Web Upstream of the Winder
η,ξ	Coordinates within an Element
ρ	Radius of Curvature
ψ	Solution of Volterra Integral
α	The Coefficient of Thermal Expansion
$\mu_{w/w}$	Friction Coefficient between Two Layers

CHAPTER I

INTRODUCTION

Roll-to-roll (R2R) manufacturing processes constitute a large sector of all manufacturing conducted today. The materials used in these processes are very long, quite thin, and susceptible to damage. R2R manufacturing involves additive processing that is rate dependent. One or more base webs must be formed. The web may be coated uniformly or selectively with one or more coatings depending on product needs. In some cases the web will be laminated to other webs that may have their unique coatings. Finally the web is cut to shape and becomes a product or part of a product. The web formation, the coating (s), laminating, etc. all occur in unique process machines due to the different rates at which these processes can occur. This requires the web to be stored and historically the only available means has been to wind the webs into rolls.

Winding is often detrimental to web and product quality. Roll defects are inevitable in the winding process, such as roll telescoping, roll blocking, buckling, bulk loss and so on, leading to inestimable economic loss. Residual stresses result from winding whose magnitude is dependent on the winding equipment, winder operating conditions such as web tension, and web and core material properties. Many web defects are caused by the magnitude of these residual stresses and prevention of the defects requires a means of determining the stresses. A winding model is a scientific prediction of the wound roll residual stresses based on mathematical calculation.

These are not simple models which would allow the calculation of residual stresses using a closed

form expression. It will be shown that these models require accretive solutions which must account for material properties that are state dependent on the residual stresses being calculated. There are often several thousand web layers in a wound roll and computational means must be employed to solve the models which estimate the residual stresses. Hakiel [4] created a popular winding model, which was first in the literature to account for all aspects that were needed to accurately predict the residual stresses. Based on Hakiel's concepts, many valuable winding models have been developed. Winding models have evolved and matured over time. These models can be placed into the following categories:

(1) 1D center winding models which predict radial and tangential residual stresses only as a function of radius are at the highest level of maturity. Axial stresses may also be calculated if plane strain conditions are assumed. A center winder applies torque to a core and the web layers wind up in spiral fashion on the core. These models assume the spiral geometry of the wound layers can be replaced with concentric layers.

(2) 2D center winding models which predict radial, tangential, axial and axisymmetric shear stresses as a function of radius and position across the roll width. These models allow residual stresses to be computed that consider variations in web thickness and length across the width.

(3) Viscoelastic 1D and 2D models which allow the study of the residual stresses through time as affected by the storage environment (temperature, moisture, etc.).

(4) Complex finite element models that account for the spiral nature of the layers in the wound roll.

The winding models discussed do not treat the bending strains in the web. The total strain in the web is a combination of the membrane stresses and strains these models do predict plus the bending strains due to winding a layer in at a unique radius into the wound roll. The total strains are important in the development of a model to predict web curl. Web curl is the inability of the web to lie in a planar state when unwinding or later when cut into a discrete product. This curl can be the result of creep due to the total strain through the thickness of homogenous, laminated and coated webs.

Laminating and coating are common R2R manufacturing processes. Often products require multiple layers that are joined by some method. Whereas the coating of web materials is common, the coating would often be considered non-structural and not affect residual winding stresses. It is not uncommon to vapor deposit aluminum on polymer films to provide an enhanced oxygen barrier or conductivity. Thus some coatings may add structural reinforcement to the base web depending on the modulus and the thickness of the coating in comparison to the modulus and thickness of the base web. In some cases webs become joined with other webs in laminating processes and the joined webs are called laminates. Laminates are typically strain matched at the site of lamination. Laminated webs that are not strain matched will curl when cut into discrete products which is typically undesirable but some products may be designed to curl.

A familiar example is sheets of label products for use in ink jet or laser printers. The label is commonly a polymer film with one surface that has been prepared for printing and the other surface prepared to receive an adhesive layer. A second web is prepared which could be a kraft paper with one surface coated with a silicone agent. The two webs are laminated together with the silicone coating on the paper in contact with the adhesive on the polymer. The laminated web is now wound and stored. When needed this roll would then be unwound and transported through a die roller which cuts a needed label size by shearing through the polymer layer but not the paper backing. The laminate may be rewound at this point or it may go directly into a sheet cutting operation where the continuous web is now cut into discrete sheets. Those sheets are packaged and delivered to the consumer who feeds them intro their printer. The consumer expects the label surface to accept the toner or ink image desired and then to be able to peel the label off of the kraft paper and then affix it to the final surface where the discrete printed label is needed. A common failure witnessed by the consumer is curl. If the discrete sheets of labels are curled they will not feed and transport properly through the printer. The origin of the curl could have been in the wound roll laminated where the sheet of labels was stored for several days or months earlier.

Since elastic and viscoelastic winding models for laminates are nonexistent, prediction and elimination of this curl is not possible. Generally speaking, a laminate, can be defined as a body made up of bonded layers of thin sheets. From the prospect of mechanics, the advantage of laminated materials is a combination of different components, leading to new or unique properties. In different processes of laminate production or laminate winding, curl is a major defect. Viscoelastic creep often occurs in rolls wound from laminated webs and the residual stresses from winding will have changed through time due to creep. Often prior to lamination, the strains in the two or more layers are matched or made equal. After lamination an unstressed coupon of laminate should have no curl about a CMD axis. If the Poisson ratios of the multiple layers are not equivalent it is possible that curl may arise about a CMD axis.

Curl is a web defect that pervades web process industries regardless if the web is homogenous or is a laminate. This research will focus on the development of predicting tools that can assess the level of curl in a web. Homogenous webs subjected to combined membrane and bending strains can curl if the web is viscoelastic. Elastic webs that are not strain matched will curl after lamination. Laminated viscoelastic webs that were strain matched at the laminator will curl when wound and stored.

One mission of this research is to predict curl in webs as a means to minimize curl and the associated economic loss. A second mission is to explore the residual stresses in laminate due to winding.

CHAPTER II

LITERATURE REVIEW

2.1 General Developments of Winding Models

2.1.1 Elastic Winding Models-1D

Winding behavior can be modeled and winding models have played an important role in the control of web quality. A good winding model is able to predict the stress in the wound roll quickly and correctly and is the key to the reduction of winding defects and economic losses in industry.

Early winding models dated back to the 1960s. Catlow&Walls [1] developed early 1D linear winding models for isotropic materials. Here the one dimension means that the stress values are only the function of the radial location in the roll. Analytical models were employed for the calculation of internal stresses of a wound roll. Winding processes were assumed to a series of concentric cylindrical layers and each layer was considered a thick pressure vessel, where the tension stress was similar to the tangential stress when the vessel is under internal pressure. Values of stresses could easily be summed due to the pressure increment effect.

The major limitation of these early winding models was the assumption of isotropic properties. In reality, most industrial materials are far from isotropic. Anisotropic commonly exists in webs

In reality, most industrial materials are far from isotropic. Anisotropic commonly exists in webs due to the material complexity. Further, the radial modulus is not a constant value and is state dependent on stress or strain. Nonetheless these models did capture the accretive behavior of winding and showed the approximated stress conditions inside the rolls.

Pfeiffer [2], in 1966, noted a logarithmic behavior between pressure and strain in a stack of web material in compression. Based on that relation Pfeiffer concluded that the radial modulus was state dependent and linearly related to the stack pressure:

$$P = K_1(e^{K_2\varepsilon_r} - 1) \rightarrow E_r(P) = \frac{dP}{d\varepsilon_r} = K_2(P + K_1) \tag{2.1}$$

where E_r is the radial Young's modulus, P is the pressure applied on the stack and ε_r is the strain that resulted in the stack. K_1 and K_2 are parameters that are fitted to the pressure versus strain data recorded form a compression test on the stack. Pfeiffer was the first to demonstrate that all wound rolls are anisotropic and that their radial modulus was linearly state dependent on pressure or nonlinearly dependent on strain (2.1).

Yagoda [3] produced a non-dimensional 1D winding model using a hypergeometric series. The model predicts web tension as a polynomial function of the radius and for the effect of the core of the web wound upon.

Hakiel's nonlinear model for wound roll [4] is a significant development in the history of winding models. This model allows for anisotropic property and a state dependent radial modulus. Hakiel approximated the radial modulus using a polynomial function:

$$E_r(P) = C_1 + C_2P + C_3P^2 \tag{2.2}$$

C_1, C_2, and C_3 coefficients are fitted to vs strain data in a stack compression test. The slope of the pressure over the corresponding strain change would be used to establish discrete values of the

radial modulus at varied pressure levels. The coefficients C_1, C_2 and C_3 were varied until the discrete modulus values were best fit at all pressure levels. It is more convenient to use expression (2.1) in industry as K_1 is typically quite small and the dimensionless value of K_2 is used to compare the state dependent radial modulus of various web materials. Hakiel combined the equilibrium, compatibility and orthotropic constitutive relations in polar coordinates to form the following second order differential equation:

$$r^2 \frac{d^2 \delta\sigma_r}{dr^2} + 3r \frac{d\delta\sigma_r}{dr} - \left(\frac{E_\theta}{E_r} - 1\right) \delta\sigma_r = 0 \tag{2.3}$$

where, σ_r is the radial stress, E_θ and E_r are the tangential and radial modulus, respectively. The expression is written in terms of incremental radial stresses ($\delta\sigma_r$), each increment representing the addition of the most recent layer. Radial stresses and incremental radial stresses vary with radius. After solving equation (2.3), the $\delta\sigma_r$ stress increments in each layer are added to the total σ_r stress that was already sustained by that layer. The radial modulus is then updated as a function of the total radial stress in each layer.

In order to solve the second order differential equation, two boundary conditions are needed. The outer boundary condition assumes that the tensile stress in the outer layer depends only on the winding tension and the radius of the newest outer layer is known. Using an equilibrium expression similar to the hoop stress equation for a thin wall pressure vessel, the pressure beneath the outer lap can be determined:

$$\delta\sigma_r|_{r=s} = -\frac{T_w|_{r=s}}{s} \tag{2.4}$$

where, T_w is the winding tension in units of load per unit width and s is the radius of the most recent layer added to the outside of the winding roll. The remaining boundary condition is derived from the imposed displacement compatibility between the outside of the core and the inside of the first

layer. The two surfaces should coincide, because the core and the layer cannot separate from or intrude into each other. This is expressed as a derivative boundary condition at the outer surface of the core ($r=r_c$):

$$[d\,(\delta\sigma_r)/dr]|_{(r=r_c)} = [(E_\theta/E_c - 1 + \upsilon_{r\theta})]\delta\sigma_r/r_c|_{r=r_c} \quad (2.5)$$

Where E_c is the core stiffness parameter which is a measure of how the surface of the core deforms under pressure. The core stiffness is defined as $E_c = \frac{P}{\varepsilon_\theta}$, where P is the external pressure.

Hakiel used the finite difference method to numerically approximate the solution of expression (2.3). The differential equation has non constant coefficients due to the radial modulus being unique within every layer and numerical solution is required. The process of obtaining the solution is similar to the process of adding a new layer. When a layer is added, the incremental stresses are computed in each layer and then summed with the previous stresses to obtain the current values. The procedure repeats until the final layer is added.

There are limitations to Hakiel's method. First, the roll is assumed to be a collection of concentric hoops of web and not a spiral. This assumption made the problem solvable. Kandadai et al. [5] and Ren et al. [6] used Abaqus to fully simulate the spiral nature of the web. By modeling the spiral form, any slippage between layers will be accompanied by changes in the residual winding stresses. If slippage occurs, results from Hakiel's model cannot predict if that slippage will continue or cease. Normal contact forces between layers increase or decrease which affects future slippage. Another important limitation is that Hakiel's model did not consider the tension loss effect, described in [2] and proposed by Good model [7], especially when dealing with soft materials (low K_2 value). Good's results indicate that the pressures within a wound roll of soft material can be lower than the values predicted by Hakiel's model. Good et al. developed a new outer boundary condition for use with equation (2.3):

$$\delta\sigma_r|_{\mathrm{r=s}} = -\left(T_w + \frac{u}{s}E_\theta\right)h/s \tag{2.6}$$

where u is the displacement in the radial position of the current outermost layer. The value of u is negative as the addition of a new outer layer subject to tension T_w results in inward deformation. Displacement is assumed axisymmetric and effectively decreases the tension in the outer layer which in turn results in lower incremental and total pressures in the wound roll. Hakiel's model did not calculate layer deformation. To implement the new boundary condition (2.6) into Hakiel's model required an estimate of the radial deformation u of the outer layer. Furthermore, a prediction the radial deformation of a layer that is just being added to the wound roll was required. Good was successful in incorporating expression (2.6) into Hakiel's model and validating the improved model through comparison with tested in-roll pressures.

These 1D winding models provide a valuable understanding of the state of stress within the wound roll, but they all incorporate the assumptions of small linear deformations and strain. These assumptions can be unrealistic for tissue and nonwoven webs. These webs have low in-plane and radial modulus, and small deformations should not be assumed. Mollamahmutoulu and Good [8] developed a 1D winding model based on large deformation theory using the finite element method. The results of this new model agree very well with models that account for tension loss.

Summary:

1D elastic models which predict stresses only as a function of radius are at the highest level of maturity. More and more situations have been considered, such as geometrical nonlinearly, material relaxation effects, and so on. These models have become an effective instrument to improve industry production, mainly through the reduction of winding defects. However, no 1D models for laminate winding have been developed, even for the simplest two-layer laminate.

2.1.2 Viscoelastic Winding Models-1D

Viscoelastic behavior is common in web materials, including laminates. The time-dependent stress-strain behavior adds complexity that is not addressed by all winding models.

Tramposch, in 1965 [9], created the first viscoelastic winding model. He was concerned with stress relaxation in rolls of magnetic tape used for data storage. The residual stresses in a roll due to winding will decay as a result of viscoelastic behavior. While some relaxation may occur during winding, the majority occurs while the wound roll is in storage. The time required to wind a roll is insignificant compared to the time rolls spend in storage. Rolls are often wound in periods of a few minutes or less whereas they can remain in storage for weeks or months at elevated temperatures and uncontrolled humidity. In this early model, the constitutive relationship was established using a four-parameter model consisting of 2 springs and 2 dashpots (schematic of 4-paramter material in pure shear) . He concluded that the wound roll of homogenous isotropic material will approach stress-free conditions when given enough time.

Later, Tramposch developed a second model that allowed anisotropic relaxation [10]. Orthotropic behavior is a very common web anisotropy. Unequal thermal expansion of hub and tape body during environmental temperature changes was analyzed. If deformations are large, errors can become unacceptable which can be a disadvantage in a model based on linear viscoelastic theory

Lin and Westmann [11], in 1989, developed a viscoelastic winding analysis to model the impact of the histories of winding, winding-pause, and winding-pause-unwinding. The winding process is viewed as the placement of a sequence of pretensioned layers starting with the hub. The boundary conditions are identical to the ones in Hakiel's 1D model. The expressions for the stress and displacement are as follows:

$$\sigma_r = \sigma_0 \int_{R_i}^{R_o} \frac{\psi(t-\tau)}{(1+\upsilon)} \left(\frac{1}{R^2} - \frac{1}{{R_i}^2} \right) dR - \sigma_0 ln \frac{R_o}{R_i} \tag{2.7}$$

$$\sigma_\theta = \sigma_0 + \sigma_0 \int_{r}^{R_0} \frac{\psi(t-\tau)}{(1+\upsilon)} \left(\frac{1}{R^2} - \frac{1}{{R_i}^2} \right) dR - \sigma_0 ln \frac{R_0}{R_i} \tag{2.8}$$

$$u = \frac{\sigma_r(1)}{E} + \int_1^r \int_\xi^{R_o} \left\{ -(1-\upsilon) J(t-\tau) \frac{\sigma_0}{R} + \int_0^{t-\tau} \left[\frac{(1-\upsilon)}{(1+\upsilon)R^2} - \frac{1}{\xi^2} \right] \frac{\psi(\eta) dJ(t-\tau-\eta)}{d(t-\tau-\eta)} d\eta \right\} dR d\xi \tag{2.9}$$

where σ_0 is the initial tension in the tape considered as a constant value, R_i and R_o are the inner radius and outer radius, E and υ are the Young's modulus and Poisson's ratio, and $\psi(t-\tau)$ is the solution of the Volterra integral equation of the second kind.

The developed relationship between stress and time accounted the analysis of a winding-pause. Different winding speeds can contribute to undesirable creep and relaxation in linear and isotropic materials. However, this model incorporated an assumption that the stress in the outer lap remained constant which would appear inconsistent in a viscoelastic development where the stresses in all layers could be affected by creep.

Qualls and Good developed a realistic orthotropic viscoelastic model of center wound rolls [12]. The model incorporates state-dependent radial modulus of the orthotropic material. The equilibrium equations in cylindrical coordinates are:

$$\text{Equilibrium: } r \frac{\partial \sigma_r}{\partial r} + \sigma_r - \sigma_\theta = 0 \tag{2.10}$$

$$\text{Compatibility: } r \frac{\partial \varepsilon_r}{\partial r} + \varepsilon_r - \varepsilon_\theta = 0 \tag{2.11}$$

$$\text{Strain-Displacement: } \varepsilon_r = \frac{\partial u}{\partial r} \quad \varepsilon_\theta = \frac{u}{r} \tag{2.12}$$

$$\text{Viscoelastic Constitution: } \varepsilon_r = \int_0^t [J_r(t-t') \frac{\partial \sigma_r}{\partial t'} + J_{r\theta}(t-t') \frac{\partial \sigma_\theta}{\partial t'}] dt' \tag{2.13}$$

$$\varepsilon_\theta = \int_0^t [J_\theta(t-t') \frac{\partial \sigma_\theta}{\partial t'} + J_{\theta r}(t-t') \frac{\partial \sigma_r}{\partial t'}] dt' \tag{2.14}$$

where $J_r(t)$ is the radial creep function and $J_\theta(t)$ is the circumferential creep function. The $J_{r\theta}(t)$ creep function couples circumferential stress (σ_θ) and radial strain (ε_r). Similarly the $J_{\theta r}(t)$ couples radial stress (σ_r) and circumferential strain (ε_θ). Using the equilibrium equation (2.10), the viscoelastic constitutive expressions (2.13, 2.14) and the compatibility equation (2.11), a second order differential equation can be written which governs how the radial stress in wound roll can vary as a function of the creep functions and time:

$$\int_0^t \left[\begin{array}{l} J_\theta(t-t')\frac{\partial}{\partial t'}(r^2\frac{\partial^2\sigma_r}{\partial r^2}) + \left\{ 3J_\theta(t-t') + J_{\theta r}(t-t') - J_{r\theta}(t-t') + r\frac{\partial}{\partial r}J_\theta(t-t') \right\} \frac{\partial}{\partial t'}(r\frac{\partial\sigma_r}{\partial r}) \\ + \left\{ r\frac{\partial}{\partial r}(J_\theta(t-t') + J_{\theta r}(t-t')) + J_\theta(t-t') + J_{\theta r}(t-t') - J_r(t-t') - J_{r\theta}(t-t') \right\} \frac{\partial\sigma_r}{\partial t'} \end{array} \right] dt' = 0 \qquad (2.15)$$

Qualls and Good used central difference approximations to simplify the equation above. The outer boundary condition was derived from the assumption that the strain in the outer layer is constant and equal to the winding stress multiplied by circumferential creep function at time zero. Replacing the circumferential strain with its definition, the outer boundary condition can be expressed as:

$$T_w J_\theta(0) = \int_0^t \left[J_\theta(t-t')\frac{\partial\sigma_\theta}{\partial t'} + J_{\theta r}(t-t')\frac{\partial\sigma_\theta}{\partial t'} \right] dt' \qquad (2.16)$$

where, T_w is the winding tension. Considering the continuity of displacement at the core, the inner boundary condition can be showed to be:

$$\frac{(\sigma_r)_j}{E_c} = (\varepsilon_\theta)_j \qquad (2.17)$$

where the j subscript refers to the current time. Finite difference approximations of the derivatives were taken in equations (2.15) and (2.16) resulting in sets of algebraic equations that were solved through time. The model successfully predicted the transient stress profiles of orthotropic viscoelastic materials with state-dependent radial modulus. Temperature changes directly influence the creep functions in polymeric materials. Qualls also formed and validated thermoviscoelastic

winding models. Winding tests were conducted at room temperature and stored at elevated temperatures on a low density polyethylene web to verify these models.

Summary:

Dealing with viscoelastic effects is not an easy problem in web winding. Selecting boundary conditions, simplification and approximation methods were necessary to reach the solution of the equations. Previous research of viscoelastic winding is mature and existing models are capable of analyzing the influence of creep in homogeneous webs stored in roll form. However, laminated webs have not been treated to date.

2.1.3 Winding Defects

The mission of winding models is to predict the residual stresses in rolls that resulted from winding. Knowledge of these residual stresses is then used to predict and mitigate damage of the web in the roll. This damage has been identified qualitatively by categorizing the damage as various types of wound roll defects.

Roisum and Frye [13][14][15][16] and Smith [17] qualitatively described multiple web defects, mainly in paper rolls, as well as the in shape and causes.

(1) Blocking

Blocking is a defect where layers in a roll stick together too aggressively. This is directly related to pressure. If the pressure between different layers is too high, the web can stick or bond to the next layer, and thus it is hard to unwind the web. The only practical method to determine the pressure that indicates blocking is to perform a compression test on a stack of web material at successively higher pressures until sticking between the layers is noted. It is likely the blocking pressure will be affected by temperature and moisture. Winding models can be used to develop winding tensions and nip loads that will prevent all internal pressures in the wound roll to be less

than the blocking pressure and thus prevent the defect. Good pointed out that thermal and viscoelastic winding models may be required to determine the maximum pressures that should be less than the blocking pressure. Laminates being wound will have dissimilar surfaces in contact as the inside of the current layer will interface with the outer surface of the layer beneath due to the spiral nature of the wound rolls. Laminate webs will block just as single layer webs, although the pressure at which blocking will occur will be unique for every single layer and laminate web.

(2) Slippage

The occurrence of slippage might cause cinching, some types of telescoping, abrasion, and so on. The consequence of slippage is usually the loss of tension control. In many cases, a parameter named the torque carrying capacity can help predict slippage. Simply speaking, the torque carrying capacity is a critical value, which is the torque that can be applied to either a winding or unwinding roll just prior to slippage occurring.

Good, in his book [18], shows based on equilibrium it would appear impossible to wind low coefficient of friction materials with a center winder ($\mu < 1/2\pi$). He estimated the torque capacity with the following expression:

$$T_{cap} = 2\pi\mu_{w/w}Pr^2W \tag{2.18}$$

where, P is the radial pressure at the radius r and $\mu_{w/w}$ is the friction coefficient between two layers of the web. It is assumed that either elastic or viscoelastic winding models have been used to determine how the internal pressure P varies with wound roll radius. Slippage in laminate rolls can be predicted with similar expressions providing the laminate winding models are developed.

(3) Curl

Curl is a common distortion shape in web materials, although most industry prefers the perfect flat web. Many reasons may induce the curl of web: (1) the core-set curl, especially for long storage time of web and (2) strain not matched for laminate web, etc. Our research mainly focuses on the viscoelastic curl for long storage time.

In an early patent, Schrader et al. [19] found that heat-tempered films have a core-set curling tendency, and they also pointed out some methods to reduce this. Some other patents also talked about reasons for the existence of core-set curl [20][21]. The reason to describe this effect is related to the rheological behavior of materials.

It is well known that, when a flat film is bent to some fixed curvature, held in this state for some time, and then released, the curvature is usually observed to drop instantaneously to some finite value and then decrease with time. J. Greener [22] developed a theoretical expression to predict the curl, and verified it experimentally.

The model predicts the values of bending recovery BR. The MD curl in winding process is similar to the bending recovery effect. BR is then defined to represent the recovery of curvature.

$$BR = \frac{R}{\rho} \tag{2.19}$$

where R is the radius of the core or position in the roll where the web is wound , and ρ is the radius of curvature of the web. Many factors may influence the curl, including the radius of core or roll, the thickness of the web, viscoelastic properties of the web, the length of storage time, environment, winding stresses, etc. If the web is flat, BR should be 0 while BR is equal to 1 if the web is totally viscoelastic.

Euler bending theory dictates:

$$M_b = \frac{D}{\rho} \tag{2.20}$$

where M_b is the bending moment per unit width and D is the bending rigidity of the film also per unit width:

$$D = \frac{EI}{(1-\upsilon^2)} = \frac{Eh^3}{12(1-\upsilon^2)} \tag{2.21}$$

where E is the Young's modulus, I is the moment of inertia of the film per unit width, h is the web thickness and υ is the Poisson's ratio. The Euler bending strains ε are [23]:

$$\varepsilon = \frac{y}{R} \tag{2.22}$$

where y is the coordinate normal to the web with an origin at the mid-plane. It is possible that frictional forces on the inner surface of the web could shift the origin of this y coordinate toward the inner surface of the web. If there were no slippage at all, the origin would be at the inner surface and all the bending strains would be elongating tensile strains.

Linear viscoelasticity can be applied here:

$$\sigma(t) = \int_0^t E(t-\varsigma)\varepsilon(\varsigma)d\xi \tag{2.23}$$

where $\sigma(t)$ is the stress, E(t) is the relaxation modulus, t and ς are the real time and a dummy time, respectively. When a viscoelastic film is wound on a rigid cylinder subject to tension, the strain distribution remains the same, and the bending stresses will begin to relax:

$$\sigma(y,t) = \frac{y}{R}\frac{E(t)}{(1-\upsilon^2)} \tag{2.24}$$

The relaxation processes in the tensile and compressive zones are expected to be dissimilar, which complexities the problem [24]. Sometimes the compressive stresses relax substantially slower than tensile stresses. E_{ten} is the relaxation modulus in tension while E_{com} is the relaxation modulus in compression.

As the web is removed form the core at $t = t_r$, the curvature will change as follows:

$$\frac{1}{R} - \frac{1}{\rho} = \frac{M_b(t_r)}{D} \tag{2.25}$$

$$M_b(t_r) = \frac{1}{(1-\upsilon^2)}\left[\int_{-H/2}^{0} E_{com}(t_r)\frac{y^2}{R}dy + \int_{0}^{H/2} E_{ten}(t_r)\frac{y^2}{R}dy\right. \tag{2.26}$$

This can be integrated to obtain the final results for the bending recovery:

$$BR = \frac{R}{\rho} = [1 - \frac{E_{ten}(t_r) + E_{com}(t_r)}{2E_0}] \tag{2.27}$$

E_0 is the initial Young's modulus, which means that the Young's modulus when the time is 0. We used the uniaxial tensile test at a certain strain rate to represent this. The bending recovery can be related to time and viscoelastic properties rather than the tension or the radius of core. Measurement of the compressive relaxation is difficult, and thus we need to analyze two extreme situations first.

When the compressive stresses relax substantially slower than tensile stresses, and thus $E_{com}(t_r) = E_0$.

$$BR_1 = \frac{1}{2}[1 - \frac{E_{ten}(t_r)}{E_0}] \tag{2.28}$$

When the relaxation of the stresses are independent of the sign of the stress, $E_{com}(t_r) = E_{ten}(t_r)$.

$$BR_2 = [1 - \frac{E_{ten}(t_r)}{E_0}] \tag{2.29}$$

When the compressive stresses relax substantially slower than tensile stresses, it can be treated simply by a constant shift factor to slow the relaxation for the compressive state.

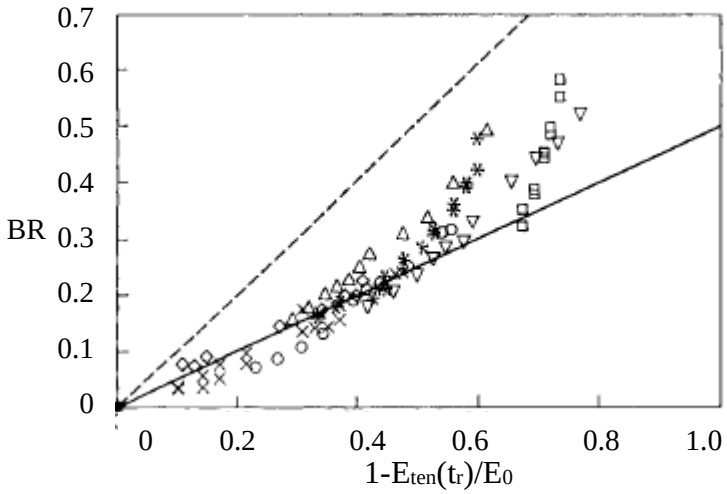

The horizontal axis is BR as in equations (2.28) and (2.29). Solid line is equation (2.28) while dashed line is equation (2.29). (*) CA, 21°C, (□) CA, 38°C, (×) PET, 21°C, (∘) PET, 38°C, (◊) MXD, 21°C, (∇) PP, 21°C.

Fig. 2.1 Instantaneous Recovery vs. Relaxed Modulus [22]

Equation (2.28) assumes that no relaxation happened for the compressive state. When $1-E_{ten}(t_r)/E_0$ is small, all the data are quite close to equation (2.29). Fig. 2.1 shows that the dissimilar relaxation exists and thus it is necessary to consider this in our future curl analysis.

Later J. Greener developed long storage time analysis for the aging effect of polymer materials [25]. Aging effect may significantly influence core-set curl in polymeric film unless the storage time is relatively short compared with the time the web age. Kidane [26] presented a 2D curl model that was based on laminate theory in 2009.

In order to solve the curl problems, measurement of the curl is necessary [27]. Swanson developed a curl measurement instrument called the Kappa Gauge [28]. This new Curl Gauge is in the units of 1/m (the inverse of the radius of curvature). The Kappa Gauge has 6 different sample lengths.

The minimum length is 50mm, while the maximum value 250mm. It is used to quantify the curl radius, such as core set curl, lamination curl, thermally induced curl and so on.

Summary

Curl defects are common in both single layer webs and laminate webs. The viscoelasticity of web materials induces the curl. It is necessary to further develop existing winding models to predict and mitigate the curl problem.

2.2 Research Objectives

Substantial research has been conducted and reported regarding the winding of webs. Even though laminating and coating webs are common web processes, no instances were found regarding winding elastic or viscoelastic models for laminated or composite webs. All entries in the literature focus on orthotropic single layer homogenous webs. Yet laminated webs and coated webs are produced commonly in industry to satisfy product requirements. Furthermore many of the developed models ignore bending strains and stresses and assume constant stresses through the depth of a wound layer. In addition the treatment of MD curl due to storage of webs in wound rolls is not sufficient. While MD curl of laminates has received some attention, MD curl of wound laminates has received no treatment. The following research objectives are proposed to fill the gaps discovered in the literature and meet the needs of the industry:

1. Development of an elastic 1D model for winding laminates or webs with substantial coatings: 1D models are useful for narrow webs where potential thickness variations are small. These models should be developed to improve the quality of wound rolls of laminated and coated webs by optimizing the winder operating conditions and the resulting wound roll residual stresses. Knowledge of these stresses can be used to prevent defects due to blocking, slippage and buckling. The new models will be verified in the laboratory using methods used for early winding models.

2. To use any winding code requires an investment of time to measure the needed input properties. Creep functions from creep tests are used as the direct input in Winder 6.3. These tests require long time to get characterization for the time period of modeling. Such models will be more useful if we characterize the viscoelastic material in short time by building a master curve by conducting creep or stress relaxation tests at elevated temperatures. If this is possible this will reduce the time investment to determine the input.

3. Control web winding defects: Curl appears in single layer or laminate webs and has received minimal attention in the literature. A curiosity regarding web rolls would be if the curl can be controlled or modified. The web would creep in long storage time. At the time the roll was unwound how has the curl been affected? Is there an optimal time to unwind the roll to minimize curl? The third research objective aims at finding answers to these questions.

2.3 Organization

Chapter 3 will focus on the development a 1D orthotropic winding model. That model will be expanded in chapter 4 to encompass the winding of laminates. Lamination curl due to strain not match will also be discussed in this chapter. Chapter 5 examines how viscoelasticity is characterized for webs and chapter 6 talks how viscoelasticity contributes to curl. Chapter 7 distills the research into conclusions and discusses the future research.

CHAPTER III

DEVELOPMENT OF 1D ELASTIC WINDING MODELS

3.1 A 1-D Single Layer Orthotropic Model

We will use the elastic constitutive equations and the assumption of plain strain to develop a pre-stress model of an orthotropic single layer. The following development is very similar to that employed by Mollamahmutoglu and Good [37]. The elastic constitutive equations in cylindrical coordinates:

$$\begin{bmatrix}\varepsilon_r\\ \varepsilon_\theta\\ \varepsilon_z\end{bmatrix}=\begin{bmatrix}\frac{1}{E_r} & -\frac{\nu_{\theta r}}{E_\theta} & -\frac{\nu_{zr}}{E_z}\\ -\frac{\nu_{\theta r}}{E_\theta} & \frac{1}{E_\theta} & -\frac{\nu_{z\theta}}{E_z}\\ -\frac{\nu_{zr}}{E_z} & -\frac{\nu_{z\theta}}{E_z} & \frac{1}{E_r}\end{bmatrix}\begin{bmatrix}\sigma_r\\ \sigma_\theta\\ \sigma_z\end{bmatrix} \tag{3.1}$$

where, the subscript r, θ and z shows the directions of radial, tangential and axials directions, respectively. ε is the strain while σ is the stress. E and υ are Young's modulus and Poisson ratios. In the lab setting, $\upsilon_{\theta r}$ and υ_{zr} are easier to measure than $\nu_{r\theta}$ and ν_{rz} for webs Maxwell's reciprocal theorem was used to eliminate those Poisson ratios that were more difficult to measure.

Generally speaking, the length of webs is much larger than the other two dimensions (width and thickness). Before entering a winder, the web in the upstream span has already contracted in the CMD direction due to the Poisson effect. If the plane strain assumption is valid the contracted

web width will remain the same as the web enters the winder. This means that the relative z or w deformation as the web transits from the entering span to the winder to outer surface of the winding roll is zero.

$$\varepsilon_z = \frac{\partial w}{\partial z} = 0 = -\frac{v_{zr}}{E_z}\sigma_r - \frac{v_{z\theta}}{E_z}\sigma_\theta + \frac{\sigma_z}{E_z} \; or \; \sigma_z = v_{zr}\sigma_r + v_{z\theta}\sigma_\theta \tag{3.2}$$

Substituting (3.2) into (3.1) yields:

$$\{\varepsilon\} = \begin{bmatrix} (\frac{1}{E_r} - \frac{v_{zr}^2}{E_z}) & (-\frac{v_{\theta r}}{E_\theta} - \frac{v_{zr}v_{z\theta}}{E_z}) \\ (-\frac{v_{\theta r}}{E_\theta} - \frac{v_{zr}v_{z\theta}}{E_z}) & (\frac{1}{E_\theta} - \frac{v_{z\theta}^2}{E_z}) \end{bmatrix} \begin{bmatrix} \sigma_r \\ \sigma_\theta \end{bmatrix} = [D]^{-1}\{\sigma\} \tag{3.3}$$

On inversion, the D matrix can be obtained:

$$[D] = \frac{E_\theta}{DEN} D_{22} = -E_\theta(E_z - E_r v_{zr}^2) \begin{bmatrix} E_r(E_\theta v_{z\theta}^2 - E_z) & -E_r(E_\theta v_{zr}v_{z\theta} + E_z v_{\theta r}) \\ -E_r(E_\theta v_{zr}v_{z\theta} + E_z v_{\theta r}) & -E_\theta(-E_r v_{zr}^2 + E_z) \end{bmatrix} \tag{3.4}$$

Where,

$$DEN = E_z\left(E_r v_{\theta r}^2 - E_\theta\right) + E_\theta(E_\theta v_{z\theta}^2 + E_r v_{zr}(v_{zr} + 2v_{z\theta}v_{\theta r})) \tag{3.5}$$

Note that, the D matrix must be positive definite to ensure that the system of finite element that will be developed can be solved. The following set of rules (3.6) must be satisfied to ensure the [D] matrix is positive definite:

$$E_r, E_\theta, E_z > 0$$

$$|v_{z\theta}| < \sqrt{\frac{E_r}{E_\theta}}, |v_{rz}| < \sqrt{\frac{E_r}{E_z}}, |v_{\theta z}| < \sqrt{\frac{E_\theta}{E_z}} \tag{3.6}$$

$$1 - v_{r\theta}v_{\theta r} - v_{\theta z}v_{z\theta} - v_{zr}v_{rz} - 2v_{\theta r}v_{z\theta}v_{rz} > 0$$

As noted Pfeiffer and Hakiel found the radial modulus to be state dependent on stack pressure which varies throughout the roll. Thus the inequalities involving Poisson's ratios and Young's modulus, specially E_r, need to be true for the range of E_r found in a roll.

A two-node axisymmetric element is shown in Fig. 3.1. The element space is defined by two nodes having radial positions r_i and r_j and radial displacements u_i and u_j

The development begins with the selection of 1D shape functions in the natural coordinate ξ shown in the master element in Fig. 3.1:

$$N_1 = \frac{1-\xi}{2} \quad N_2 = \frac{1+\xi}{2} \tag{3.7}$$

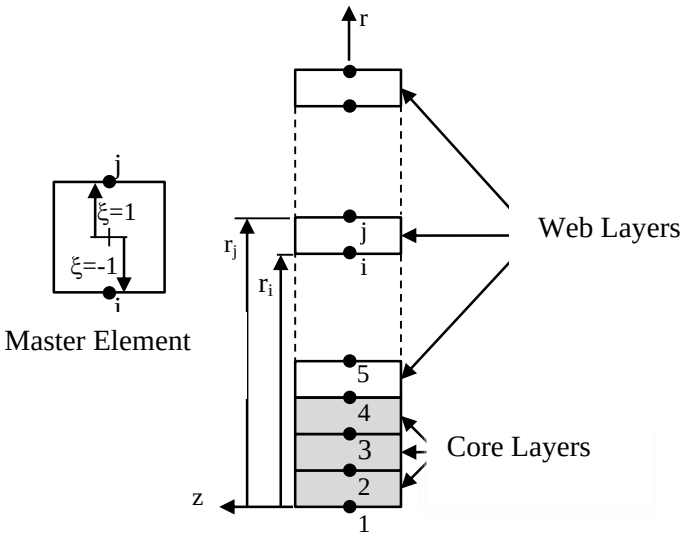

Fig. 3.1 1D Axisymmetric Finite Element Model of Wound Roll

These shape functions will be used in an isoparametric formulation to interpolate the radial locations (r) and the radial deformations (u) within the 1D axisymmetric finite element:

$$r = [N_i \quad N_j] \begin{Bmatrix} r_i \\ r_j \end{Bmatrix} \tag{3.8}$$

$$u = [N_i \quad N_j]\begin{Bmatrix} u_i \\ u_j \end{Bmatrix} \tag{3.9}$$

Equation (3.8) can be rearranged to produce a coordinate map equation relating the ξ and r coordinates. Note that r_j-r_i is the undeformed web thickness h:

$$\xi = \frac{2r - (r_i + r_j)}{r_j - r_i} = \frac{2r - (r_i + r_j)}{h} \tag{3.10}$$

With the deformations (3.9) known the strains can be determined. The radial strain is:

$$\varepsilon_r = \frac{du}{dr} = \frac{du}{d\xi}\frac{d\xi}{dr} = \begin{bmatrix} -\frac{1}{h} & \frac{1}{h} \end{bmatrix}\begin{Bmatrix} u_i \\ u_j \end{Bmatrix} \tag{3.11}$$

For purposes of stiffness development the tangential strain will be determined at the centroid of the finite element where $\bar{r} = \frac{r_i + r_j}{2}$:

$$\varepsilon_\theta = \frac{u}{r} = \begin{bmatrix} \frac{N_i}{r} & \frac{N_j}{r} \end{bmatrix}\begin{Bmatrix} u_i \\ u_j \end{Bmatrix} = \begin{bmatrix} \frac{1}{2\bar{r}} & \frac{1}{2\bar{r}} \end{bmatrix}\begin{Bmatrix} u_i \\ u_j \end{Bmatrix} \tag{3.12}$$

$$\varepsilon_z = \gamma_{rz} = 0 \text{ (Plane Strain Assumption)} \tag{3.13}$$

The non-zero strains are thus:

$$\begin{Bmatrix} \varepsilon_r \\ \varepsilon_\theta \end{Bmatrix} = \begin{bmatrix} -\frac{1}{h} & \frac{1}{h} \\ \frac{1}{2\bar{r}} & \frac{1}{2\bar{r}} \end{bmatrix}\begin{Bmatrix} u_i \\ u_j \end{Bmatrix} = [\bar{B}]\{u\} \tag{3.14}$$

The concept of pre-stress (σ_0) and pre-strain (ε_0) is often used in finite element derivations to accommodate thermal stress and strain. This concept will be employed here to introduce the MD stress in the web due to web tension in the winder tension zone. The strain energy in a finite element (U) is:

$$U_e = \frac{1}{2}\int_0^{2\pi}\int_A \{\sigma\}^T\{\varepsilon\} r\, dA\, d\theta - \int_0^{2\pi}\int_A \{\sigma\}^T\{\varepsilon_o\} r\, dA\, d\theta \tag{3.15}$$

Substituting the developed representations for stress and stain yields:

$$U_e = \frac{2\pi}{2}\{q\}^T \int_A \{\bar{B}\}^T[D]\{\bar{B}\}\bar{r}\, dA\{q\} - 2\pi\{q\}^T \int_A \{\bar{B}\}^T[D]\{\varepsilon_o\}\bar{r}\, dA \tag{3.16}$$

The element stiffness matrix $[K_e]$ is integral to the 1st term in equation (3.16) and the 2nd term is a statement of work potential involving deformations and equivalent forces $\{f_e\}$ at nodes:

$$U_e = \frac{1}{2}\{q\}^T[K_e]\{q\} - \{q\}^T\{f_e\} \tag{3.17}$$

$$[K_e] = 2\pi \int_A \{\bar{B}\}^T[D]\{\bar{B}\}\bar{r}\, dA = 2\pi\bar{r}A_e\{\bar{B}\}^T[D]\{\bar{B}\} = 2\pi\bar{r}hW\{\bar{B}\}^T[D]\{\bar{B}\} \tag{3.18}$$

where W is the web width. Substituting equations (3.14) and (3.4) into (3.18) yields:

$$[K_e] = \begin{bmatrix} \frac{\pi W}{2}\left(\frac{4\bar{r}}{h}D_{11} + \frac{h}{\bar{r}}D_{22} - 4D_{12}\right) & rW\left(\frac{h}{2\bar{r}}D_{22} - \frac{2\bar{r}}{h}D_{11}\right) \\ \pi W\left(\frac{h}{2\bar{r}}D_{22} - \frac{2\bar{r}}{h}D_{11}\right) & \frac{\pi W}{2}\left(\frac{4\bar{r}}{h}D_{11} + \frac{h}{\bar{r}}D_{22} - 4D_{12}\right) \end{bmatrix} = \begin{bmatrix} k_{11} & k_{12} \\ k_{21} & k_{22} \end{bmatrix} \tag{3.19}$$

The force vector $\{f_e\}$ is integral to the 2nd term in equation (3.18):

$$f_e = 2\pi \int_A \{\bar{B}\}^T[D]\{\varepsilon_o\}\bar{r}\, dA = 2\pi\bar{r}hW\{\bar{B}\}^T[D]\{\varepsilon_o\} = 2\pi\bar{r}hW\{\bar{B}\}^T\{\sigma_o\} \tag{3.20}$$

Substituting equation (3.14) into (3.20) yields:

$$\{f_e\} = 2\pi\bar{r}hW\begin{Bmatrix}\frac{\sigma_\theta}{2\bar{r}} - \frac{\sigma_r}{h} \\ \frac{\sigma_\theta}{2\bar{r}} + \frac{\sigma_r}{h}\end{Bmatrix}_0 \tag{3.21}$$

The only pre-stress in the outer layer is the tangential stress (σ_θ) which is equivalent to the web stress due to web tension (T_w) and there is no radial pre-stress component (σ_r). Also a tensile (σ_θ) stress in the outer lap would produce forces in a positive r direction at nodes *i* and *j* that would result in a negative contact pressure between the outer layer and the layer beneath. Thus a negative value of web stress is substituted into equation (3.21) and the force vector reduces to:

$$\{f_e\} = -\pi hWT_w\begin{Bmatrix}1 \\ 1\end{Bmatrix} \tag{3.22}$$

The winding tension (T_w) in equation (3.22) can take any form as a function of wound roll radius chosen. With a developed stiffness matrix and force vector the development of the finite element formulation is nearly complete. The stiffness matrix (3.19) can be used recursively to develop element stiffness matrices for the core and for the layers of web material added to the core. An example is shown in equation (3.23) in which the changes in deformation (u_i) are being sought as a result of accreting the third web layer. Note the core is being crudely modeled here with 2 axisymmetric elements, in most cases 5 core layers has been found sufficient to model the core accurately. Each web layer is modeled with 1 axisymmetric element, also found to be sufficient to achieve convergence of results.

$$\begin{bmatrix}
k_{11\boxed{c1}} & k_{12\boxed{c1}} & 0 & 0 & 0 & 0 \\
k_{12\boxed{c1}} & k_{22\boxed{c1}} + k_{11\boxed{c2}} & k_{12\boxed{c2}} & 0 & 0 & 0 \\
0 & k_{12\boxed{c2}} & k_{22\boxed{c2}} + k_{11\boxed{w1}} & k_{12\boxed{w1}} & 0 & 0 \\
0 & 0 & k_{12\boxed{w1}} & k_{22\boxed{w1}} + k_{11\boxed{w2}} & k_{12\boxed{w2}} & 0 \\
0 & 0 & 0 & k_{12\boxed{w2}} & k_{22\boxed{w2}} + k_{11\boxed{w3}} & k_{12\boxed{w3}} \\
0 & 0 & 0 & 0 & k_{12\boxed{w3}} & k_{22\boxed{w3}}
\end{bmatrix}
\begin{Bmatrix}\delta u_1 \\ \delta u_2 \\ \delta u_3 \\ \delta u_4 \\ \delta u_5 \\ \delta u_6\end{Bmatrix} =
\begin{Bmatrix}0 \\ 0 \\ 0 \\ 0 \\ -\pi h_w WT_w \\ -\pi h_w WT_w\end{Bmatrix} \tag{3.23}$$

The assembly of the stiffness matrices begins with assembling all the core matrices. Several elements should be used to model the core which is usually considerably thicker than the web. Since the finite element will allow at best constant values of stress within the domain of the element ($\sigma = D\bar{B}u$), several elements are needed to properly characterize the mechanical behavior of the core. The accretive solution begins with one web layer being added to the core. Note that one web and two web layer solutions had to precede that shown in equation (3.23) such that the D_{ij} terms in (3.4) were known for the web layers that depend on the state dependent radial modulus that varies with pressure. The changes in deformation that result from solving the independent set of equations such as those shown in equation (3.23) can then be used to determine the increments in stress within each element due to the addition of the most recent layer. Such a computation is shown here for element W2:

$$\left\{\delta\sigma_{\boxed{W2}}\right\} = \begin{Bmatrix}\delta\sigma_r \\ \delta\sigma_\theta\end{Bmatrix} = \left[D\right]_{\boxed{W2}}\left[\bar{B}\right]_{\boxed{W2}}\begin{Bmatrix}\delta u_4 \\ \delta u_5\end{Bmatrix} \tag{3.24}$$

Equation (3.2) can then be used to determine the change in axial stress ($\delta\sigma_z$) in element W2:

$$\delta\sigma_z = v_{zr}\delta\sigma_r + v_{z\theta}\delta\sigma_\theta \tag{3.25}$$

Changes in stresses would be calculated for each element of the core and for all layers in the wound roll. The total stresses in a particular layer are determined by summing all the changes in stress in that layer from the point when that layer was added until the most recent layer *n* was accreted on the wound roll. For layer W2:

$$\left\{\sigma\right\}_{\boxed{W2}} = \begin{Bmatrix}\sum_{i=2}^{n}\delta\sigma_{ri\boxed{W2}} \\ \sum_{i=2}^{n}\delta\sigma_{\theta i\boxed{W2}} + T_w \\ \sum_{i=2}^{n}\delta\sigma_{zi\boxed{W2}}\end{Bmatrix} = \begin{Bmatrix}\sigma_r \\ \sigma_\theta \\ \sigma_z\end{Bmatrix}_{\boxed{W2}} \tag{3.26}$$

The total pressure in layer W2 is now known ($P=-\sigma_r$) and can be used to update the radial modulus (E_r) using equation (2.1) for this element. The stiffness matrix for element W2 can then be updated using equation (3.19). These calculations in equation (3.26) are repeated for all *n* layers in the wound roll. Then a new set of equations similar to those shown in (3.23) is formed to solve for the differential displacements throughout the wound roll due to the addition of the *n+1* layer. The differential displacements for each node can be summed to determine the total deformation of each node due to all the layers added outside of a given node. Equations similar to (3.23) through (3.26) are assembled repeatedly and solved until a defined number of layers are wound onto the core or a defined outer roll radius is achieved.

3.2 Validation

1D winding models have been verified at various levels. The interlayer pressure can be measured using steel shim on narrow rolls quite accurately. The steel shim is often enveloped in brass shim which is called a pull tab and wound into rolls. The pull force required to induce slip between the steel and brass shim is related to the pressure between layers in the wound roll. The relationship is best obtained by inserting these pressure transducers into a stack of the web material to be wound. A material testing system is used to subject the stack to various pressures and the force required to induce slip is measured at each stack test pressure.

Table 3.1 Winding, Web and Core Properties for Winding Newsprint

Web Thickness (mm)	0.071	Core Inner Radius (cm)	3.81
Finish Radius (cm)	13.35		
Web Width (cm)	15.26	Core Outer Radius (cm)	4.45
Winding Stress (MPa)	5.17		
Web Properties		**Core Properties**	
$E_\theta=E_z$ (MPa)	3,370	$E_r=E_\theta=E_z$ (GPa)	200
K_1 (KPa)	1.175		
K_2	45.14	$\nu_{\theta r}=\nu_{zr}=\nu_{z\theta}$	0.3
$\nu_{\theta r}=\nu_{zr}=\nu_{z\theta}$	0.3		

The model developed herein will be verified for a newsprint web with the properties shown in Table 3.1. Note that orthotropic property input is possible for both the web and the core.

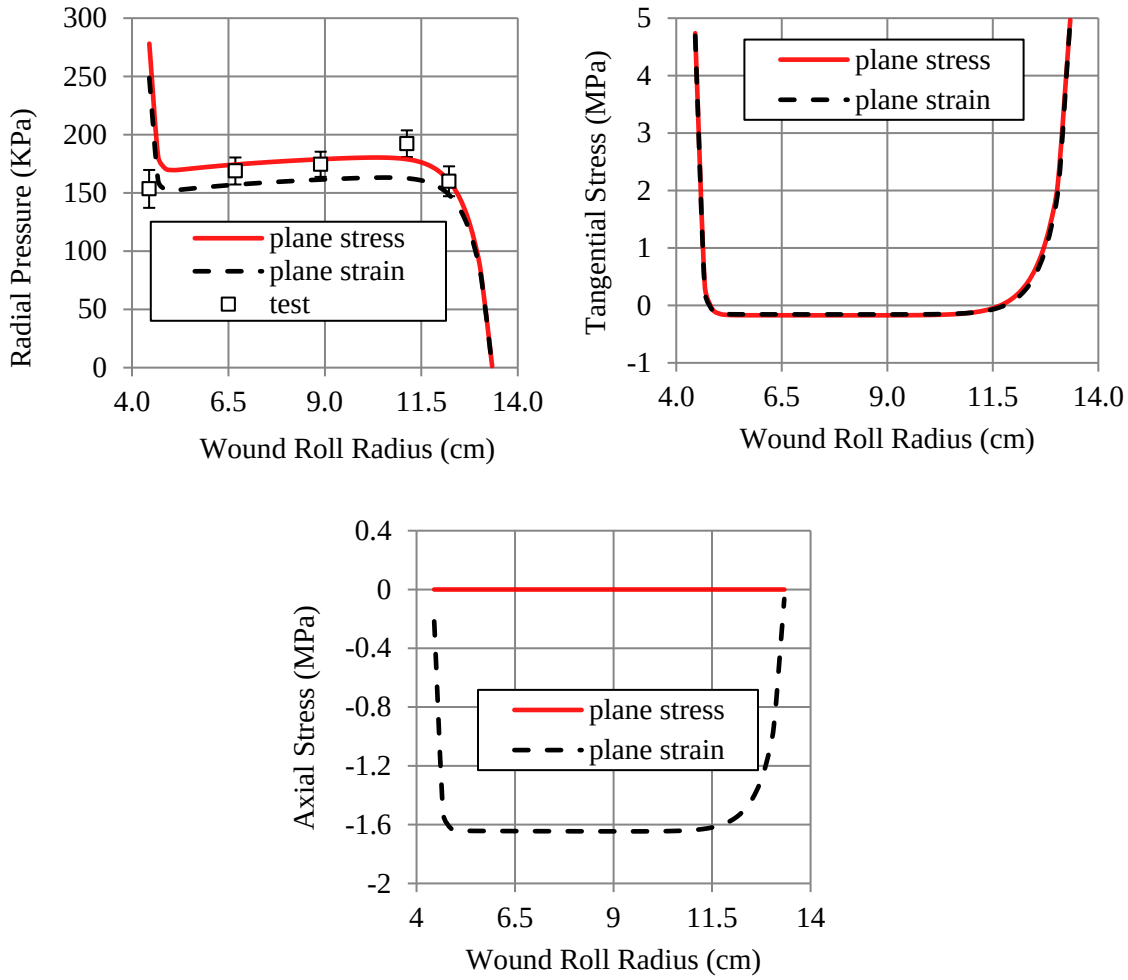

Fig. 3.2 Verification of Orthotropic Winding Model on Newsprint

The results of the verification tests are shown in Fig. 3.2. The test data points are the average pressure measurements from 3 winding tests where pull tab pressure transducers were wound into the rolls consistently at the wound roll radial positions shown in the charts. The error bars show the standard deviation of the data at each radius. Model results are shown for both plane stress and plane strain material behaviors. The plane strain model developed herein can produce plane stress behavior if ν_{zr} and $\nu_{z\theta}$ are set to zero refer to expression (3.2). In general the comparison of model

results with tests is very good with the test results comparing somewhat better with the plane stress model behavior. The web width was inadequate to achieve the plane strain behavior. Note the tangential stresses (σ_θ) resulting from the two material behaviors are essentially equal. Substantial negative axial stresses can be developed when plane strain behaviors are achieved. In plane strain conditions the axial stresses tend to vanish at the outer lap and in this case near the core which was axially much stiffer than the web in this example.

CHAPTER IV

DEVELOPMENT OF LAMINATE WINDING MODEL

4.1 1-D Two-layer Laminate Model

4.1.1 Assumptions

A stiffness matrix and force vector for a plane strain homogenous web was developed in equations (3.19) and (3.22) respectively. Those developments will be extended to a two layer laminate web. It will be assumed that the agent used to bond the layers together in the laminator does not contribute to the stiffness of the laminate. It will also be assumed that the behavior of a stack of laminates in compression will be characterized in a compression test similar to that described in section 2.1.1.

A laminate is now accreted to the winding roll and a stiffness matrix and a force vector for the laminate is needed. Equations (3.19) and (3.22) can be used to determine the stiffness and forces the two layers (1 and 2) in the laminate:

$$K_{(1)} = \begin{bmatrix} K_{1ii} & K_{1ij} \\ K_{1ij} & K_{1jj} \end{bmatrix}, f_{(1)} = \begin{Bmatrix} f_{1i} \\ f_{1j} \end{Bmatrix} \; and \; K_{(2)} = \begin{bmatrix} K_{2jj} & K_{2jk} \\ K_{2jk} & K_{2kk} \end{bmatrix}, f_{(2)} = \begin{Bmatrix} f_{2j} \\ f_{2k} \end{Bmatrix} \tag{4.1}$$

where, i, j and k refer to the nodes in Fig. 4.1. Since the two layers have node j in common the direct stiffness assembly method can be used to combine the stiffness matrices and force vectors:

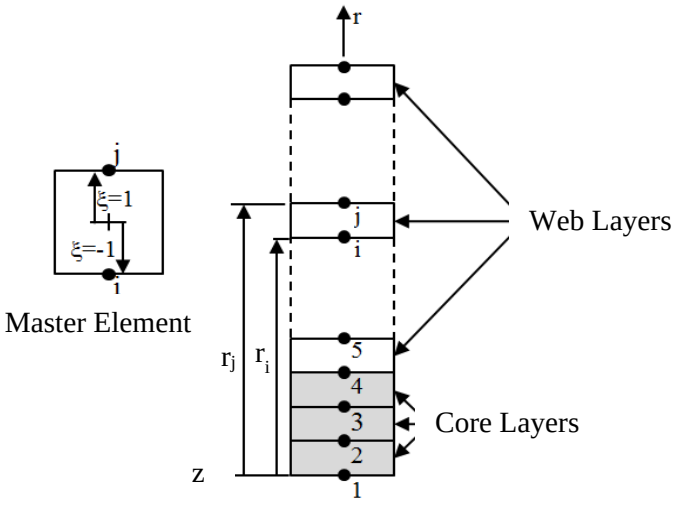

Fig. 4.1 A 1D Axisymmetric Laminate Finite Element

$$K_{Laminate} = \begin{bmatrix} K_{1ii} & K_{1ij} & 0 \\ K_{1ij} & K_{1jj} + K_{2jj} & K_{2jk} \\ 0 & K_{2jk} & K_{2kk} \end{bmatrix} \; and \; f_{Laminate} = \begin{Bmatrix} f_{1i} \\ f_{1j} + f_{2j} \\ f_{2k} \end{Bmatrix} \tag{4.2}$$

where:

$$\begin{aligned} K_{1ii} &= \frac{\pi}{2} w \left(\frac{4\bar{r}}{h} D_{11} + \frac{h}{\bar{r}} D_{22} - 4D_{12} \right)\Big|_{(1)} & K_{2jj} &= \frac{\pi}{2} w \left(\frac{4\bar{r}}{h} D_{11} + \frac{h}{\bar{r}} D_{22} - 4D_{12} \right)\Big|_{(2)} \\ K_{1ij} &= \pi w \left(\frac{h}{2\bar{r}} D_{22} - \frac{2\bar{r}}{h} D_{11} \right)\Big|_{(1)} & K_{2jk} &= \pi w \left(\frac{h}{2\bar{r}} D_{22} - \frac{2\bar{r}}{h} D_{11} \right)\Big|_{(2)} \\ K_{1jj} &= \frac{\pi}{2} w \left(4D_{12} + \frac{h}{\bar{r}} D_{22} + \frac{4\bar{r}}{h} D_{12} \right)\Big|_{(1)} & K_{2kk} &= \frac{\pi}{2} w \left(4D_{12} + \frac{h}{\bar{r}} D_{22} + \frac{4\bar{r}}{h} D_{12} \right)\Big|_{(2)} \end{aligned} \tag{4.3}$$

and

$$f_{(1)} = \begin{Bmatrix} f_{1i} \\ f_{1j} \end{Bmatrix} = -\pi h W T_w|_{(1)} \begin{Bmatrix} 1 \\ 1 \end{Bmatrix} \; and \; f_{(2)} = \begin{Bmatrix} f_{2j} \\ f_{2k} \end{Bmatrix} = -\pi h W T_w|_{(2)} \begin{Bmatrix} 1 \\ 1 \end{Bmatrix} \tag{4.4}$$

The subscripts (1) and (2) in equations (4.3) and (4.4) denote stiffness and force terms associated with layers 1 and 2 in the laminate. The stresses in layers 1 and 2 will be unique and will depend on conditions at the laminator which will be discussed later in section 4.1.3. An accretive solution similar to that shown for the single orthotropic layer in equation (3.23) can now be developed and

solved for the changes in radial deformation of the nodes (δu_i). Those nodal changes in deformation can then be used to solve for changes in stress in all layers using equation (3.24).

4.1.2 Numerical Oscillation and Condensation Method

When solutions were attempted of the laminate winding model described numerical oscillations were witnessed in some cases in the stresses output. In other cases the solution of the set of equations was not possible. If identical material properties were input for the two layers of the laminate, the oscillations vanished and solution of the sets of equations was always possible. The problem stemmed from the assumption that both layers of the laminate shared an identical equation (2.1) for the radial modulus (E_r). The problem was solved using a condensation method.

The equilibrium of the two-layer laminate can be stated as:

$$\begin{bmatrix} K_{1ii} & K_{1ij} & 0 \\ K_{1jj} & K_{1jj}+K_{2jj} & K_{2jk} \\ 0 & K_{2jk} & K_{2kk} \end{bmatrix} \begin{Bmatrix} \delta u_i \\ \delta u_j \\ \delta u_k \end{Bmatrix} = \begin{Bmatrix} f_{1i} \\ f_{1j}+f_{2j} \\ f_{2k} \end{Bmatrix} \tag{4.5}$$

The condensation method will be used to remove the internal degree of freedom at node *j*. These equations from equation (4.5) can be re-ordered as follows:

$$\begin{bmatrix} \begin{bmatrix} K_{1ii} & 0 \\ 0 & K_{2kk} \end{bmatrix} & \begin{bmatrix} K_{1ij} \\ K_{2jk} \end{bmatrix} \\ \begin{bmatrix} K_{1ij} & K_{2jk} \end{bmatrix} & \begin{bmatrix} K_{1jj}+K_{2jj} \end{bmatrix} \end{bmatrix} \begin{Bmatrix} \begin{Bmatrix} \delta u_i \\ \delta u_k \end{Bmatrix} \\ \{\delta u_j\} \end{Bmatrix} = \begin{Bmatrix} \begin{Bmatrix} f_{1i} \\ f_{2k} \end{Bmatrix} \\ \{f_{1j}+f_{2j}\} \end{Bmatrix} \tag{4.6}$$

This can be rewritten symbolically as:

$$\begin{bmatrix} [K_{rr}] & [K_{rc}] \\ [K_{cr}] & [K_{cc}] \end{bmatrix} \begin{Bmatrix} \{\delta u_r\} \\ \{\delta u_c\} \end{Bmatrix} = \begin{Bmatrix} \{r_r\} \\ \{r_c\} \end{Bmatrix} \tag{4.7}$$

The condensed stiffness matrix is:

$$K_{condensed} = [K_{rr}] - [K_{rc}][K_{cc}]^{-1}[K_{cr}] = \begin{bmatrix} K_{1ii} - \dfrac{K_{1ij}^2}{K_{1jj} + K_{2jj}} & \dfrac{-K_{1ij}K_{2jk}}{K_{1jj} + K_{2jj}} \\ \dfrac{-K_{1ij}K_{2jk}}{K_{1jj} + K_{2jj}} & K_{2kk} - \dfrac{K_{2jk}^2}{K_{1jj} + K_{2jj}} \end{bmatrix} \quad (4.8)$$

And the condensed force vector is:

$$f_{condensed} = \{r_r\} - [K_{rc}][K_{cc}]^{-1}\{r_c\} = \begin{Bmatrix} f_{1i} - \dfrac{K_{1ij}}{K_{1jj} + K_{2jj}}\left(f_{1j} + f_{2j}\right) \\ f_{2k} - \dfrac{K_{2jk}}{K_{1jj} + K_{2jj}}\left(f_{1j} + f_{2j}\right) \end{Bmatrix} \quad (4.9)$$

The condensed stiffness matrix and force vector can now be used in an accretive solution identical to that posed earlier for accreting single layers of web as given in equation (3.23). After solving for the changes in deformation due to a new outer laminate the changes in stress, the total stresses and the radial modulus in each layer must be updated. To compute the changes in stress requires the recovery of the deformation associated with the internal node *j* in each condensed laminate element. That deformation can be recovered using:

$$\begin{aligned} \{\delta u_c\} &= [K_{cc}]^{-1}([K_{cr}]\{\delta u_r\} - \{r_c\}) \\ \{\delta u_j\} &= \left[K_{1jj} + K_{2jj}\right]^{-1}\left([K_{1ij} \quad K_{2jk}]\begin{Bmatrix}\delta u_i \\ \delta u_k\end{Bmatrix} - \{f_{1j} + f_{2j}\}\right) \end{aligned} \quad (4.10)$$

Now equation (3.24) can be used to determine the changes in stress in each layer of all the laminates that have been wound onto the roll. The total stresses are obtained using equation (3.26) but the winding stress in each layer of the laminate will be unique (T_{w1} or T_{w2}).

4.1.3 Strain Matched versus Non Strain Matched Laminating Conditions

Laminates are often strain matched at the site of lamination. Laminated webs that are not strain matched will curl when cut into discrete products which is often undesirable. It is not always possible to set the web tensions in the layers entering the laminator to achieve strain matching.

Nonetheless the laminate must be wound and the winding tension in the laminate layers are important input with regard to the winding residual stresses. To achieve strain matching requires the web stress in each layer to be controlled prior to lamination according to the MD modulus of that layer:

$$\varepsilon_{MD} = \frac{T_{w1}}{E_{MD1}} = \frac{T_{w2}}{E_{MD2}} \tag{4.11}$$

The web layer tensions (T_{w1} and T_{w2}) prior to lamination should be in equilibrium with the total tension T in the laminated web where A_1 and A_2 are the cross sectional areas of layers 1 and 2, respectively:

$$T = T_{w1}A_1 + T_{w2}A_2 \tag{4.12}$$

The total tension T in the laminate can vary depending on the tension zone in the web line. In the winder tension zone if the total tension is T, equations (4.13) can be used to determine the winding stress in each layer of the laminate:

$$T_{w1} = \frac{TE_{MD1}}{E_{MD1}A_1 + E_{MD2}A_2} \; and \; T_{w2} = \frac{TE_{MD2}}{E_{MD1}A_1 + E_{MD2}A_2} \tag{4.13}$$

In non-strain matched conditions the web layer tensions are set independently (T_{layer1} and T_{layer2}) upstream of the laminator. Although strain matching the layers is desirable when considering curl defects it is not always possible to transport webs upstream of the laminator at tensions that would be required to strain match the two webs. It is assumed the total web tension may differ from the exit of the laminator to the entry of the winder. If the laminate web tension at the entry to the winder is T, the winding tension for layers 1 and 2 will be:

$$T_1 = \frac{T_{layer1}}{T_{layer1} + T_{layer2}} * T \;\; and \;\; T_2 = \frac{T_{layer2}}{T_{layer1} + T_{layer2}} * T \tag{4.14}$$

4.2 Verification of the 1D Laminate Winding Model

4.2.1 Abaqus Verification

An Abaqus model can be used here to verify some results from the 1D code. The process of winding simulation in Abaqus is shown in Fig. 4.2 below:

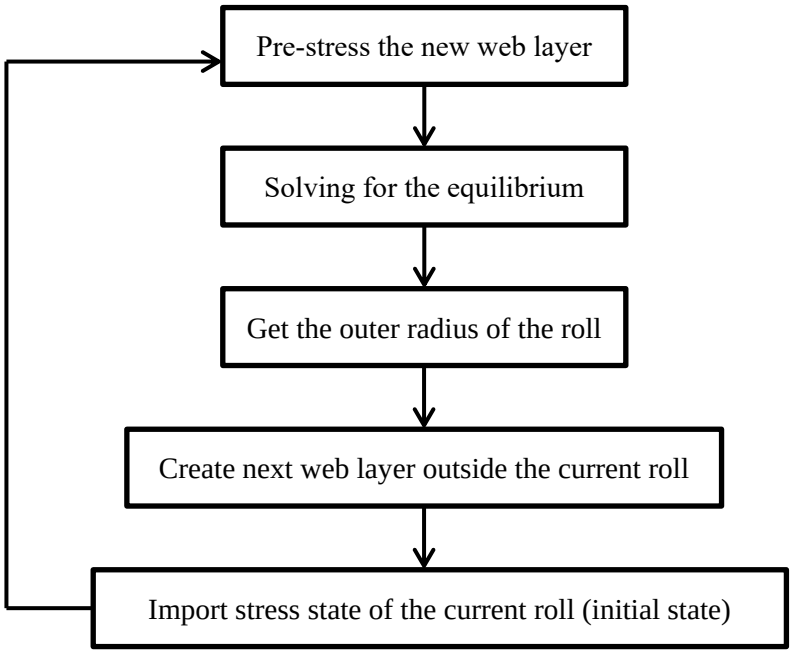

Fig. 4.2 Simulation Process of Abaqus for Laminate Winding

A homogeneous web with constant orthotropic properties is verified firstly because of its simplicity. Geometry and materials properties are in the table below:

Table 4.1 Material Properties for a Homogeneous Web

$E_{w\theta}$ (psi)	E_{wz} (psi)	E_{wr} (psi)	$\nu_{w\theta r}$	ν_{wzr}	$\nu_{wz\theta}$	E_c (psi)	ν_c
711,000	711,000	30,000	0.30	0.24	0.30	2.9E6	0.30

Table 4.2 Geometry Properties for a Homogeneous Web

R_{in} (in)	R_{out} (in)	R_{final} (in)	t(in)	W(in)	Core Layers #1.5
1.5	1.75	3.3	0.02	20	5

Note that, T (the total laminate tension) is equal to 320 lbf. A comparison of the result of the 1D model and the Abaqus simulation are show in Fig. 4.3.

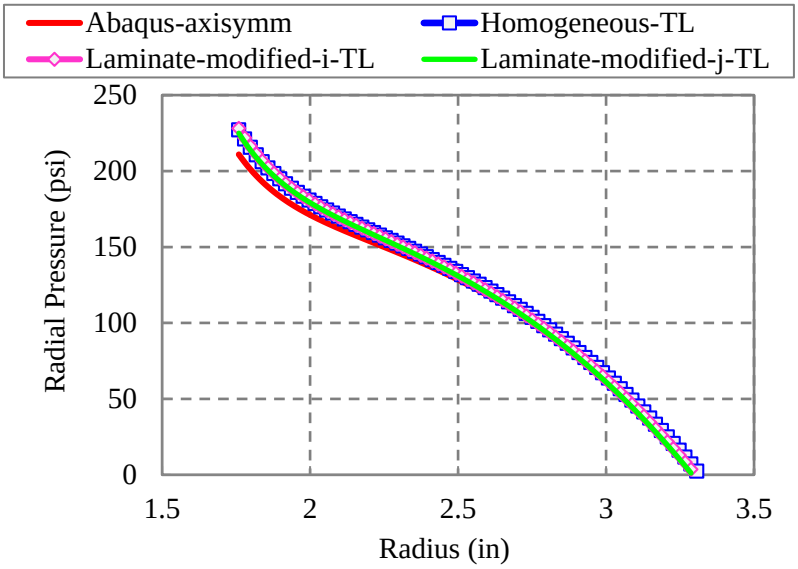

Fig. 4.3 Verification of Radial Stress for Homogenous Webs

From Fig. 4.3, the 1D Laminate Winding Model compares well for a homogenous orthotropic web with constant modulus input. Although this is not a state dependent modulus, results show that the 1D code has good accuracy. There are some minor differences in the results from the Abaqus model and the 1D code. In Abaqus model the thickness of the laminate is 0.02'', while the 1D code uses 0.01'' as the thickness of each layer of the laminate.

The next step in verifying the 1D laminate winding model was to allow the two layers of the laminate to have unique orthotropic properties. These properties are listed in Table 4.3.

Table 4.3 Material Properties for an Orthotropic Web (i and j)

Laminate i	$E_{w\theta}$	E_{wz}	E_{wr}	$\upsilon_{w\theta r}$	υ_{wzr}	$\upsilon_{wz\theta}$	t_i
	711 ksi	711 ksi	30 ksi	0.30	0.24	0.30	0.01in
Laminate j	$E_{w\theta}$	E_{wz}	E_{wr}	$\upsilon_{w\theta r}$	υ_{wzr}	$\upsilon_{wz\theta}$	t_j
	400 ksi	400 ksi	30 ksi	0.30	0.13	0.30	0.01in

Table 4.4 Geometry Properties for an Orthotropic Web

R_{in}	R_{out}	R_{final}	E_c	υ_c
1.5 in	1.75 in	3.64 in	2.9E6 psi	0.3

Note the total tension T is equal to 16 lbf. A comparison of the results from the 1D laminate model and Abaqus simulations are shown in Fig. 4.4.

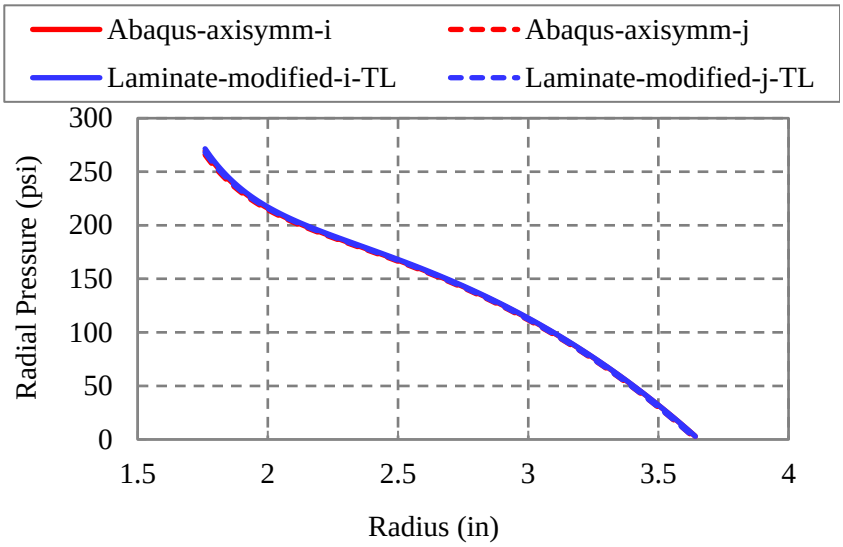

Fig. 4.4 Verification of Radial Stress for Orthotropic Webs

In Fig. 4.4, we observe that the Abaqus results and laminate winding results overlap, thus the 1D laminate Winding Model compares very well with the Abaqus model for a constant orthotropic web with constant E.

4.2.2 Lab Test Verification-Strain Matched Conditions

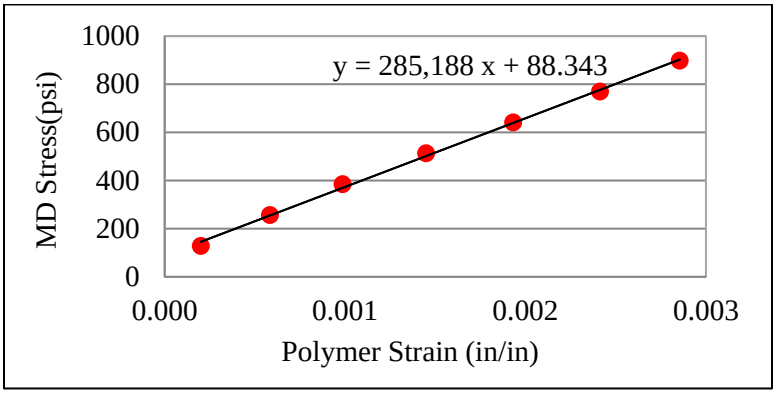

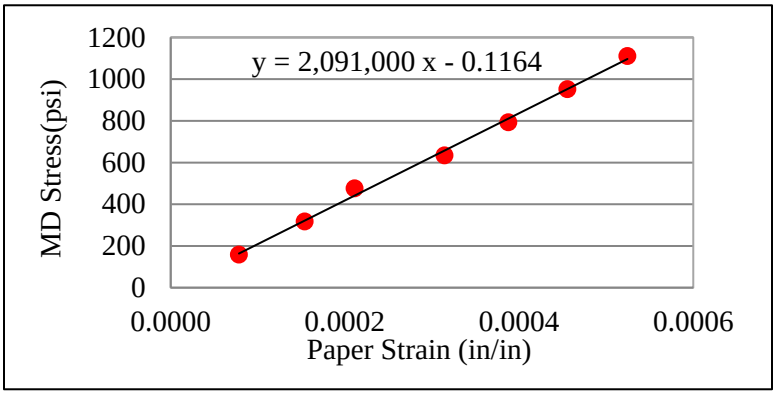

Fig. 4.5 Tangential Modulus Tests for Paper and Polymer

An existing 2-layer laminate was used to verify our model. The laminate has a paper layer and a polymer layer. The web was narrow in width (6 inches), and plane stress conditions were assumed to apply. The properties of the web materials needed to be measured, including web thickness, MD modulus, and radial modulus. The modulus was measured multiple ways in an effort to investigate the effect of the adhesive. The Poisson's ratio ($\upsilon_{\theta r}$) that couples a tangential stress to a radial strain was assumed 0.3 for both webs.

1) Web Materials Tests-E_θ: The paper thickness was measured to be 0.0021'' and the polymer thickness was found to be 0.0026''. Samples of the polymer and paper webs soft long were subjected to force/deformation testing. After collection of the data, the deformations were

converted to strains ($\Delta L/L$) and the forces were converted to stress (F/A) by dividing by the cross sectional area of the web. In Fig. 4.5, the x-axis is the dimensionless strain and the y-axis is the MD stress in the units of psi. The slope of this data is the modulus of elasticity. The MD modulus of polymer is 285 ksi and the modulus of the paper is about 2,090 ksi. Both of paper and polymer are in the elastic range from Fig. 4.5, and the tension in this thesis will satisfy the elastic range.

2) Web Material Tests-E_r: The laminated sample roll consists of two base webs (polymer and paper) and an adhesive. Individual stack compression tests on the base materials without adhesive were run. Next, layers of the base materials into a stack were interleaved to simulate a laminated stack without adhesive. Finally a stack cut from the sample roll with adhesive was subjected to compression tests.

From Pfeiffer's model, we know that:

$$P = K_1(e^{K_2\varepsilon_r} - 1) \tag{4.15}$$

$$E_r = \frac{dP}{d\varepsilon_r} = K_2(P + K_1) = K_2(K_1 - \sigma_r) \tag{4.16}$$

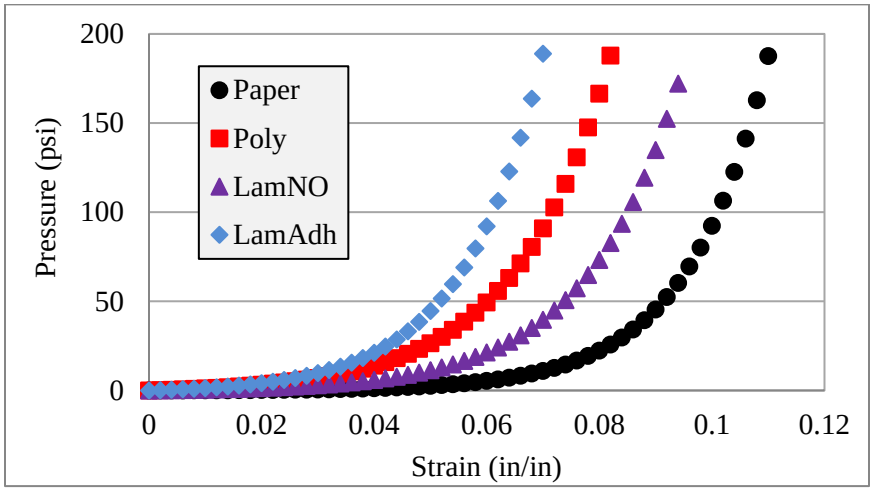

Fig. 4.6 Stack Tests for Laminate Webs

where, paper-paper layer alone, polyer-polymer layer alone, LamNO-Without adhesive and LamAdh- laminate with adhesive. The four pressures versus strain sets of data in Fig 4.6 were curve fit using expression (4.15). The K_1 and K_2 parameters were varied with the least total error resulted between the data set and the curve fit. The K_1 and K_2 parameters that resulted from this exercise are shown in Table 4.5, where we set up the pressure range is 0-150 psi for the curve fit.

Table 4.5 Pheiffers Material Constantans of the Laminate

	Paper	Polymer	No Adhesive	Adhesive
Range (psi)	150	150	150	150
K_1 (psi)	0.08	1.40	0.58	1.31
K_2	70.81	59.81	60.69	71.69

3) Winding Tests: A strain matched 2-layer laminate was used in winding tests to verify the model. The laminate is composed of a paper layer and an oriented polypropylene polymer layer. The inputs provided to the laminate winding code are shown in Table 4.6, the polypropylene is layer i and paper is layer j. All input was measured except for the Poisson ratio terms which were assumed.

Table 4.6 Input for Laminate Winding Model: Strain Matched Case

Core inner radius	0.0381m (1.5 in)
Core outer radius	0.0445m (1.75 in)
Roll final radius	0.1334m (5.25 in)
$E_{w\theta i}$, E_{wzi}	1.96 GPa (285,188 psi)
$E_{w\theta j}$, E_{wzj}	14.41 GPa (2,091,000 psi)
Web: $\nu_{\theta ri}$, ν_{zri}, $\nu_{z\theta i}$, $\nu_{\theta rj}$, ν_{zrj}, $\nu_{z\theta j}$	0.3
E_{cr}, E_{cq}, E_{cz}	206.7 GPa (30 Mpsi)
$\nu_{\theta rc}$, ν_{zrc}, $\nu_{z\theta c}$	0.3
Web width w	0.1524 m (6 in)
Thickness h_i and h_j	66.04 μm (0.0026 in), 53.34 μm (0.0021 in)
E_r (K_1, K_2)	9.03 KPa (1.31 psi),71.1
T, winding tension	32 N (7.2 lb)

Results for the strain matched case are shown in Fig. 4.7. This is a narrow web which has not achieved plane strain conditions. The model result shown in Fig. 4.7 is for the plane stress case

which was achieved by input of zero for the Poisson ratios ν_{zri}, $\nu_{z\theta i}$, ν_{zrj}, and $\nu_{z\theta j}$. When winding laminates there is a choice of which layer faces the outside of the roll. The model shows no effect whether the paper or the polypropylene is chosen for layers *i* or *j*. The winding tests were conducted with the paper facing outwards three times and then with the polypropylene facing outward three times. The test data points in Fig. 4.7 are the average of three pressure measurements taken with pull tabs and the error bars indicate the standard deviation of the data. Use of the statistical t-test indicated that the data taken with the paper facing outward could not be claimed different than the data collected when the polypropylene faced outward. The agreement between the model for plane stress conditions and the test data is good. The tangential stress results show that the paper, whose in-plane modulus was roughly 7 times larger than that of the polypropylene, bore significantly larger stress at the outside of the roll. This was expected as a result of the strain matched condition.

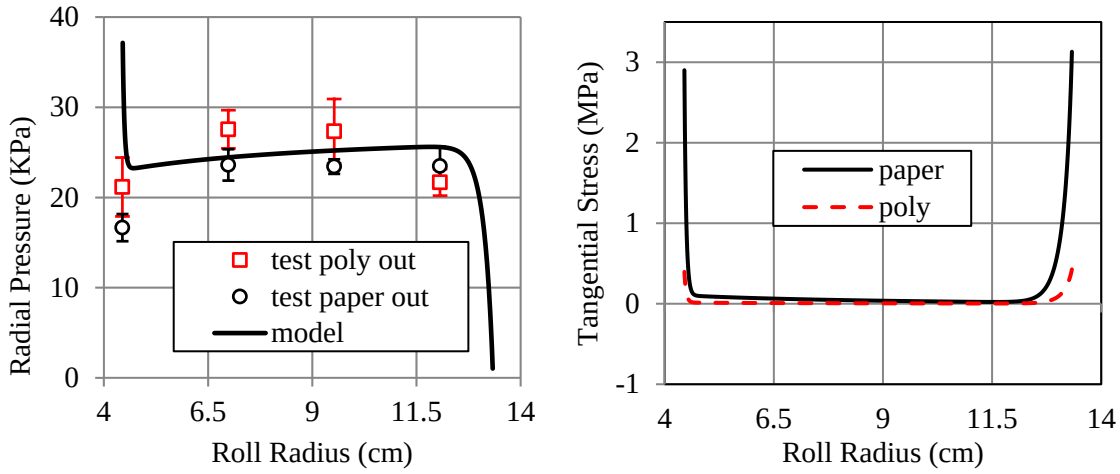

Fig. 4.7 Strain Matched Case T=2.1N/cm

As discussed earlier the laminate winding model developed shows no influence on output regarding which layer properties are input for layer i and layer j. To determine if this was a physical reality tests were conducted. We conducted 4 sets of laminate winding tests 1.2pli and 2 pli winding tensions, polymer ply out and paper ply out. Each test was repeated 5 times. All the test results are

presented in Fig. 4.8. T-test was employed here to analyze the data. In mathematic statistics, the t-test is a useful method to determine if two sets of data are significantly different from each other.

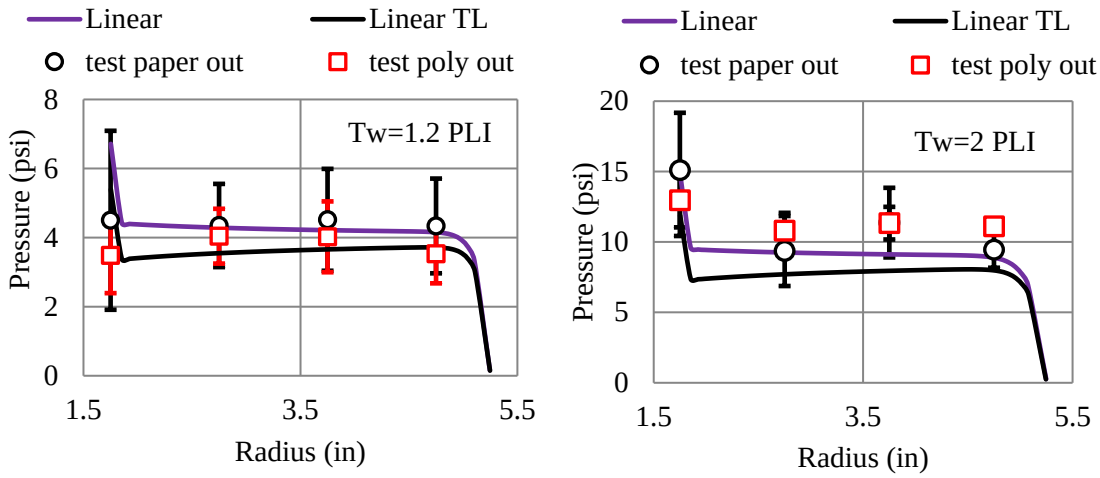

Fig. 4.8 Average of 5 Times Repeated Tests for the Laminate

We wanted to explore if the polymer or paper ply faced outward affected the roll pressure. The t-test result showed that there is no significant difference between the two situations. Thus both the model and the winding test results concur that which ply faces outward has no impact on the pressure in the wound roll. There would be an impact on tangential and axial stresses.

4.2.3 Lab Test Verification-Non Strain Matched Conditions

We desired to further verify the model on laminates where strain matching may or may not have occurred. Compared with strain-match situation, winding tension in each layer changed if the strain matching did not occur. In order to verify our model which is capable of considering the non-strain matched condition, 8 test rolls were wound. Two cases were tested in which the laminating tensions in each layer were varied.

The web tension downstream of the laminator can differ from the laminate tension in the winder tension zone. Equation (4.14) was employed to determine the tensions in the laminate layers in the winding model. Pull tabs were wound into the edge of the winding roll as shown in Fig. 4.9.

Fig. 4.9 Machine Set Up for Laminate Web Winding Tests

Table 4.7 Input for Laminate Winding Model: Non-Strain Matched Case

Core inner radius	0.089 m (3.5 in)	
Core outer radius	0.105 m (4.15 in)	
Roll final radius	0.2517 m (9.91 in)	
$E_{w\theta i}$, E_{wzi}	6.12 GPa (887,600 psi)	
$E_{w\theta j}$, E_{wzj}	2.07 GPa (300,000 psi)	
Web: $\nu_{\theta ri}$, ν_{zri}, $\nu_{z\theta i}$, $\nu_{\theta rj}$, ν_{zrj}, $\nu_{z\theta j}$	0.3	
E_{cr}, E_{cq}, E_{cz}	68.9 GPa (10 Mpsi)	
$\nu_{\theta rc}$, ν_{zrc}, $\nu_{z\theta c}$	0.3	
Web width w	0.6858 m (27 in)	
Thickness h_i and h_j	55.88 μm (0.0022 in), 66.04 μm (0.0026 in)	
E_r (K_1, K_2)	1.01 KPa (0.146 psi),117.1	
	Case A	Case B
Laminating Tension i	302.5 N (68 lb)	355.9 N (80 lb)
Laminating Tension j	89.0 N (20 lb)	44.5 N (10 lb)
T, winding tension	95.6 N (21.5 lb)	

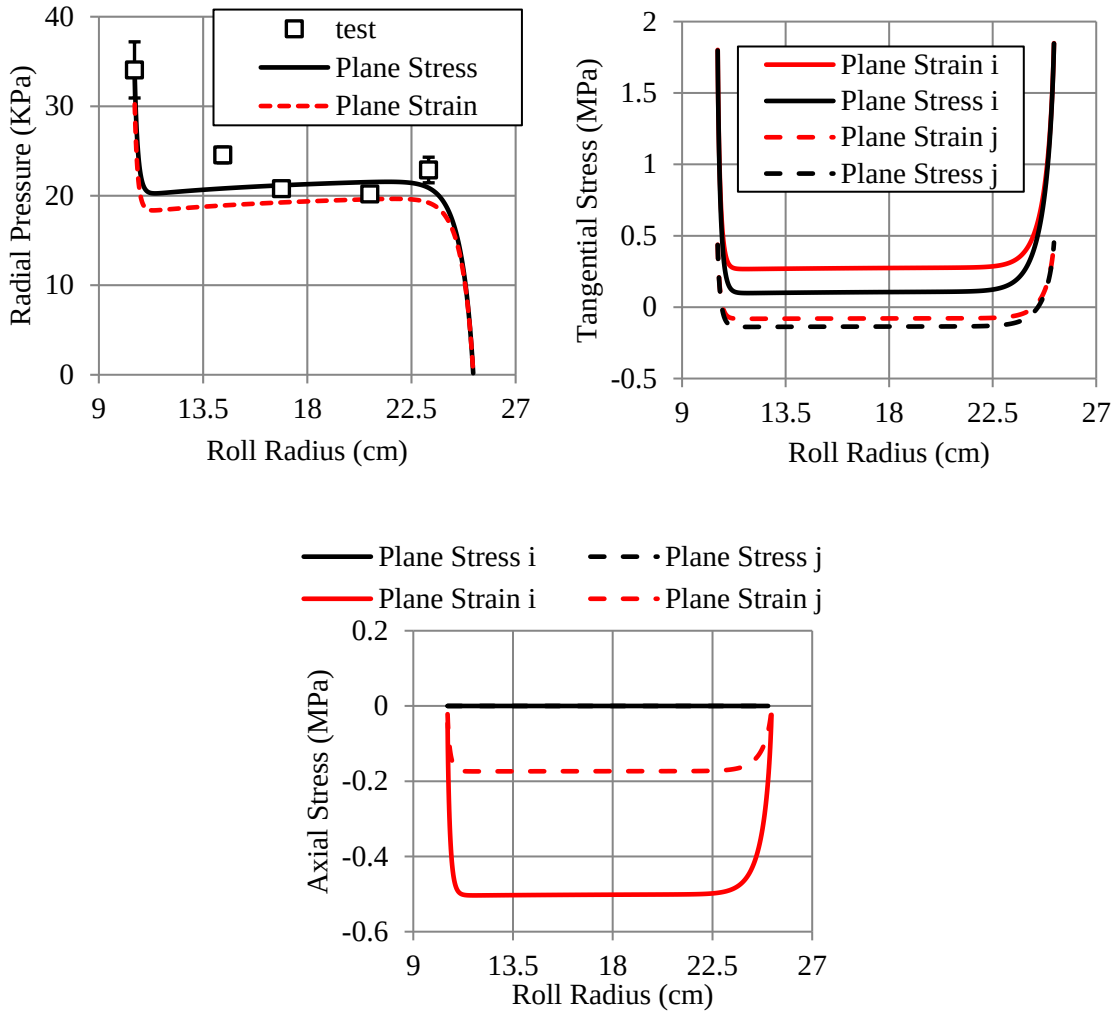

Fig. 4.10 Model and Test Results: Non-Strain Matched Case A

Results are shown in Fig. 4.10 for both plane stress and plane strain material behaviors. The winding tests were conducted 3 times and the pressure test data in Fig. 4.10 represent the average of the pressure measurements at each radial location. The height of the error bars represents the standard deviation of the data. The test pressures agree best with the plane stress case but the plane strain results agree reasonably well too. Tangential and axial stresses throughout the roll are shown as well for both material behaviors.

Results are also shown in Fig. 4.11 for a Case B where the web tensions at the laminator were set markedly different from Case A but the tension in the laminated web at the winder was the same.

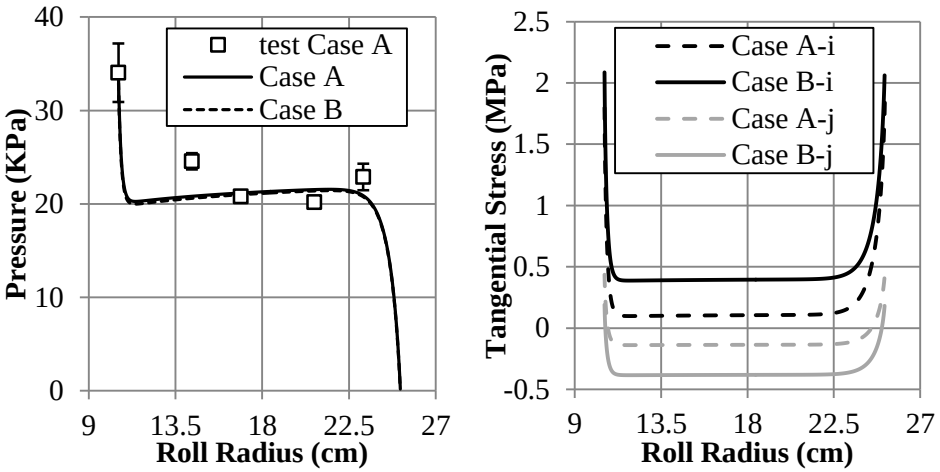

Fig. 4.11 Effects of Lamination Tension, Non-Strain Matched Cases

Note the model shows no difference in pressure for Cases A and B. This indicates pressure is being affected by total winding tension and not the laminating tensions. The tangential stresses are affected by the lamination tensions and although not shown here by winding tension too.

4.3 Influence of Bending Stress

The elastic bending strains and stresses exist at some level in single layer and laminate webs wound into rolls. Bending effects were not considered in the early winding models discussed in chapter 2. These winding models were developed to consider only the membrane stresses in the web and the pressure throughout the radius range of a wound roll.In the development of the bending stresses the distance from the reference axis (y_0, z_0) to the centroid axis (y, z) of the laminate z_0^* is needed:

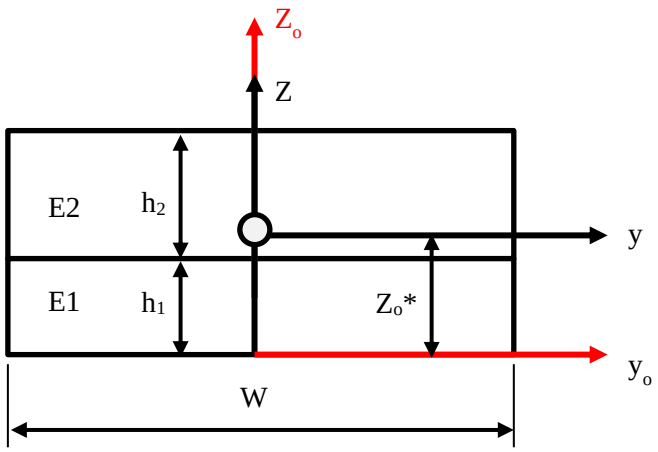

Fig. 4.12 Cross Section of Laminate

The distance to the centroid axis is determined by the equation:

$$z_0^* = \frac{\frac{h_1^2}{2} + \frac{E_2}{E_1} h_2 (h_1 + \frac{h_2}{2})}{(h_1 + \frac{E_2}{E_1} h_2)} = \frac{E_1 h_1^2 + E_2 h_2 (2h_1 + h_2)}{2(E_1 h_1 + E_2 h_2)} \tag{4.17}$$

Where E_1, E_2, h_1, h_2 are the Young's modulus and thickness of layer 1 and layer 2,respectively.

The strain must be continuous and linear in the thickness direction, which means that the stress changes abruptly at the contact surface. The general equation for the stress in a non-homogeneous beam with axial and bending loads and a temperature change [29].

$$\sigma_{xx} = \frac{E}{E_1} [\frac{P^*}{A^*} - \frac{M_z^* I_{yy}^* - M_y^* I_{yz}^*}{I_{yy}^* I_{zz}^* - (I_{yz}^*)^2} y - \frac{M_y^* I_{zz}^* - M_z^* I_{yz}^*}{I_{yy}^* I_{zz}^* - (I_{yz}^*)^2} z - E_1 \alpha T] \tag{4.18}$$

Where, A^* is the modulus weighted area and can be shown as:

$$A^* = \sum_{i=1}^{n} A_i^*, \quad A_i^* = \frac{E_i}{E_1} A_i \tag{4.19}$$

For the laminate web winding process, there is no temperature change and there is no initial curve in the web. We only need to consider the bending effect on the machine direction. The stress through the thickness as a function of z location is:

$$\sigma_{xx} = \frac{E}{E_1}\left(\frac{P}{A^*} - \frac{M_y z}{I_{yy}^*}\right) \tag{4.20}$$

Where, P is the axial or MD loads, E is the young's modulus of each layer. We usually choose the young's modulus of the bottom layer as E_1.

$I_{y_0 y_0}^*$ is the modulus weighted area moment of inertial about the reference axis.

$$I_{y_0 y_0}^* = \frac{E_1}{E_1}\left[\frac{w h_1^3}{12} + \left(\frac{h_1}{2}\right)^2 w h_1\right] + \frac{E_2}{E_1}\left[\frac{w h_2^3}{12} + \left(h_1 + \frac{h_2}{2}\right)^2 w h_2\right] \tag{4.21}$$

I_{yy}^* is the modulus weighted area moment of inertial about the centroid axis:

$$I_{yy}^* = I_{y_0 y_0}^* - (\bar{z}_0^*)^2 A^* \tag{4.22}$$

The bending moment and stiffness will be related to the radius of the winding roll r:

$$\frac{1}{r} = \frac{M_y}{E I_{yy}^*} \qquad M_y^* = \frac{E_1 I_{yy}^*}{r} \tag{4.23}$$

The final stress in each layer of laminate can now be developed:

$$\sigma_{xx} = \frac{E}{E_1}\left(\frac{P^*}{A^*} - \frac{M_y^* z}{I_{yy}^*}\right) = \frac{E}{E_1}\left(\frac{P^*}{A^*} - \frac{E_1 z}{r}\right) \tag{4.24}$$

Similar to the homogenous beam, the stress is the function of the z direction, but z is relative to the centroidal axis. We can integrate this stress though the thickness to find the average axial stress in each layer of laminate. The average axial stress in each layer becomes the input to the force vector we use in our finite element winding model:

$$T_{w1} = \frac{P}{A^*} - \frac{w\int_{-z_0^*}^{-z_0^*+h_1} \frac{E_1 z}{r} dz}{w^* h_1} = \frac{P}{A^*} - \frac{E_1}{2rh_1}[(-z_0^* + h_1)^2 - z_0^{*2}] \tag{4.25}$$

$$T_{w2} = \frac{E_2}{E_1}\frac{P}{A^*} - \frac{w\int_{-z_0^*+h_1}^{-z_0^*+h_1+h_2} \frac{E_2 z}{r} dz}{w^* h_2} = \frac{E_2}{E_1}\frac{P}{A^*} - \frac{E_2}{2rh_1}[(-z_0^* + h_1 + h_2)^2 + (-z_0^* + h_1)^2] \tag{4.26}$$

We see that T_{w1} and T_{w2} are now influenced by the radius r at which the layer was wound onto the roll. We incorporated this expression into a new version of the laminate winding model in order to explore the difference with the model which did not consider the bending stress in each layer.

The model input was for strained match condition to compare the difference (Table 4.6). The paper ply will face out in this example.

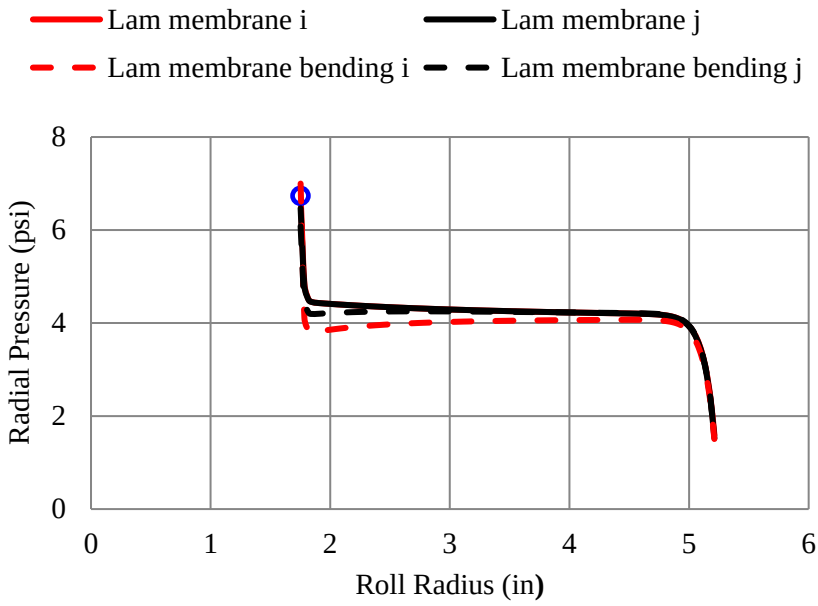

Fig. 4.13 Radial Pressure Including the Bending Effect

The pressures are nearly identical. Thus the bending stresses have little influence on roll pressures. The tangential stress should change significantly due to existence of the bending stress in each layer.

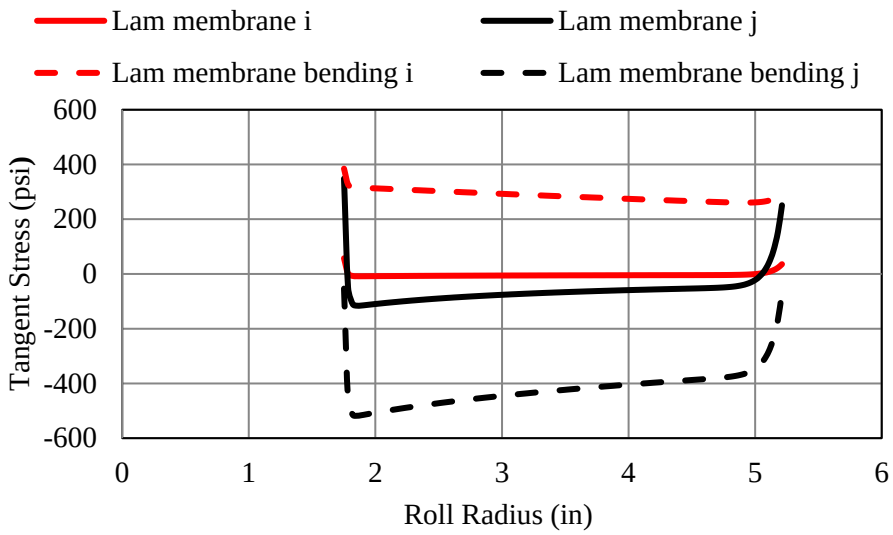

Fig. 4.14 Tangential Stress Including the Bending Effect

These bending effects cannot be neglected in the investigation of web curl, which is dependent on accurate representation of the tangential stains and stresses and their impact on creep and curl.

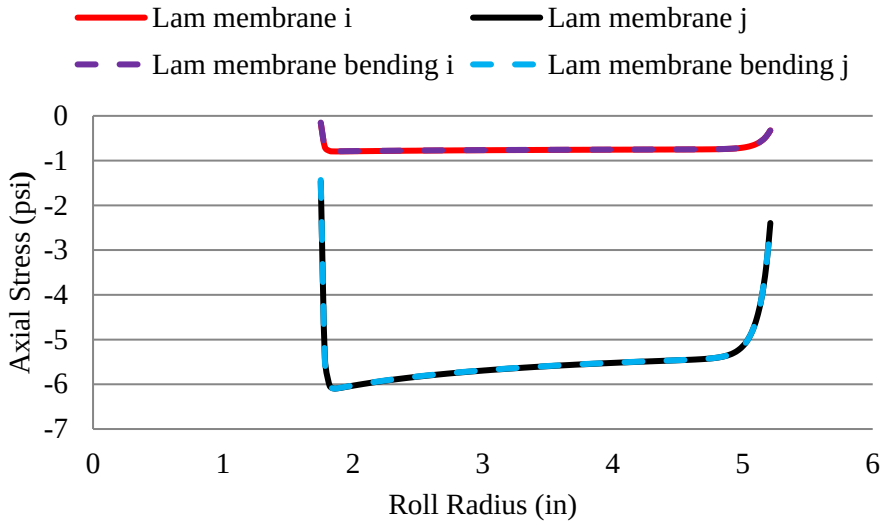

Fig. 4.15 Axial Stress Including the Bending Effect

The axial stresses are almost unaffected by bending. Laminated webs can be formed from 2 to n webs depending on product needs. The stiffness matrix presented in (4.2) and force vector in (4.4)

will become more complex as the number of layer increases. Also unique to multiple-layer laminates is the allocation of tension of each layer. In the laminate winding, the winding tension cannot be input directly in units of stress, the laminate plies may hang the same strain level. If strain matched at the laminator, the winding tension will now have the units of force. Assuming strain matching at the laminator;

$$\varepsilon_{MD} = \frac{T_{w1}}{E_1} = \frac{T_{w2}}{E_2} = \cdots = \frac{T_{wn}}{E_n} = \frac{T}{\sum_{i=1}^{n} E_i A_i} \tag{4.27}$$

From equilibrium:

$$T = T_{w1}A_1 + T_{w2}A_2 + \cdots + T_{wn}A_{1n} \tag{4.28}$$

where T is the total winding tension and the T_{wi} are the stresses induced in each ply due to T.

The tension for j[th] layer of n-layer laminate is:

$$T_{wj} = \frac{TE_j}{\sum_{i=1}^{n} E_i A_i} \tag{4.29}$$

4.4 An Equivalent Single-Layer Laminate Model

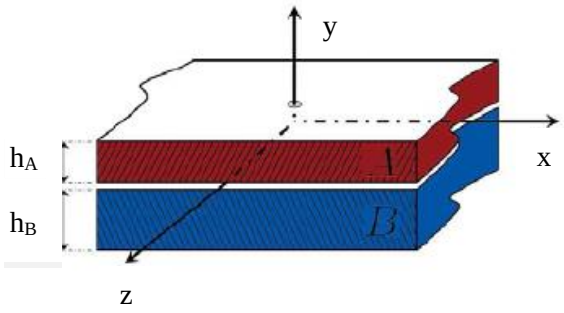

Fig. 4.16 Equivalent Modulus of Laminate

The previous laminate winding models developed in this chapter were finite element formulations that treat each layer of the laminate as a finite element. The multiple layers and the properties of those layers can be treated as an equivalent single layer web. This offers the advantage of using our previous winding models directly for laminate. It is possible that a similar development would be feasible for laminate viscoelastic winding models. For elastic winding the winding model would accrete a single layer whose thickness is $h_A + h_b$ for a 2 ply laminate. Then an equivalent MD modulus is calculated to represent the entire layer in the x (MD) and y (CMD) directions:

$$E_{cx} = \frac{E_A h_A + E_B h_B}{h_A + h_B} \tag{4.30}$$

$$E_{cy} = \frac{E_A E_b (h_A + h_B)}{E_A h_A + E_b h_B} \tag{4.31}$$

where, E is the Young's modulus and h is the thickness. Since the radial modulus is state dependent, it has to be determined by performing a compression test on a stack of laminates and fitting Pfeiffer's curve to the pressure strain data. This ensures that coefficients account for the dissimilar web surfaces in contact and the effects of the adhesive.

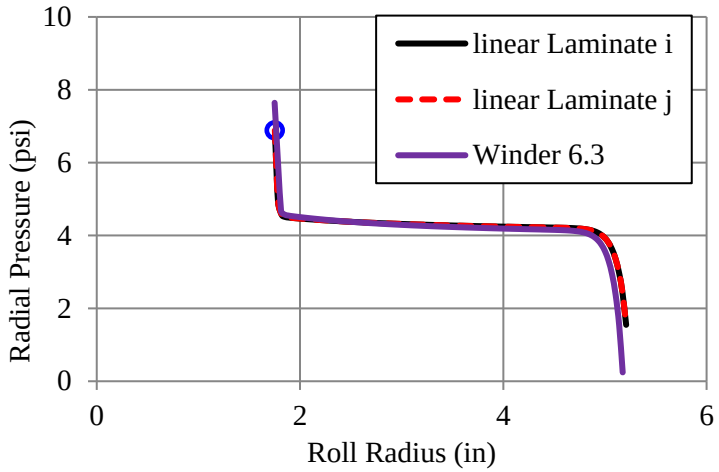

Fig. 4.17 Elastic Strain Matched Verification for Radial Pressure

To demonstrate how well this approach can work an equivalent layer was developed for the strain matched 2-layer case where the input was presented in Table 4.6. The winding tension was set at 1.2pli, equivalent to the case 1 and 3. The pressure results are shown in Fig. 4.17. The equivalent layer properties were input to a single layer winding code (Winder 6.3). Note that the agreement between Winder 6.3 and 1D finite element laminate winding model is quite good. A non- strain matched case was also investigated using the input data in Table 4.7. Pressure is shown for a winding tension of 21.5 pounds in Fig. 4.18. Again good agreement is witnessed.

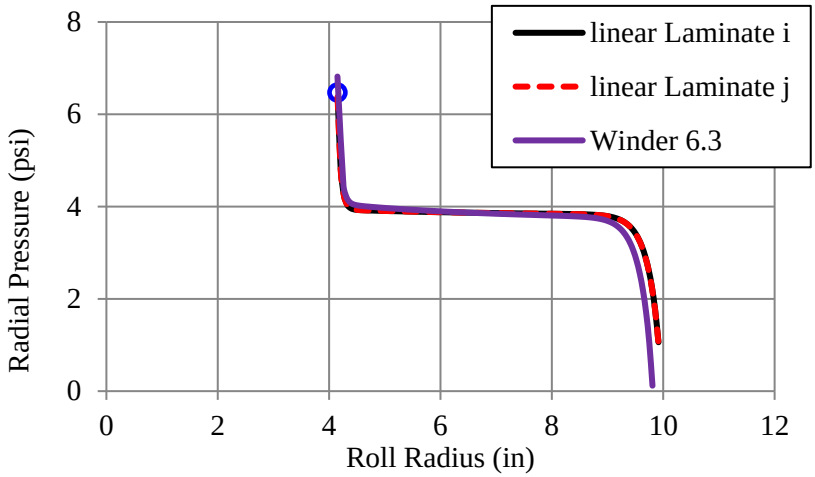

Fig. 4.18 Elastic Part-Strain not Match Verification for Radial Pressure

4.5 Elastic Curl for Laminate

Laminates are often strain matched at the site of lamination. Laminated webs that are not strain matched will curl when cut into discrete products which is often undesirable. It is not always possible to set the web tensions in the layers entering the laminator to achieve strain matching. In pure bending of beam, the relationship between bending moment M and the radius of curvature is in equation (4.32):

$$M = \frac{EI}{\rho} \rightarrow \rho = \frac{EI}{M} \tag{4.32}$$

Due to strain mismatch, lamination winding tension T_1 and T_2 will form a moment to the neutral axis. The procedure to estimate the radius of curvature of strain mismatch condition is:

(1) Determine the neutral axis of laminate web.

(2) Calculate the total moment.

(3) Use equation (4.32) to predict the radius of curl.

In chapter 2, we talked about Kidane's 2D model to predict the laminate curl. Non-equal strain in different layers of the laminate, lead to curl. Kidane, in his paper [26], discussed the prediction of MD and CD curl by using laminate theory. MD and CD strain for the i[th]layer was given as follows:

$$\varepsilon_i^{MD} = \frac{T_i}{E_i t_i} \quad \varepsilon_i^{CD} = -\upsilon_i \varepsilon_i^{MD} \tag{4.33}$$

where ε_i^{MD} and ε_i^{CD} are machine direction strain and cross machine direction strain of the i[th] layer of web. T_i is given in fore per unit length,

When the strains are calculated through the equations above, the modified load can be substituted into the traditional laminate theory equations.

$$\begin{Bmatrix} N_x^T \\ N_y^T \\ N_{xy0}^T \end{Bmatrix} = \Delta T \sum_{k=1}^{n} \begin{bmatrix} Q_{11} & Q_{12} & 0 \\ Q_{12} & Q_{11} & 0 \\ 0 & 0 & Q_{11} \end{bmatrix} \begin{Bmatrix} \alpha_L \\ \alpha_T \\ 0 \end{Bmatrix} (h_k - h_{k-1}) \tag{4.34}$$

$$\begin{Bmatrix} M_x^T \\ M_y^T \\ M_{xy}^T \end{Bmatrix} = \frac{1}{2} \Delta T \sum_{k=1}^{n} \begin{bmatrix} Q_{11} & Q_{12} & 0 \\ Q_{12} & Q_{11} & 0 \\ 0 & 0 & Q_{11} \end{bmatrix} \begin{Bmatrix} \alpha_L \\ \alpha_T \\ 0 \end{Bmatrix} \left(h_k^2 - h_{k-1}^2\right) \tag{4.35}$$

where N and M are the equivalent forces and moments due to temperature difference ΔT. Q is the stiffness matrix element and α is the coefficient of thermal expansion.

Kidane's 2d curl prediction model is applicable for estimating curl in both MD and CMD directions for a number of web processes, including lamination. During the laminating process, the strains of different layers should theoretically be the same to prevent MD curl for all tensions in the laminate (perfect bonding condition). However, in reality the problem is more complicated due to the existence of strain matching loss, which means that the strain will not the same, and thus laminate winding will want to curl when unwound. By using these equations above combined with laminate elastic and viscoelastic winding model developments, curl can be predicted. If the layers in a laminate have different Poisson ratios, CMD curl can be expected at laminate web tensions other than the combined tensions in the two webs at the laminator. After a discrete product is cut from a web there will be no tension and some CMD curl may result.

CHAPTER V

VISCOELASTIC CHARACTERIZATION OF WEB MATERIALS

Some web curl defects are the combined result of the total membrane bending stresses and viscoelastic creep. Before discussing the curl analysis, it is necessary to characterize viscoelastic properties correctly and quickly. This chapter focuses on the viscoelastic characterization of the web.

5.1 Viscoelastic Models and Methods

5.1.1 Wiechert Model

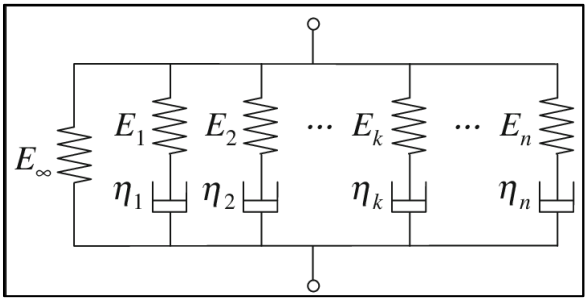

Fig. 5.1 Generalized Maxwell Model (Wiechert Model)

The Wiechert model (General Maxwell Model) in Fig. 5.1 is widely used in viscoelastic analysis. One term Wiechert model (Standard Linear Solid Model) is in Fig. 5.2.

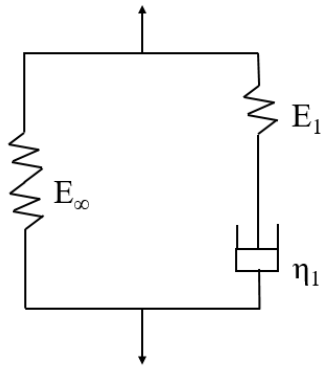

Fig. 5.2 Standard Linear Solid Model (One Term Wiechert Model)

The constitutive equation of the model is:

$$\sigma + p_1\dot{\sigma} = q_0\varepsilon + q_1\dot{\varepsilon} \tag{5.1}$$

The p and q terms in equation (5.1) are related to the elastic constants (E_∞,E_1) and the viscosity term (η_1) in the standard linear solid model.

$$p_1 = \frac{\eta_1}{E_1}, \quad q_0 = E_\infty, \quad q_1 = \frac{E_\infty + E_1}{E_1}\eta_1 \tag{5.3}$$

Using the Laplace Transform to convert the constitutive equation (5.1):

$$\bar{\sigma} + p_1 s\bar{\sigma} = q_0\bar{\varepsilon} + q_1 s\bar{\varepsilon} \tag{5.4}$$

If we consider the application of a step strain $\varepsilon(t) = \varepsilon_0 H(t)$ to the model, and corresponds to the relaxation response of the materials the resulting stress in the s domain is:

$$\bar{\sigma}(s) = \frac{\varepsilon_0}{s}\left(\frac{q_0 + q_1 s}{1 + p_1 s}\right) \tag{5.5}$$

The creep response can be written as:

$$\sigma(t) = E(t)\varepsilon_0 \tag{5.6}$$

and the inverse of the Laplace Transform of equation (5.5), produces the relaxation function:

$$E(t) = E_\infty + E_1 exp\left({-t}/{(\eta_1/E_1)}\right) \tag{5.7}$$

If an elastic element in parellel with n Maxwell elements, the relaxation function can be expressed as an n-term Prony series:

$$E(t) = E_\infty + \sum_{i=1}^{n} E_i e^{\left(-\frac{t}{\lambda_i}\right)} \tag{5.8}$$

where, E_∞ is the equilibrium modulus, E_i are relaxation modulus and λ_i ($\lambda_i = \eta_i/E_i$) are relaxation times . The Wiechert model (5.8) will be used to compare different viscoelastic characterization methods at the end of this chapter.

5.1.2 Merchant Model

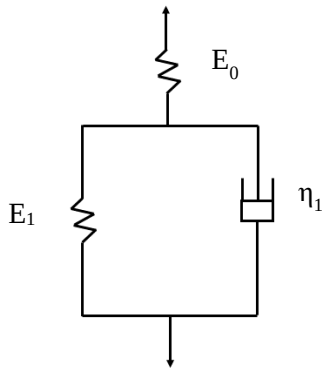

Fig. 5.3 One Dimensional Merchant Model with One Kelvin Element

An elastic spring, in series with a Kelvin element, is called the Merchant model. The constitutive equation of the Merchant model is (5.1). The p and q terms in equation (5.1) are related to the elastic constants (E_0,E_1) and the viscosity term (η_1) in the Merchant model.

$$p_1 = \frac{\eta_1}{E_0 + E_1}, \quad q_0 = \frac{E_0 E_1}{E_0 + E_1}, \quad q_1 = \frac{E_0 \eta_1}{E_0 + E_1} \tag{5.9}$$

Using the Laplace Transform to convert the constitutive equation into (5.4).

If we consider the application of a step stress $\sigma(t) = \sigma_0 H(t)$ to the model, and corresponds to the creep response of the materials the resulting strain in the s domain is:

$$\bar{\varepsilon}(s) = \frac{\sigma_0}{s}\left(\frac{1 + p_1 s}{q_0 + q_1 s}\right) \tag{5.10}$$

The creep response can be written as:

$$\varepsilon(t) = J(t)\sigma_0 \tag{5.11}$$

and the inverse of the Laplace Transform of equation (5.10), produces the creep function:

$$J(t) = \frac{1}{E_0} + \frac{1}{E_1}\left(1 - exp\left({}^{-t}/_{(\eta_1/E_1)}\right)\right) \tag{5.12}$$

If an elastic element in series with n Kelvin elements, the creep function can be expressed as an n-term Prony series:

$$J(t) = J_0 + \sum_{i=1}^{n} J_i \left(1 - \exp\left({}^{-t}/_{\tau_i}\right)\right) \tag{5.13}$$

where, $J_0 = 1/E_0$ is the inverse of instantaneous elastic modulus, J_i are the creep compliances and $\tau_i = \eta_i/E_i$ are the retardation times. Compared with Burger's model (a Maxwell element in series with Kelvin elements), the equilibrium modulus (when time t is infinity) is not zero, which is necessary for solid materials. In this thesis, the Merchant model is used for creep function expression unless stated otherwise.

5.1.3 Time-Temperature Superposition Method

When viscoelastic data measured at a temperature different from the reference temperature is plotted as a function of frequency or time in double logarithmic scale, the horizontal and vertical shifts of the data to those at the reference temperature give a single superposed curve called the master curve. This superposition of viscoelastic data is called the principle of time-temperature superposition (TTS) [39]. The superposition principle is based upon the premise that the processes involved in molecular relaxation or rearrangements occur at greater rates at higher temperatures.

A master curve of the modulus at a chosen reference temperature corresponds to a curve of the values of the modulus for the full range of frequencies developed from the modulus values measured at a various temperatures based on the shift factor. The purpose of determining shift factors is to build a smooth master curve that allows the modulus to be estimated for various temperature and time. Master curves are made to fit by shifting curves along the time axis. We estimated the horizontal shift factor from the log time chart.

The storage modulus E' data acquired at 20°C and 30°C (Fig. 5.4) will be used as an example to discuss the determination of the shift factor. At 20°C, when the frequency is 0.292 Hz the modulus E' is 235MPa, which is similar to the value when f is 6.309 Hz at 30°C. Equation (5.9) will be used to express the superposition process:

$$E'(\omega, T) = E'_{T_0}(\omega_r, T_0) = E'_{T_0}(\omega a_T, T_0) \tag{5.14}$$

Where $E'(\omega, T)$ is the storage modulus at temperature T and angular frequency ω, and $E'_{T_0}(\omega a_T)$ is the storage modulus at reference temperature T_0transferred from temperature T, due to the shift of a_T from x. In Fig. 5.5, shift factor $a_T = Log(\omega_r/\omega) = Log(0.292/6.309) = -1.4$.

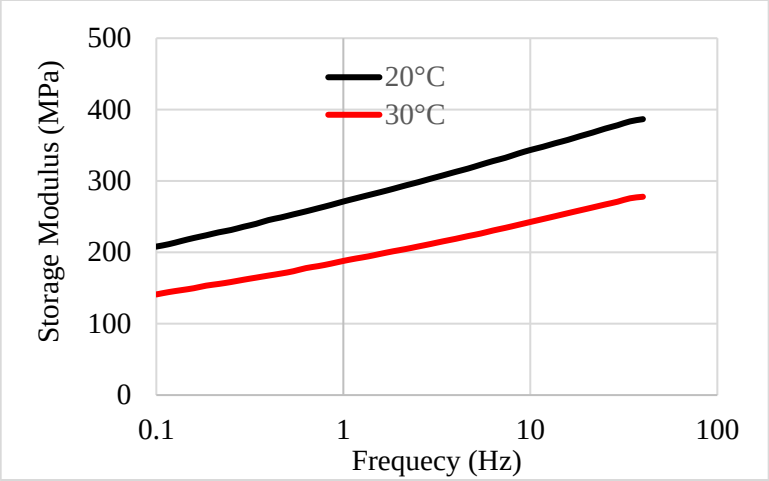

Fig. 5.4 Storage Modulus at Temperature 20°C and 30°C

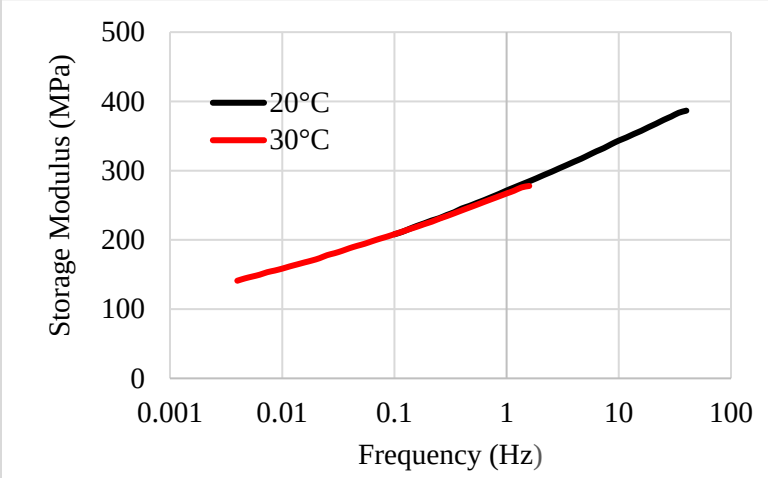

Fig. 5.5 Storage Modulus at Reference Temperature 20°C

5.2 Viscoelastic Characterization

At the beginning we used a Differential Scanning Calorimeter (DSC) instrument to determine the glass transition and melting temperatures. From the DSC test, we did not see obvious glass transition effect or melting effect between -40°C to 90°C. This determined the range of temperature for all the tests in this section.

5.2.1 Ordinary Lab Creep Test

Before conducting the creep test, the Instron machine was used to conduct the elastic tensile test for the LDPE. Samples were cut into strips one inch wide and at least 12 inches in length (10 inches for the test). For these tests, a strain rate of 1in/in/min was prescribed. All tests were conducted at ambient temperature of approximately 70°F. The average LDPE modulus from 2 tests is 22,200psi from data in Fig. 5.6.

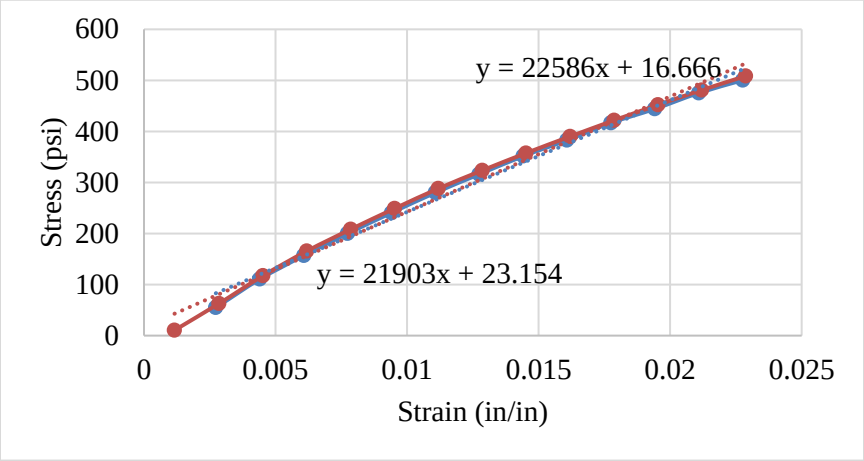

Fig. 5.6 Instron Test Results of LDPE

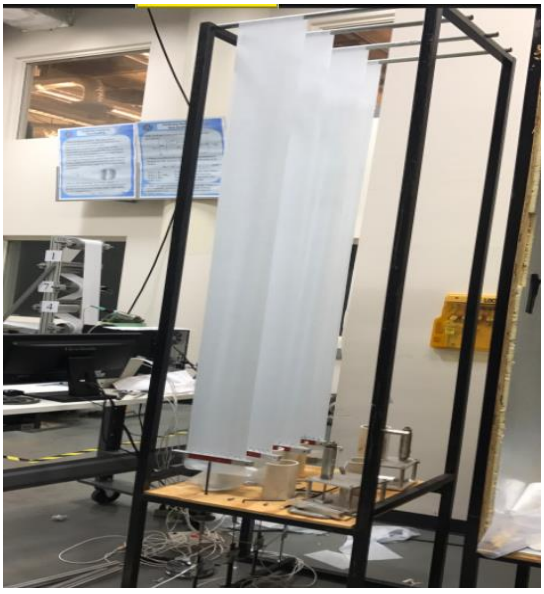

Fig. 5.7 WHRC Lab Creep Test Set Up

When a constant stress is applied to a viscoelastic specimen, the strain increases with time, a phenomenon called creep. An experimental setup to measure creep is shown in Fig.5.7. Displacements are measured via the digital sensors, and thus continuous data acquisition is available. For these experiments, 4 inches wide strips of 0.02inch thickness LDPE specimen approximately 90 inches in length were prepared. The cross-section area of LDPE is about $A_e = 2 * (4^{"})(.02^{"})$. These creep tests were conducted at 15, 25, 35 lbs. (tensile stresses of 93.75, 156.25, 218.75 psi) at 70°F for a period of 7 days. There are dynamic effects when the dead weights are placed and thus we have to subtract the initial data. Test procedures are as follows:

(1) The intent is to subject the 3 web samples to different loads (15, 25,35lbs) and hence stresses at the same time.

(2) The loads are applied with dead weights which rest on stands until we are ready to begin the test.

(3) The stands are retracted and the webs now support the dead weights. Displacement transducers capture the displacement of each web sample due to the unique stress applied.

(4) The displacements are recorded through time and are used to calculate the strains values according to time, then building the creep curve.

(5) The Excel solver routine (GRG nonlinear method) is used to determine the J and τ coefficients in equation (5.13) which best fit the test creep data through time. The creep function is then known.

Fig. 5.8 displays the test data from the displacement sensors after removing the beginning dynamic effects.

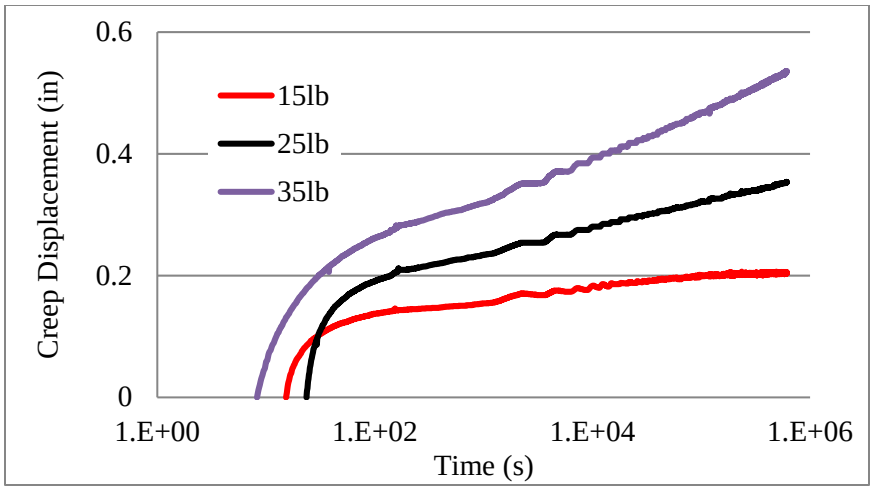

Fig. 5.8 Increase of Creep Displacement with Time

If the displacement is divided by the length of specimen and the stress, the difference among different load is small in Fig. 5.9. This means that the LDPE can be considered as linear viscoelastic material.

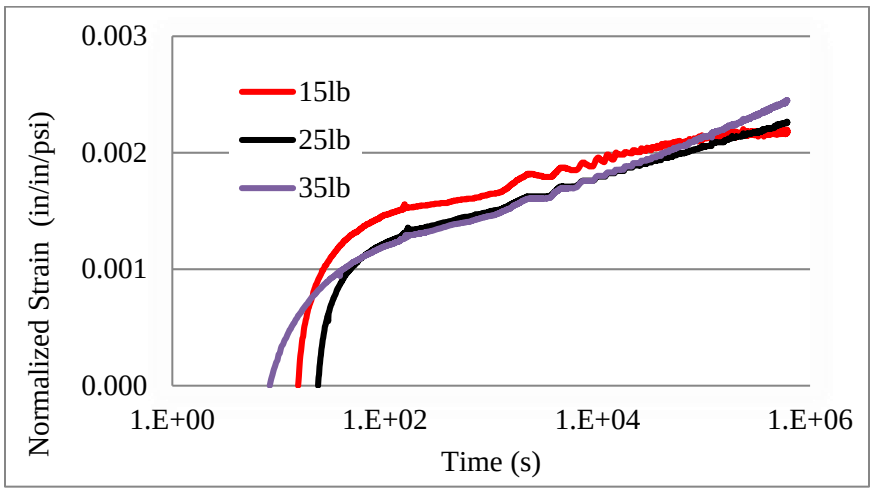

Fig. 5.9 Normalized Strain with Time

A Merchant model was fitted to the normalized creep experiment data. Creep function is expressed as equation (5.13).We used the Solver in Excel to calculate the coefficients for the creep function

that best fit the test data. It was found that 3 Prony terms were sufficient. The 3 terms Prony series for the LDPE creep function from 7 days of testing is shown in Table 5.1:

Table 5.1 3 Terms Creep Function for LDPE at 70°F

J_0(1/psi)	J_1(1/psi)	τ_1(s)	J_2(1/psi)	τ_2(s)	J_3(1/psi)	τ_3(s)
1/22,200	1.467e-05	13	5.376e-06	1445	7.913e-06	100,512

The creep terms and retardation times are determined automatically using solver. In some case, the retardation times had to be estimated manually firstly to provide a good starting point. Creep function from Table 5.1 compares well with test data in Fig. 5.10.

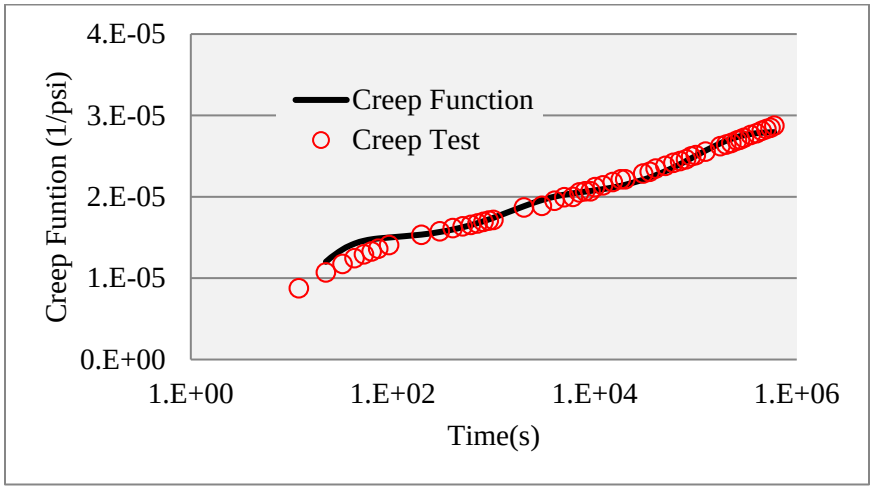

Fig. 5.10 Measured Creep Function for LDPE at 35lbs

Similar creep test was conducted at an elevated temperature 110°F in Table 5.2.

Table 5.2 4 Terms Creep Function for LDPE at 110°F

J_0(1/psi)	J_1(1/psi)	τ_1(s)	J_2(1/psi)	τ_2(s)	J_3(1/psi)	τ_3(s)	J_4(1/psi)	τ_4(s)
1/22,200	1.40e-05	1E03	1.19E-05	1E04	1.87E-05	1E05	1.32E-05	1E06

5.2.2 Creep Master Curve

The principle of time-temperature superposition extends the range of frequencies (DMA) or times (creep, relaxation) of viscoelastic properties. The master curve may be used to predict material behavior that has not been actually measured. A constant stress is applied to the specimen very quickly (about 0.2s) and then the strain is measured through time. Results from various temperatures are utilized to build the master curve to analyze the creep property of the web materials over long time periods. In this case we will use the RSA G2 TA Instruments machine to measure creep data through time at various test temperatures. We estimated the horizontal shift factor from the log time chart, and then adjusted it in an effort to obtain a smooth curve. A standard creep curve usually exhibit three regions, primary creep, secondary creep and tertiary creep. Secondary creep region is a linear part which should be used to build the master curve. Superposition and shifting is generally limited to the steady-state regime of the creep phenomenon. The dimension of specimen is length 1.6in*width 0.2in*thickness 0.0211in. Detailed procedure is as follows:

1 Stress Control (PID) TA machines does this automatically.

2 Axial Stress Set Up. Specimen is prevented from buckling with temperature changes and the stress cannot be too large. This procedure is not necessary if we preheat the specimen in the chamber before the test.

3 Step Creep (Temperature, Duration, Stress, and Data Acquisition): The test duration should be sufficient to determine the shift factor for different temperatures. 1Mpa is applied for all tests.

4 Temperature Set Up for the Next Specimen: Duration of each temperature is 10mins (600s) in this test. The temperature we chose: 23, 27.5, 30, 32.5, 35, 37.5, 40, 43, 45, 47.5, 50, 52.5, 55 °C.

Fig. 5.11 Blade Holder for the Specimen

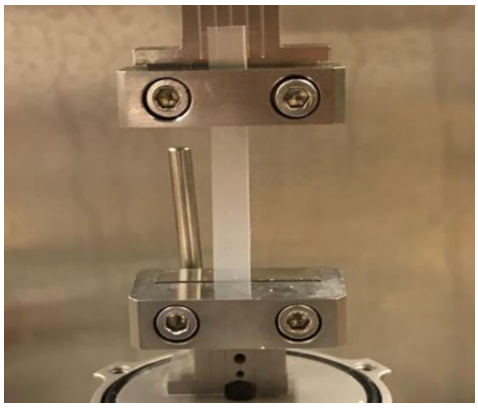

Fig. 5.12 Creep Master Test at Room Tem

We used a blade holder to improve the accuracy for cutting specimens. This produced greater repeatability in the results. Prior to each test, we put the specimen into the clamps but did not tighten them. Then we increased the temperature to allow thermal expansion before the creep test. The creep and time data recorded are shown in Fig. 5.13.The beginning part has been removed (about the first 10s for this test). Now, we used 23°C as the reference temperature. Master curve is as plotted in Fig. 5.14 through shift factor in Table 5.3.

Table 5.3 Creep Master Curve Shift Factors for Reference T 23°C

T	27.5°C	30°C	32.5°C	35°C	37.5°C	40°C	43°C
a_T	0.6	1.4	1.7	2.7	3.0	3.1	4.4
T	45°C	47.5°C	50°C	52.5°C	55°C	57°C	Ref 23°C
a_T	4.7	5.1	5.7	6.2	7.1	7.9	0

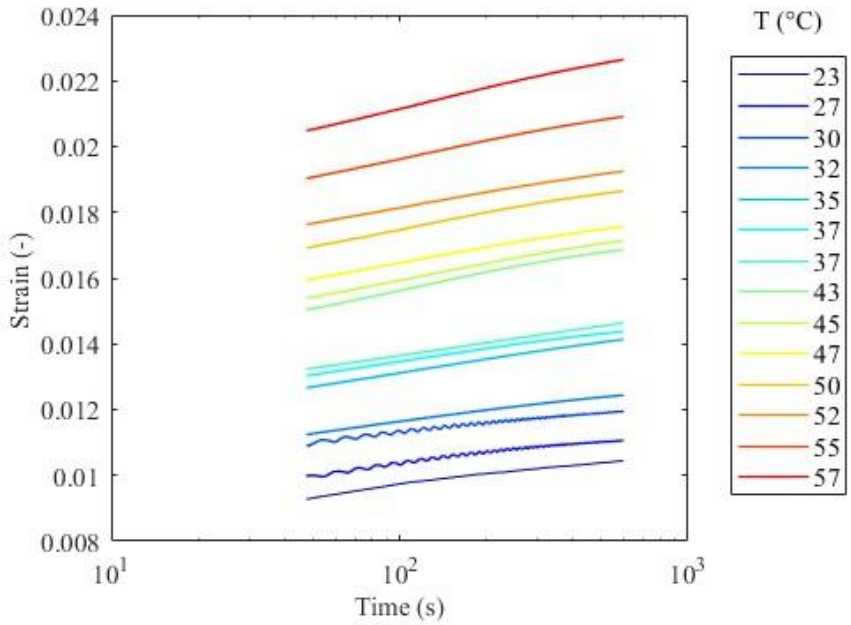

Fig. 5.13 Creep Master Curve Test Results at 1Mpa (145psi)

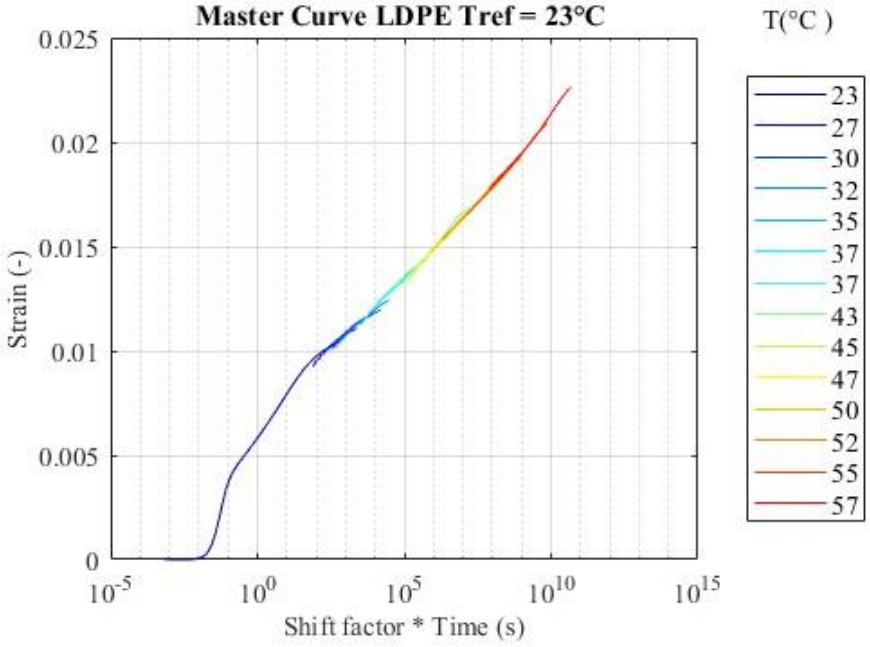

Fig. 5.14 Creep Master Curve for LDPE at Reference Temperature 23°C (1Mpa)

From Fig. 5.14, the beginning part (less than 0.01s) is close to 0 due to the accuracy of test. The realistic process of applying load to the specimen is a gradual process rather than a step stress.

5.2.3 Relaxation Master Curve

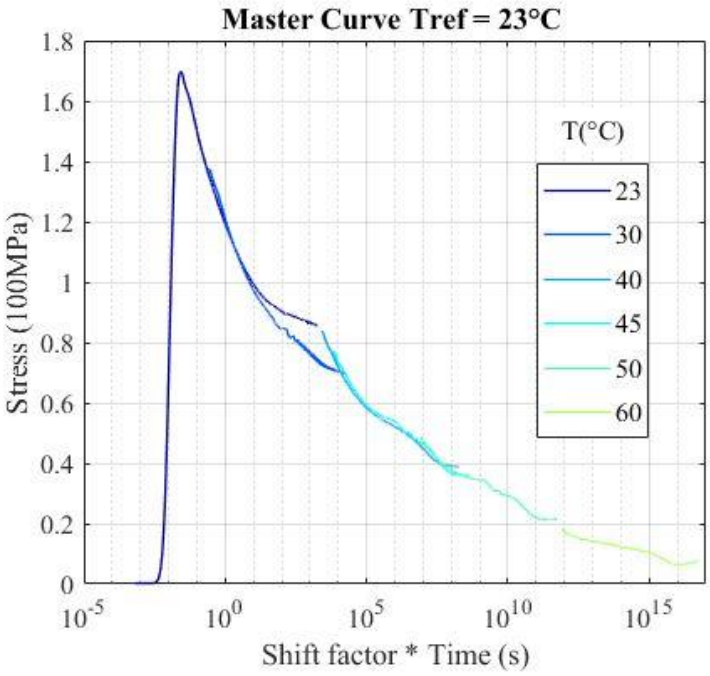

Fig. 5.15 Relaxation Master Curve for LDPE at Reference Temperature 23°C (1% strain)

Xin Chen, a student from WHRC lab performed relaxation tests on the same LDPE web material. We include these tests here for comparison with the creep tests. RSA G2 TA Instrument machine is used to measure relaxation data through time at various test temperatures. The dimension of the specimen is length 1.97in*width 0.53in*thickness 0.0211in.

1 Step Relaxation: 1% strain is applied for all tests.

2 Temperature Set Up for the Next Specimen: Duration of each temperature is 30mins (1800s) in this test and the temperature we chose 23, 30, 40, 45, 50, 60°C.

Table 5.4 Relaxation Master Curve Shift Factors for Reference T 23°C

T	30°C	40°C	45°C	50°C	60°C
a_T	1	5	5.4	8.5	13.5

5.2.4 DMA Master Curve

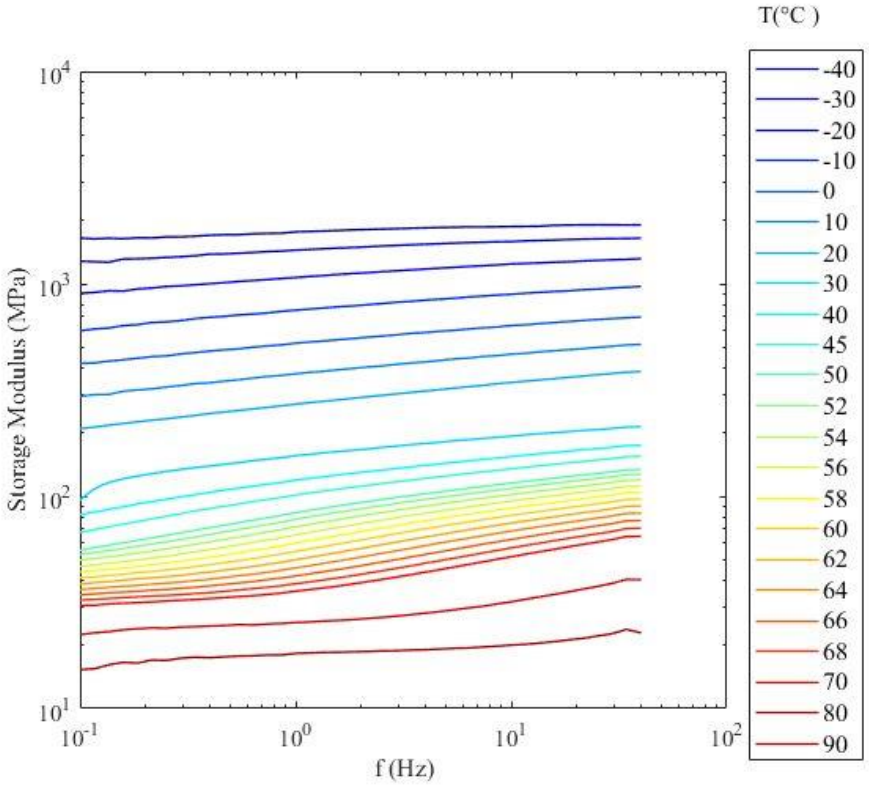

Fig. 5.16 Storage Modulus Results from DMA Test at Different Temperatures

Any progress that would allow us to decrease the time required to provide input to a model makes those models more usable and useful. Fast and accurate viscoelastic property measurement is needed for curl and winding viscoelastic models. Dynamic Mechanical Analysis could be a useful method for our application. The dynamic mechanical analysis involves subjecting a specimen to a sinusoidal strain through time t of the form:

$$\varepsilon(t) = \varepsilon_0 \sin(\omega t) \tag{5.15}$$

where $\varepsilon(t)$ is the strain at time t, ε_0 is the maximum strain, ω is the frequency of oscillation.

If the material is viscoelastic linear, this results in a stress that is also sinusoidal in time, but the stress will lag the strain by a phase angle δ in expression (5.16):

$$\sigma(t) = \sigma_0 \sin(\omega t + \delta) \tag{5.16}$$

The complex modulus is treated as a complex number:

$$\frac{\sigma}{\varepsilon} = E' + iE'' \tag{5.17}$$

Where E' is the storage modulus, which is for the elastic response (spring nature), and E'' is the loss modulus which is the dashpot part for viscous behavior.

The storage and loss modulus cannot be used in our research directly. We must convert them into relaxation functions or creep functions. The relaxation function can be expressed as a discrete set of exponential decays (5.8). Equations (5.18) and (5.19) are the relationships between relaxation modulus and storage or loss modulus (λ_i are the relaxation times in Wiechert model).

$$E'(\omega) = E_\infty + \sum_{i=1}^{N} E_i \frac{(\omega\lambda_i)^2}{1 + (\omega\lambda_i)^2} \tag{5.18}$$

$$E''(\omega) = \sum_{i=1}^{N} E_i \frac{\omega\lambda_i}{1 + (\omega\lambda_i)^2} \tag{5.19}$$

Through DMA frequency sweep tests, we can obtain $E'(\omega)$ and $E''(\omega)$. In equations (5.18) and (5.19), E_∞, N, λ_i and E_i are the unknown. From frequency sweep tests on the DMA, equations (5.18) and (5.19) are become a set of nonlinear statically indeterminate equations. After E_∞ and all of E_i are obtained, the relaxation function can be expressed as equation (5.8).Many previous researches focus on the method about the conversion from the dynamic modulus to relaxation function [32][33][34].

Dimensions of these specimens were: length 1.6in*width 0.2in*thickness 0.0211in. The thickness was the average of several measurements. The range of frequency was set from 0.1Hz to 40Hz (0.63 to 251rad/s), and 23 temperatures were tested between -40°C to 90°C. Both storage and loss modulus test were recorded. Only the storage modulus data was utilized to obtain the master curve since the loss modulus measurement was not as stable as the storage modulus. Increasing the temperature decreases the viscosity and thus it can be shifted to express the storage modulus at low frequency. Low temperatures are used to obtain the modulus at high frequency. Fig. 5.16 is the frequency sweep storage modulus data.

Table 5.5 DMA Shift Factors for Reference T 20°C

T	-40°C	-30°C	-20°C	-10°C	0°C	10°C	20°C
a_T	11.5	9.3	7	4.8	3.0	1.4	0
30°C	40°C	45°C	50°C	52°C	54°C	56°C	58°C
-1.7	-2.4	-2.9	-3.4	-3.6	-3.8	-4.05	-4.3
60°C	62°C	64°C	66°C	68°C	70°C	80°C	90°C
-4.6	-4.9	-5.25	-5.65	-6.1	-6.6	-10	-13

Fig. 5.17 is the DMA master curve at the reference temperature 20°C based on shift factors from Table 5.5.

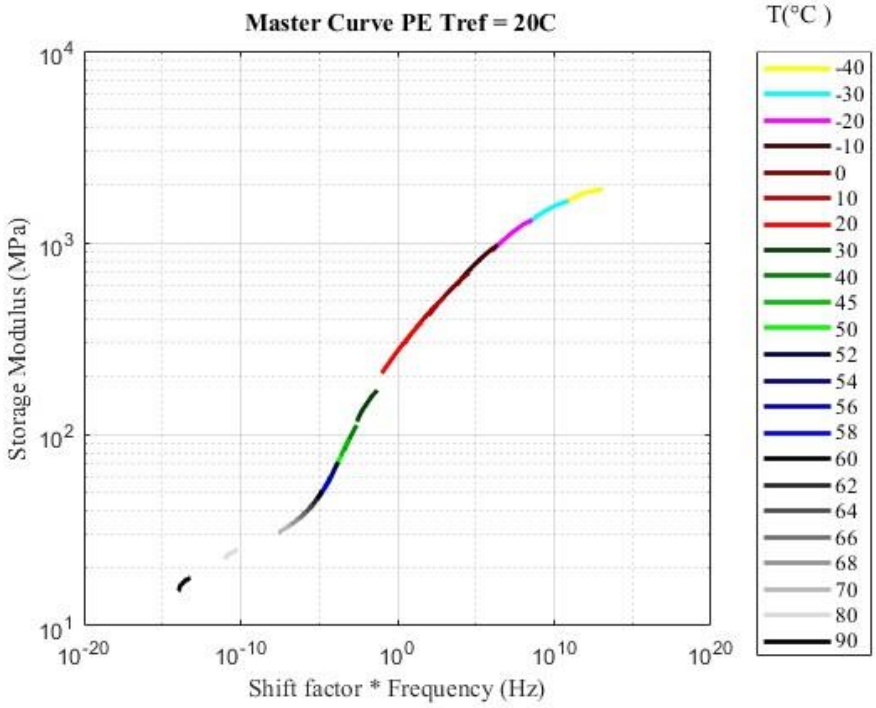

Fig. 5.17 DMA Master Curve at Reference Temperature 20°C

5.2.5 Comparison of the Different Methods

Wiechert model (General Maxwell Model) is used in this section and thus the relaxation function is shown in equation (5.8). The purpose of this section is to fit different test results into the Wiechert model to compare them. A numerical method is conducted in this section to evaluate the creep response of the model:

From viscoelastic constitutive relations:

$$\sigma(t) = E_\infty \varepsilon(t) + \sum_{i=1}^{n} E_i \int_0^t exp\left({}^{(-t+s)}/_{\tau_i}\right) \dot{\varepsilon}(s) ds \tag{5.20}$$

$$\sigma(t+\Delta t) = E_\infty \varepsilon(t+\Delta t) + \sum_{i=1}^{n} E_i \int_0^{t+\Delta t} exp\left({}^{(-(t+\Delta t)+s)}/_{\tau_i}\right) \dot{\varepsilon}(s) ds \tag{5.21}$$

where,

$$h_i^t = E_i \int_0^t exp\left({}^{(-t+s)}/_{\tau_i}\right) \dot{\varepsilon}(s) ds \tag{5.22}$$

The integration part is divided into (0,t) and $(t, t+\Delta t)$), and midpoint approximation is used to simplify the $(t, t+\Delta t)$) part:

$$\sigma(t+\Delta t) = E_\infty \varepsilon(t+\Delta t) + \sum_{i=1}^{n} \left[h_i^t e^{-\Delta t/\tau_i} + E_i e^{-\Delta t/2\tau_i} \left(\varepsilon(t+\Delta t) - \varepsilon(t) \right) \right] \tag{5.23}$$

Reorganize equation (5.23):

$$\left(E_\infty + \sum_{i=1}^{n} E_i \, e^{-\Delta t/2\tau_i} \right) \varepsilon(t+\Delta t) = \sigma(t+\Delta t) + \sum_{i=1}^{n} E_i \, e^{-\Delta t/2\tau_i} \, \varepsilon(t) - \sum_{i=1}^{n} h_i^t e^{-\Delta t/\tau_i} \tag{5.24}$$

Equation (5.25) is the final recursive formula:

$$\varepsilon(t+\Delta t) = \frac{1}{E_\infty + \sum_{i=1}^{n} E_i \, e^{-\Delta t/2\tau_i}} \left(\sigma(t+\Delta t) + \sum_{i=1}^{n} E_i \, e^{-\Delta t/2\tau_i} \, \varepsilon(t) - \sum_{i=1}^{n} h_i^t e^{-\Delta t/\tau_i} \right) \tag{5.25}$$

When the Wiechert model is known, or from initial guess, equation (5.25) is applied in creep test to calculate the estimated strain, which is used to compare with creep test results. All the relaxation time terms are chosen the optimization determines the moduli to fit the data.

Fig.5.18 is the Wiechert model for creep test from section 5.2.1 based on equation (5.25) (Values of E and λ will be in appendix). Since the WHRC lab creep test is only 7-day test, the number of term is fewer than other methods.

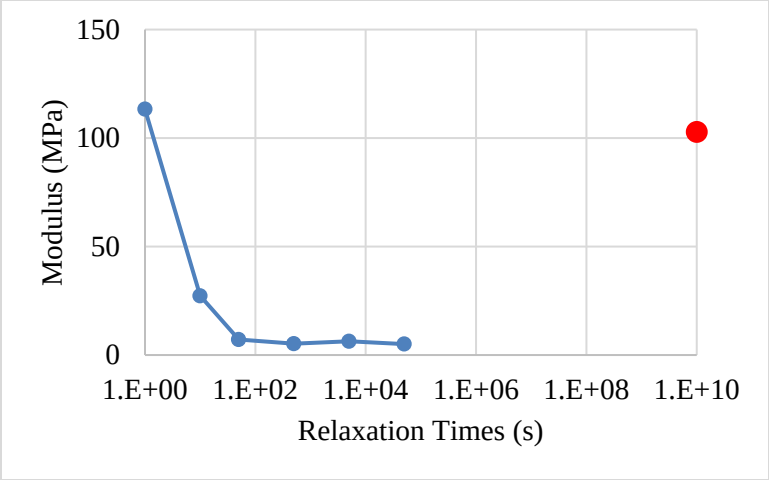

Fig. 5.18 Wiechert Model for Lab Creep Test

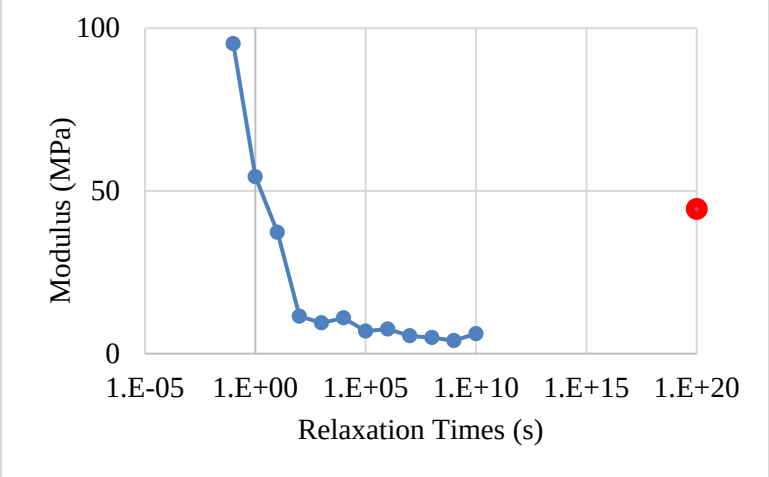

Fig. 5.19 Wiechert Model for Creep Master Curve Test

Fig.5.19 is the Wiechert model for creep master curve test from section 5.2.2 (Values of E and λ will be in appendix).

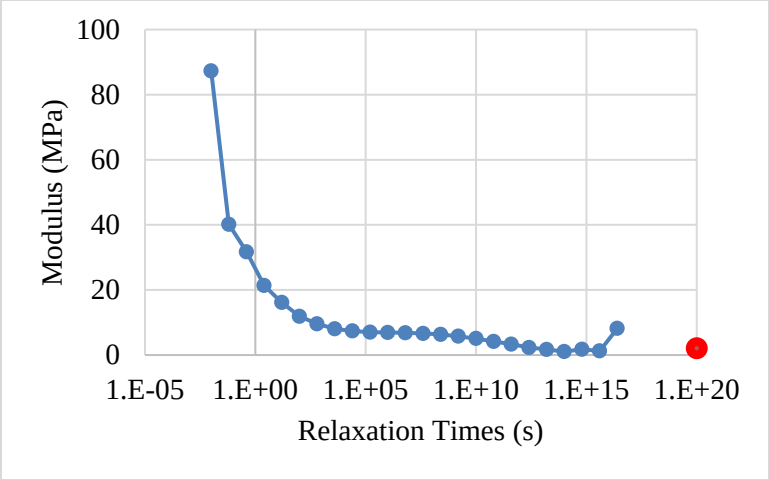

Fig. 5.20 Wiechert Model for Relaxation Master Curve Test

Fig.5.20 is the Wiechert model for relaxation test from section 5.2.3 (Values of E and λ will be in appendix).

Equation (5.18) is used to characterize the relationship between storage modulus and Wiechert modulus.

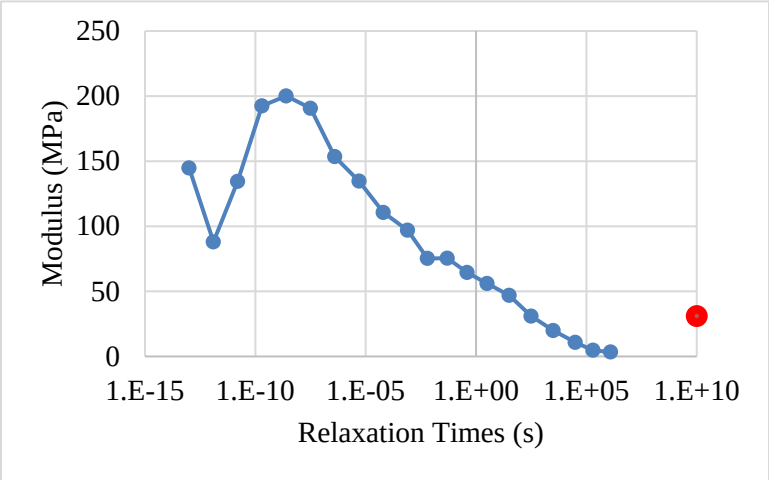

Fig. 5.21 Wiechert Model for DMA Test

We can compare all the methods we used to characterize the viscoelasticity property of LDPE.

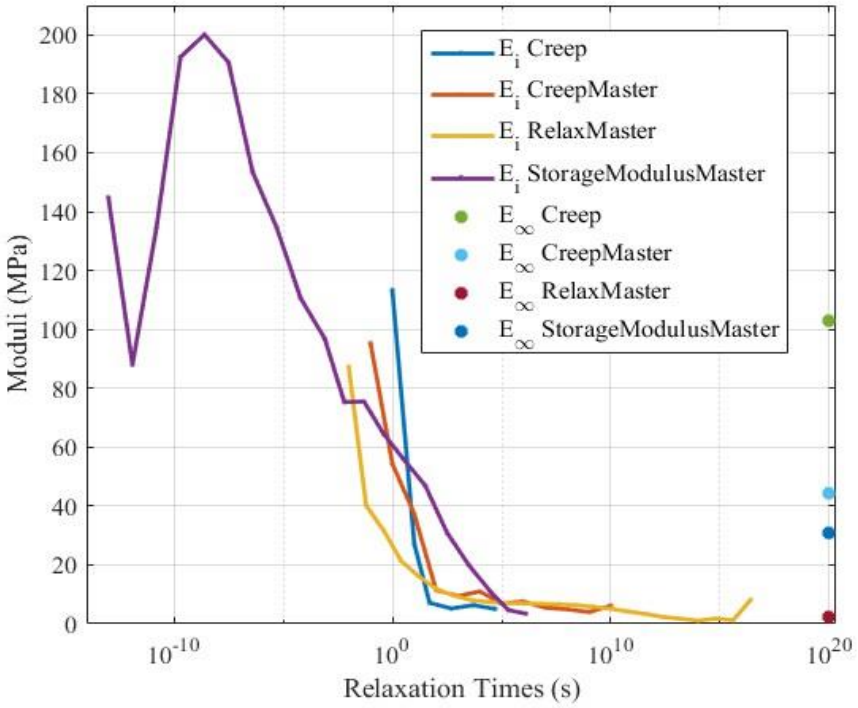

Fig. 5.22 Moduli vs Relaxation Time

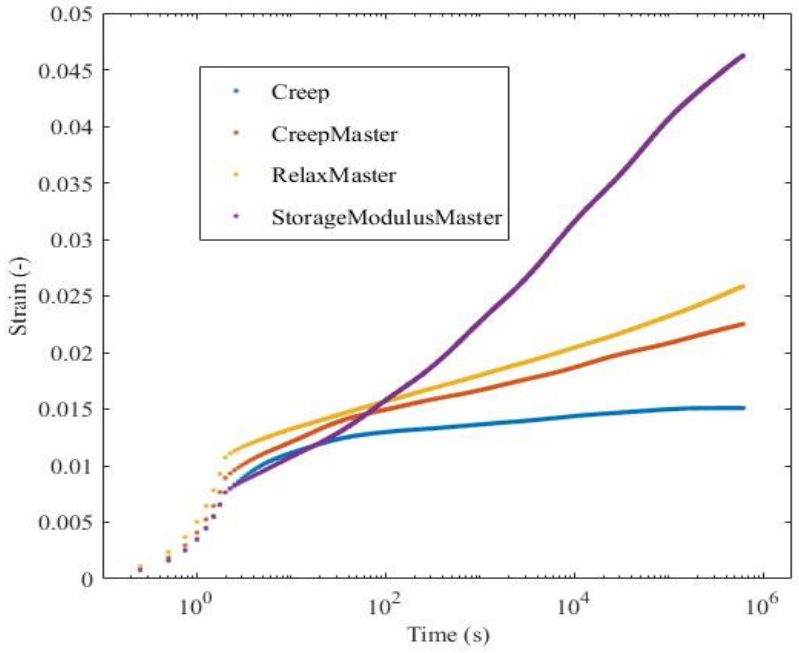

Fig. 5.23 Comparison all Characterization Methods in Creep Test

Fig.5.22 compare the moduli values for all relaxation times. Fig.5.23 represents the resulting creep curve for each model in the condition of the WHRC creep test. In the time domain from 10 to 100,000 seconds, there is reasonable agreement for all the methods except the DMA method. The DMA method shows a much faster relaxation, compared with other methods. Experimental errors might be partly responsible, but the difference in the results remains mostly unexplained.

Performing creep or relaxation tests in the smaller TA Instrument machines combined with time-temperature superposition method required less than 3 hours. Finally it required half a day to obtain the storage modulus data from the DMA method. The advantage of TTS method is obvious. Both creep and relaxation master curves are able to characterize viscoelastic property of LDPE for more than 10^{10} seconds (hundreds of years) storage time, while the time cost of the test is less than half a day. In addition, the master curve captured the beginning of the creep or relaxation effect, which cannot be obtained from WHRC creep test due to the dynamic effect of the set up. The main error in master curve tests might be due to the thermal expansion, which leads to an overestimation of the creep strain.

The advantage of WHRC lab creep test is its simplicity of operator. The experimental fault tolerance of the method is high, while the accuracy might not be reliable enough if faster creep happens at the beginning. Both relaxation master curve results and WHRC creep test will be used in next chapter for curl analysis. From equation (5.21), stress at a certain rate can be calculated, and thus stress strain relationship for strain rate is shown in Fig. 5.24 based on the relaxation master curve in Fig. 5.20:

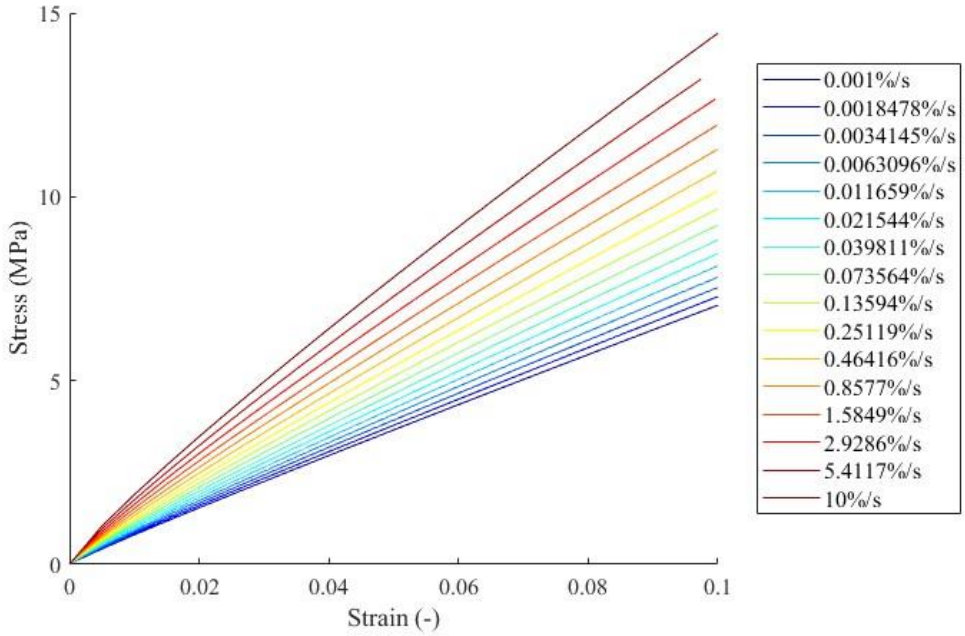

Fig. 5.24 Stress-Strain Relationship at Different Strain Rate

If the strain rate is 1in/in/min and the final strain is 0.025, which is the same as we did Instron test in section 5.2.1, the instantaneous Young's modulus is about 19,100psi, compared with 22,200 psi from Instron test.

CHAPTER VI

MACHINE DIRECTION CURL ANALYSIS

Curl for a single layer web due to viscoelastic behavior is similar to the bending recovery described in chapter 2. If the single layer is wound into a roll, the curl behavior can become more complex. The membrane and tangential stresses vary with radius in a wound roll. There are also tangential stresses due to bending a web to the spiral shape it assume in a wound roll. It is hard to find a way to consider both the orthotropic viscoelastic behavior and the boundary between tensile and compressive stresses which may affect creep through the depth of a layer. For a laminate, the curl problem becomes more complex. There are several reasons that laminate can become a curled web, but the main reason is strain mismatch during lamination or one sided surface treatments. Near the core of a wound roll, where the radius of a stored layer may approach that of the core curl is common because of the influence of creep due to bending strains inside the roll. Curl can also occur in laminates because of the imperfect bonding conditions between two layers.

I have found that Abaqus can analyze the curl problem. The web can be partitioned to consider the dissimilar relaxation process in the tensile and compressive stress zones of the web in Abaqus, if the tensile and compressive creep behaviors differ.

Qualls developed a viscoelastic winding model [30] can predict the change of radial pressure and tangential stress for different storage times. Based on this model, a new version of Winder 6.3 was developed to predict curl. When a constant strain is applied to a flat web, the stress decreases.

as the storage time increases. At unloading, a residual viscoelastic stress cannot disappear instantly Viscoelastic webs would into rolls will exhibit bending recovery and curl defect when unwound.

6.1 Curl Analysis of Single Layer Homogeneous Viscoelastic Webs

6.1.1 Curl Analysis of Homogenous Webs Wound into Rolls

The simplest curl calculations for webs wound into rolls would result from ignoring the effects of winding membrane residual stresses entirely. After a period of time t_r in storage process the web would be unwound and the curl radius ρ of unstressed web would be measured. Curl radius of bending recovery would be calculated using either expression (2.28) or (2.29) and knowledge of the radius r at which the layer was wound into the roll.

$$BR_1 = \frac{1}{2}[1 - \frac{E_{ten}(t_r)}{E_0}] \tag{6.1}$$

$$BR_2 = [1 - \frac{E_{ten}(t_r)}{E_0}] \tag{6.2}$$

Mollamahmutoglu's converting routine in section 5.1.2 is used here to covert the creep function from Table 5.2 (WHRC lab creep test) into the relaxation function (6.3):

$$E(t) = 13697 + 6842 * e^{-t/1325} + 1661 * e^{-t/89630} \tag{6.3}$$

From equation (6.3), the relaxation modulus exponentially decreases as the storage time increases. Substitute (6.3) into (6.1) and (6.2), relation between BR and storage time is shown as in Fig. 6.1.

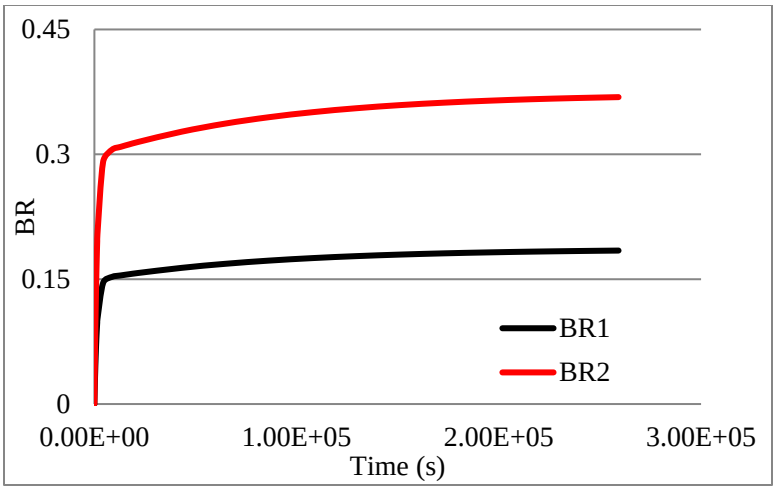

Fig. 6.1 Bending Recovery Values versus Storage Time

6.1.2 An Abaqus Model for MD Curl Analysis

6.1.2.1 Viscoelastic Input for Abaqus

Abaqus/CAE allows the user to input isotropic viscoelastic parameters from either experimental test data or Prony coefficients. Abaqus uses relaxation parameters, which can be input one of four ways: direct specification of the Prony series parameters, inclusion of creep test data, inclusion of relaxation test data, or inclusion of frequency-dependent DMA data obtained from sinusoidal oscillation experiments. Direct Prony creep terms can be used as direct input to Abaqus but the parameters from a pure shear creep test must be input. Shear creep tests are not easily conducted on thin web materials in the lab. For test input, there are two types of domain: time domain and frequency domain. Shear and volumetric tests are the only two inputs allowed in time domain, while dynamic mechanical analysis (DMA) test results are input in frequency domain.

Uniaxial creep tests in tension are convenient in the laboratory. It is necessary to transform this data to parameters that can be input in Abaqus. In Abaqus, if we want to use shear creep test data, two inputs are needed: the normalized shear compliance $j_s(t)$ and the relaxation time τ.

$$j_s(t) = G_0 J_s(t) \tag{6.4}$$

Where, $J_s(t)$ is the shear compliance, G_0 is the shear modulus at the initial time t=0. Based on the relationship G=E/(2(1+ν)), Young's modulus relates an elastic stress to an elastic strain.

In this research, creep function from Fig. 5.2 (two terms Prony series) is used to simulate in Abaqus model later, and the input in the Abaqus model is in Table 6.1:

Table 6.1 Shear Creep Test Inputs for Abaqus

Linear, Isotropic, Prony Series Definition			
I	G(I)	K(I)	TAU(I)
1	0.308	0.308	1325s
2	0.075	0.075	89,630s

Besides the creep test data, DMA test results can be used as direct viscoelastic inputs in Abaqus as in Fig. 6.2.

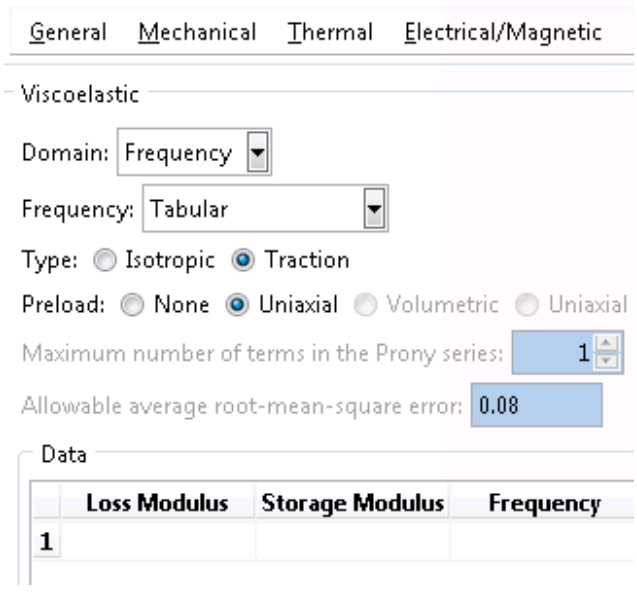

Fig. 6.2 DMA Direct Input in Abaqus

6.1.2.2 Isotropic Viscoelastic Abaqus Model for Isotropic Relaxation Behavior

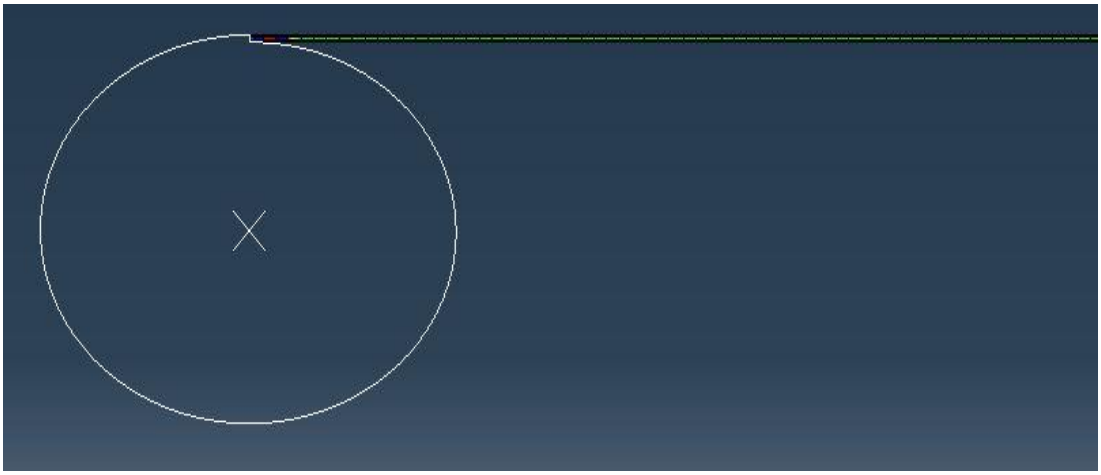

Fig. 6.3.a Abaqus Model for Curl Analysis before Winding

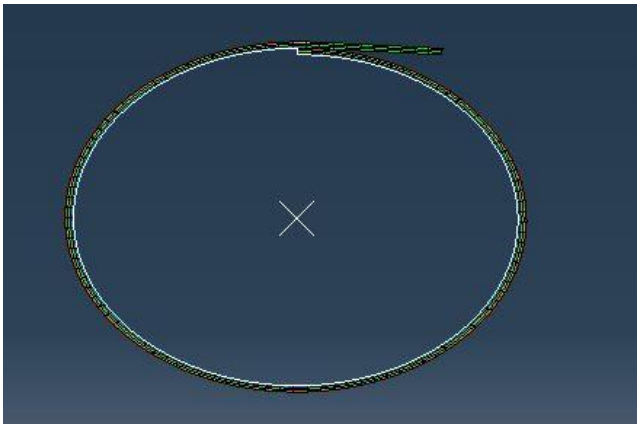

Fig. 6.3.b Abaqus Model for Curl Analysis after Winding

Fig. 6.3.a and b are the Abaqus models before and after winding step.

The purpose of this section is to demonstrate MD curl can be simulated using Abaqus. Simulation results will be used to compare with results of other models in later sections.

We simulated an LDPE 6 inches in width and 0.02 inches in thickness. The core is an analytical surface whose outside radius is 0.5 inches. The web is given isotropic elastic properties with

Young's modulus of 22,200psi and Poisson's ratio of 0.3. Both of the elastic and the viscoelastic property input come from Table 5.1. The web material is viscoelastic for every step in this simulation. Since the minimum relaxation time is1325s from input data, while the winding time is less than 10s, the winding process is still similar to the elastic state.

Table 6.2 Step Description of Curl Simulation

Step Name	Time	Step Content
Pretension	1 (s)	800 psi tension is applied to the right surface of web
Winding	1.25 (s)	1 lap of web are wound on the core
Storage	1 (day) or 3 (day)	2 different storage times are set up
Unwinding	1.25 (s)	Opposite rotation of the winding process
Release Tension	1 (s)	Winding tension was released very quickly
Final State	100 (s)	Eliminate dynamic effect

In the final state, the deformed coordinates (at 1s of final state) of the web are used to determine the amplitude of the curl. Fig. 6.4 shows the final deformed state of the web stored for 1 day, unwound and released. The deformed coordinates of each node were probed along the MD direction. Three consecutive nodes were used to define an arc and compute the arc radius. Inverting the radius of the arc yields the curvature of the center node. The curvature divided by the radius of the core is used to evaluate the bending recovery.

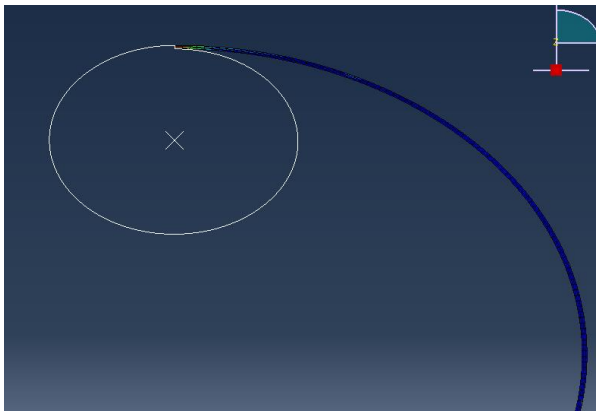

Fig. 6.4 Final State of Web for 1day Storage Time after Unwinding and Tension Release

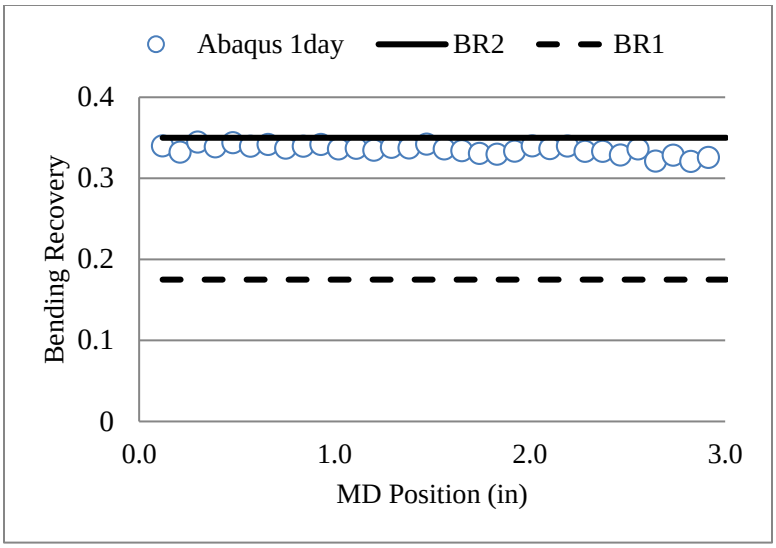

Fig. 6.5.a Theory of BR and Abaqus Results 1Day Storage

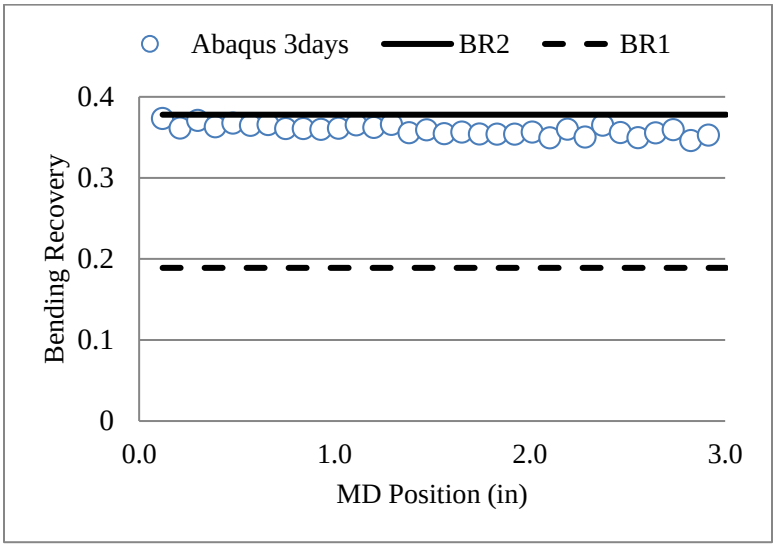

Fig. 6.5.b Theory of BR and Abaqus Results 3Days Storage

From Fig 6.5a and b, it is not hard to imagine that viscoelastic effects will be significant when the storage time is long. During the storage process, the web is forced to the shape of the core, and the stress through the web depth will relax. With more time for the bending stress to relax in storage, more curl will result. After about 2 days the result did not change, because the largest time constant in the creep function we used was 89,630 seconds or 1.05 days. Additional creep or changes in

bending recovery would not be predicted by the model. The constant values of curl radius might oscillate are due to influence of core and the step in winding radius that results where the second layer overlaps the start of the first layer. The relaxation modulus function input (6.3) was assumed to be applicable for tensile and compressive stresses and strains. As we expected, the Abaqus results are close to BR_2 given by expression (6.2) and shown in Fig. 6.1. The Abaqus results compare with theory well.

6.1.2.3 Consideration for Dissimilar Relaxation Behavior

Matsuoka points that there is difference between the stress-relaxation in tension and in compression [24]. Greener suggests that compressive stresses will relax at a substantially slower rate than tensile stresses for many materials. We discussed this in the literature review, and it is contended that the linear-viscoelastic response of a sample in uniaxial compression could be treated by shifting the relaxation in tension by a constant shift factor. This provided a method to model this in Abaqus. A layer is divided into two parts, each part has 1/2 the thickness of the web. Each portion of the web was given the same elastic parameters but different relaxation times.

The cases for curl in the literature are for pure bending. The web would be subject to tensile stress above the neutral plane and compressive stress below as shown Fig. 6.6. In this case we can divide the web into 2 equal thickness portions with different relaxation properties.

The winding problem is not pure bending. We apply torque either through the core or a nip roll or both to wind the roll. This induces the web tension (T) in the winder tension zone. As the web approaches the winder it has only tensile stress (T_w) due to web tension. As the web becomes the outer layer of the winding roll it will assume the radius of curvature (R) of the layer beneath. Now there are bending strains and stresses in addition to the tensile stresses that were due to web tension. There may be no compressive MD stress in the web or there may be a small zone ($<t/2$) of compressive stress near the bottom of the web.

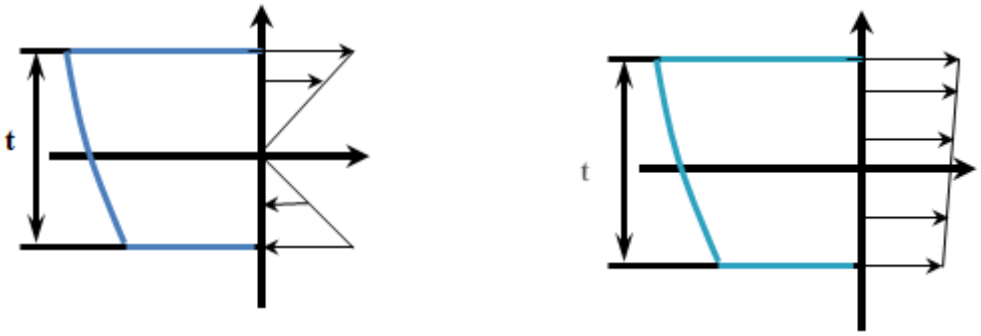

(a) Pure Bending (b) Tensile

Fig. 6.6 Stress in Pure Bending and Tensile State

For dissimilar relaxation processes, relaxation times for compressive state of web are assumed a large number, whose coefficients are determined by the material.

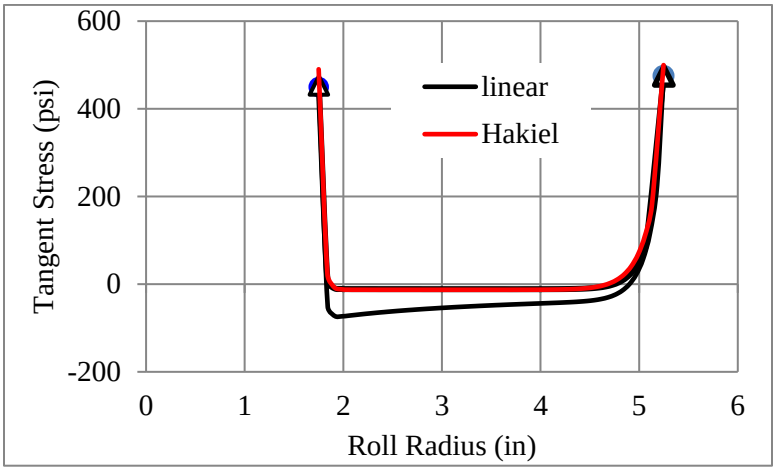

Fig. 6.7 Tangential Stress after Winding Process through the Radius

Use of winding models shows that the membrane tangential stress in a wound roll varies with radius as shown in Fig. 6.7. The interior of the roll has small tangential stress and thus during storage, most of the interior web is influenced by bending stress only, except the innermost and outermost layers of web. The dissimilar relaxation process may affect the curl in the interior of the roll. The low tangent stress in this region will assure compressive stresses due to bending and thus dissimilar relaxation, if dissimilar relaxation exists. If the web stress is tensile throughout the

thickness, the dissimilar relaxation consideration will increase the curl rather than reduce the curl in Abaqus results.

6.2 Curl Simulation Using Viscoelastic Winding Models

Qualls [30] development of a viscoelastic winding model demonstrated that state dependent orthotropic elastic material characterization was necessary during the winding phase of his solution. He also demonstrated that orthotropic creep compliance characterization was necessary for the storage phase of his solution. Ren et al., [6] demonstrated how the state dependent orthotropic elastic properties in winding simulations could be addressed with VUMAT and UMAT subroutines for Abaqus Explicit and standard Implicit simulations. It may be possible to model orthotropic creep behaviors using the VUMAT and UMAT subroutines. However, the exits to subroutines to update properties are very time consuming and several computational hours are required to simulate the winding of a few layers.

Based on existing winding model 6.3, a new version of the existing viscoelastic winding model has been developed to calculate the radius of curl at a certain radius after winding based on bending recovery theory.

6.2.1 Bending Recovery Theory to Develop Winder 6.3

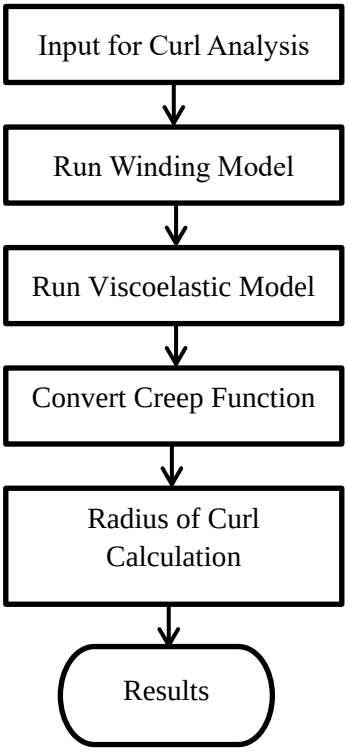

Fig. 6.8 Flow Chart of Curl Analysis in Winder 6.3

Winder 6.3 requires creep function viscoelastic inputs for the web material. The conversion between creep functions and relaxation functions was discussed in Appendix B. Details of the conversion procedure come from Mollamahmutoglu et al. [31].

To calculate the curl radius, we return to equations (6.1) and (6.2) again. We do not want to consider differential relaxation firstly.

$$\rho_{(r)} = r/BR_2 = r/\left[1 - \frac{E_{ten}(t_r)}{E_0}\right] \tag{6.5}$$

where $\rho_{(r)}$ means the radius of curvature at the radius of r.

E_0 is the initial Young's modulus, which means that the Young's modulus when the time is 0. We used the instantaneous MD Young's modulus to represent this. . $E_{ten}(t_r)$ is the relaxation modulus that we can converting the creep functions input to Winder 6.3. In Winder 6.3, the radius of each layer is known and the state dependent radial modulus is considered.

Adjustment of dissimilar relaxation is a manual choice, because although common in web materials, it is not a universal phenomenon. The tangential stress is not large in the middle of roll for some winding situations (Fig. 6.7), which means that some part of the web is in a compressive state. If so, BR_2 might need to be replaced by BR_1. The difference between relaxation processes in tensile and compressive zones is difficult to quantify for webs, the measurement of MD creep in compression would require short sample lengths to prevent buckling. However, the effect may be assumed negligible, if the bending stress is relatively small compared with winding tension. If it is not, the real curl value will be smaller than the model prediction. Abaqus was used to consider this in section 6.1.2, but different creep functions are not easily assigned to each layer in Winder 6.3. An estimating method, which used a curl compensation coefficient is introduced to estimate the effect.

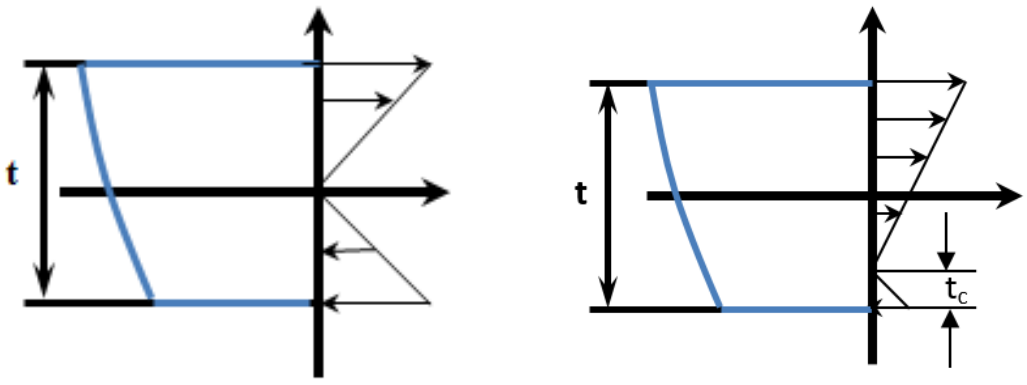

(a) Tensile (b) Compressive

Fig. 6.9 Tensile and Compressive Zone Factor

In pure bending, half of the web is in the tensile zone, and the other half is in the compressive state. When we apply a winding tension to the web, the tensile zone stays in the tension, while part or all of compressive zone becomes tensile. A new factor is introduced, t_p ($t_p = 2t_c/t * 100\%$) to express the remaining compressive zone. The range of t_p is [0, 1). From the single layer bending recovery, when t_p=0(means no compressive zone), the adjust coefficient is 1(no adjust). When t_p is closed to 1(most compressive part still keep the same state), the adjust coefficient is 0.5(the curl is adjusted about 50%).

In Winder 6.3, the winding tension and the tangential stress at different radius are known values, thus whether the layer of web is in tensile or compressive state can be determined. It is assumed that the adjust coefficient is only the function of t_p. Linear interpolation is used to calculate the adjust coefficient. The final curl is the multiplication of original curl and adjust coefficient. This is a convenient way to consider dissimilar relaxation.

6.2.2 Curl Simulation Verification

6.2.2.1 Curl Test Procedure

The curl test procedures follow:

(1) The web was wound and unwound several times. In between winding and unwinding it was stored at 150°F for about 5 hours. The curl of innermost layer and outermost layer are measured until the initial curl was less than 2 on the Kappa Gauge*(mentioned at the end of section 2.1), which is assumed flat in our test.

(2) The web was wound at a selected winding tension and stored for 1 day.

(3) Curl was measured in the outmost layer. The roll was unwound so that web sample could be harvested that was adjacent to the core during storage. This allowed us to measure the curl in what was the innermost layer in the roll during storage.

(4) Procedure was repeated for different winding tensions.

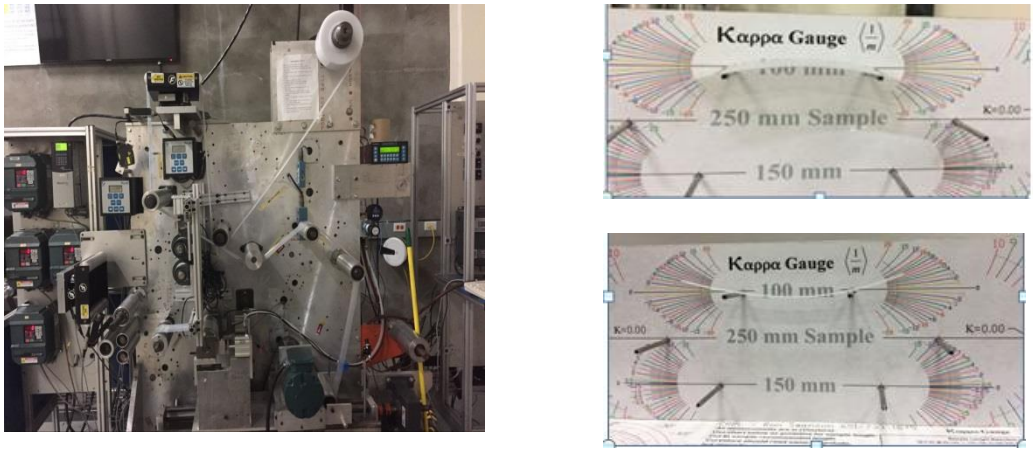

(a) 3M Winding Machine (b) Kappa Gauge

Fig. 6.10 3M Winding Machine and Curl Measurement through Kappa Gauge

6.2.2.2 Curl Test and Model Results

The final radius of the roll decreased after each test because of the web harvested to make the curl measurements from previous tests. Generally the test results compare well with model predictions. For the outermost layer, the web is loose due to relaxation and a small radial pressure, and thus test results are smaller than the theoretical value. For the innermost layer, the quality of the wound roll is not good since it is difficult to maintain winding tension as the winder starts. We know that winding tension significantly influences the radial pressure in a wound roll. Winding tension does not have significant influence on curl as shown by tests and modeling. The radial location of the layer in the wound roll will have influence on the curl. High temperature accelerates the creep process and therefore increases the curl.

Since the first layer of web is influenced by the core splice, we usually harvest the third or fourth layer to measure the radius of curl as the innermost layer. For the Kappa Gauge measurement, 100mm and 150mm samples are recommended when the curl is larger than 10(m^{-1}). In Tables 6.4 and 6.6, model (WHRC) means that WHRC creep test is used as the input, while model (Master) means that relaxation master curve is as the input in Winder 6.3. 3 LDPE wound rolls are used for these tests. The results in the following tables refer to wound rolls 1,2 and 3. Per the procedure (see page 92) these rolls were conditioned to reduce any existing curl prior to these tests. The wound roll from which curl test were conducted is recorded here to be able to trace these results:

Table 6.3 Geometry and Winding Tension for Curl Test **(**70°F)

Test	Wound Roll	T (lb)	Inner Radius (in)	Outer Radius (in)
1	1	9	1.75	4.75
2	1			4.50
3	1			4.35
4	1	18		4.30
5	1	5		4.30

Table 6.4 Comparison between Lab Tests and Model Results for Single-Layer Curl (70°F)

Test	Innermost Layer (Kappa 1/m)			Outermost Layer(Kappa 1/m)		
	Measured	Model (WHRC)	Model (Master)	Measured	Model (WHRC)	Model (Master)
1	6.5	7.77(19.5%)	9.6(47%)	2.5	2.94(17.6%)	3.56(42.4%)
2	9.0	7.77(-13.6%)	9.6(6.7%)	3.5	3.1(-11.4%)	3.76(7.5%)
3	8.5	7.77(-9.1%)	9.6(12.9%)	2.5	3.21(28.4%)	3.89(55.6%)
4	8.5	7.77(-9.1%)	9.6(12.9%)	2.5	3.24(29.6%)	3.93(57.2%)
5	9.0	7.77(-13.6%)	9.6(6.7%)	2.5	3.24(29.6%)	3.93(57.2%)

The real measurement cannot be instantaneous and it was conducted about 10s after removal. Some relaxation process may happen during the time, especially when relaxation happens significantly at the beginning. In Greener's paper [22], he used Young's modulus in tensile test at 1in/in/min strain rate to represent E(0). In order to reduce the possible recovery that occurs before

the curl measurement, Young's modulus in tensile test at 0.6in/in/min strain rate (from relaxation master curve) is chosen in this section to represent E(0) for the model (master curve). All he input for the Winder 6.3 is in Appendix C.

For the innermost layer, the test results agree with the model prediction with errors ranging from -14 to 20% for room temperature. In all tests but two the error was negative which means the model predicts less curl than the test produce. For the outermost layer, the curl is less as expected but the %errors can be larger since these are small numbers. Initial Kappa measurement less than 2 might be not flat enough for the outermost layer since its value is small.

Table 6.5 Geometry and Winding Tension for Curl Test **(**110°F)

Test	Wound Roll	T (lb)	Inner Radius (in)	Outer Radius (in)
6	2	9	1.75	3
7	2			3
8	3			5
9	3			5

Table 6.6 Comparison between Lab Tests and Model Results for Single-Layer Curl (110°F)

Test	Innermost Layer (Kappa 1/m)			Outermost layer (Kappa 1/m)		
	Measured	Model (WHRC)	Model (Master)	Measured	Model (WHRC)	Model (Master)
6	11	10.3(-6.3%)	17.3(57%)	3.5	6(71%)	10(>100%)
7	11	10.3(-6.3%)	17.3(57%)	3.5	6(71%)	10(>100%)
8	12	10.3(-14.1%)	17.3(44%)	3.5	3.6(3%)	6(71%)
9	13	10.3(-20.8%)	17.3(33%)	3.5	3.6(3%)	6(71%)

Tables 6.5 and 6.6 display the set up and results at elevated temperature. The input is in Appendix C. From Table 5.4, shift factor is estimated at 5.2 for 110°F (43°C). The possible reason for the large errors from the master curve relaxation input is that the thermal expansion was not treated correctly when the procedures were set up. This needs to be solved in future characterization tests.

Review of results in Tables 6.6 and 6.4 demonstrate that storage at elevated temperature will result in smaller curl radius and larger curl by Kappa measurement.

6.2.3 Laminate Viscoelastic Model

In section 4.5, equivalent single-layer laminate elastic winding model was introduced. For viscoelastic laminate, equation (4.30) can be applied in the MD and CMD directions. Since the radial modulus is a nonlinear state dependent term, stack test is always necessary rather than any estimation. We developed equation (4.30) into (6.6):

$$E_{lam}(t) = \frac{E_A(t)h_A + E_B(t)h_B}{h_A + h_B} \tag{6.6}$$

where $E_{lam}(t)$ is the equivalent relaxation function for laminate, $E_A(t)$ and $E_B(t)$ are the relaxation function for each layer, and h_A and h_B are the thickness of each layer, respectively. The equivalent creep function is still function of time. $E_{lam}(t)$ is also function of time, which is considered as the equivalent relaxation function of the laminate. Excel Solver is used to obtain the equivalent relaxation function. This relaxation function can be converted to creep functions, which is the direct input in Winder 6.3. This extension has been developed for Winder 6.3 but has not been verified.

6.3 Online Measurement

6.3.1 Anticlastic Curl Theory

Now assume a layer of LDPE web which can creep at room temperature and creep faster at elevated temperature has been stored in a cylindrical shape in a wound roll for some storage time. Creep occurs as a function of bending and membrane stresses and time.

When this roll is unwound we would expect it to have varying levels of MD curl that we could measure. Samples would be cut to establish a stress free state, and then make the measurement with a Kappa gage. If we wished to know how the curl varied through the wound roll we would destroy the web by cutting many samples and making several Kappa gage measurements.

A web with MD curl will elastically curl in the CMD direction when unwound under tension due to anticlastic bending. Lab tests were conducted to quantify the relationship between MD curl and CMD curl. An on-line measurement instrument for monitoring the CMD curl has been developed. The measured CMD curl was used to estimate the MD curl that must have been present in the web in the wound roll. This On-line measurement method was used to verify our previous curl tests.

The bending moment M that would be required to make an 0.02" thick LDPE web conform to the shape of a .5" radius cylindrical roller would be:

$$\mathrm{M} = \frac{\mathrm{D}}{\mathrm{r}} = \frac{\mathrm{EI}}{\mathrm{r}(1-\upsilon^2)} = \frac{\mathrm{Ewh}^3}{12\mathrm{r}(1-\upsilon^2)} = \frac{22200 * 4 * 0.02^3}{12 * 0.5(1-0.3^2)}) = .13010989\mathrm{in} - \mathrm{lb} \tag{6.7}$$

Timoshenko plate theory [23] demonstrates that a moment M on web two opposite edges of a rectangular plate generates an anticlastic surface. The web could conform to a cylindrical surface only if there is a second bending moment M_y which is applied on the moment M_y applied to the other two edges of the web:

$$M_x = M/w = .13010989/4 = .032527lb - in/in \tag{6.8}$$

$$M_y = M_x * \upsilon = .032527 * 0.3 = .009758lb - in/in \tag{6.9}$$

$$w = -\frac{M_x}{2D(1-\upsilon^2)}x^2 + \frac{\upsilon M_x}{2D(1-\upsilon^2)}y^2 \tag{6.10}$$

CMD bending stresses are induced by the moment M_y on the outer surface and inner surface of the web:

$$\sigma_{y,CMD} = \pm\frac{6M_y}{t^2} = \pm\frac{.058549}{0.02^2} = \pm 146psi \tag{6.11}$$

If we were to unwind this roll of material into a web line, the web tension would elastically pull out the curled shape of the web, however due to anticlastic bending a CMD curl will be induced that we intend to measure and then relate to the MD curl without destroying the web. If the web assumed an MD curl of radius MDR while in storage and if the MD curl was drawn flat by tension when unwinding then theoretically the out-of-plane deformation in the CMD would be:

$$w = \frac{\upsilon M_x}{2D(1-\upsilon^2)} = \frac{\upsilon}{2\,R_{MD}(1-\upsilon^2)}y^2 \tag{6.12}$$

The 2nd derivative of w is related to the CMD curl radius CMDR:

$$\frac{\partial^2 w}{\partial y^2} = \frac{\upsilon}{R_{MD}(1-\upsilon^2)} = \frac{1}{R_{CMD}} \tag{6.13}$$

Thus potentially we should be able to measure a CMD radius of curvature in the free span of:

$$R_{CMD} = R_{MD}\frac{1-\upsilon^2}{\upsilon} \tag{6.14}$$

This is only an estimate of the radius of the CMD curl after unwinding. It is expected that out-of-plane web constraint at rollers, web elasticity, web tension and span geometry would affect the measured CMD curl radius.

6.3.2 Characterizing the Relationship between MD and CMD Curl

Several 18 inches specimen (LDPE) were prepared. All of the specimen are wound and then stored in 150°F about 2 hours to remove the initial curl once. We used the Kappa gage to measure the curvature (both MD and CMD) for several samples as shown in the following table:

Table 6.7 Initial MD and CMD Curl of Specimen

Specimen	1	2	3	4	5
MD Curl Kappa(in)	2.50(16)	2.00(20)	1.25(31)	4.25(9.0)	1.0(39)
CMD Curl Kappa(in)	3.00(13)	1.00(39)	3.75(10)	5.25(7.5)	1.0(39)

It is found that the web can have curl in both the MD and the CMD directions in a stress free state. Some CMD curl can exist independently from MD curl and anticlastic bending. This could affect the accuracy of an online measurement system.

Keyence LK031 laser displacement sensors were used in online measurement. The sensors are mounted 30 mm (1.2 in) away from the undeformed web plane. The measuring range is ± 5 mm (+0.2 in). In the CMD direction, one sensor is targeted at the middle of the web, and the other two are quite symmetric at about 3.8 cm (1.5 in) away. The length of vertical test span is 18 inches. The relationship between MD and CMD curl was characterized by tests.

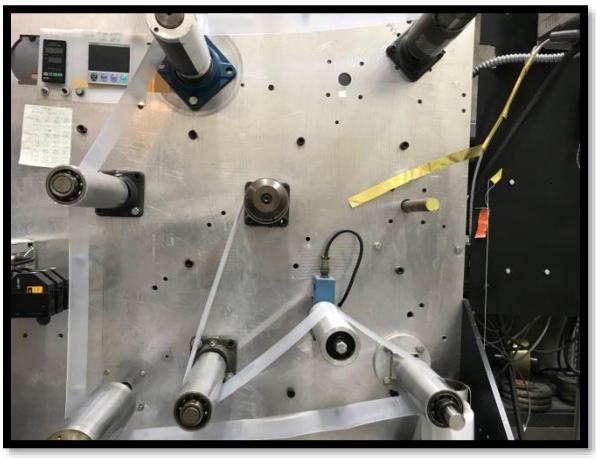

Fig. 6.11 Web Path for Online Measurement Characterization

(1) To conserve web 5 different LDPE specimens were prepared about 16 feet in length with known MD curl levels (the Kappa Gauge was used to measure the MD curl).

(2) Each web sample was then transported under tension through the test span shown on the previous slide. It is important to ensure the 3 Keyence laser sensors are targeted accurately in the CMD as shown in Fig. 6.11. When we start moving the web there will be some length of web that will pass before the guide system will bring the web laterally to a steady state positions (we usually delete the results until the web is tracking properly).

(3)These samples were so short and thus they are manually assisted the winding and unwinding rolls in order to gain the target winding tension from the control panel as quickly as possible (3lbs,6lbs,9lbs).

(4) The data was recorded from the 3 Keyence sensors from which I inferred the radius of CMD curvature. These values oscillated some and averaged values were recorded.

(5) Every MD curl test was repeated at least 3 times. Finally, a relationship between initial MD curls (no tension) and CMD curl (online under tension) is obtained.

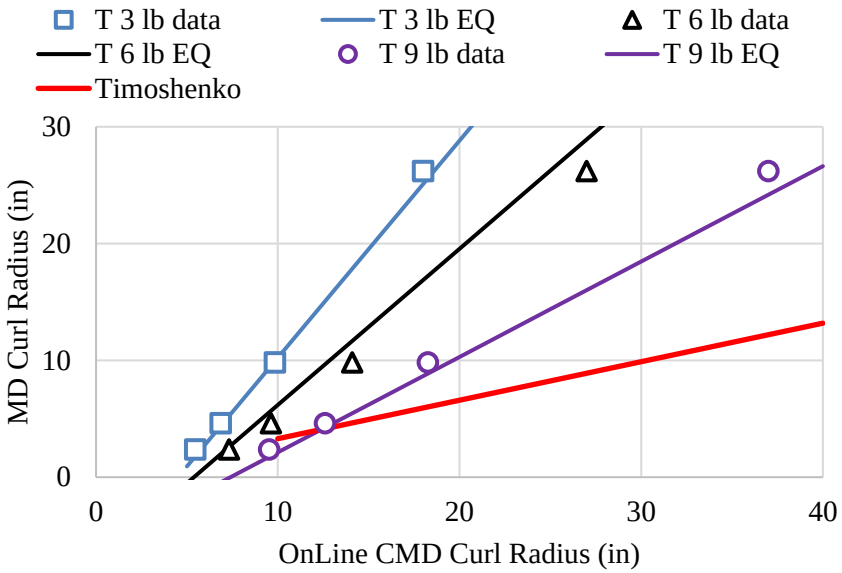

Fig. 6.12 Relationship between MD and CMD Curl versus Timoshenko Theory

Test data shows a linear relationship between MD and CMD Curl as the Timoshenko expression does. The test data demonstrates the slope between MD and CMD curl is dependent on web tension whereas the Timoshenko expression shows dependence only on Poisson's ratio. For this web and test span the regression curve can be to infer the MD Curl in a stress free state from the CMD Curl with the web in tension. Expression (6.15) is the test data regression to show the relationship between MD and CMD curl.

$$R_{MD}(in) = [-0.174 * T(lb) + 2.380] * R_{CMD}(in) + [0.388 * T(lb) - 9.531] \qquad (6.15)$$

6.3.3 Online Measurement and Winder 6.3 Curl Analysis

We only measured the curl of innermost layer and outermost layer in section 6.2.2. The standard we used is that the initial Kappa is less than 2, which we thought the whole roll should be flat enough through the radial direction. Online measurement method is used to verify this. LDPE web rolls were still used in this online measurement test. The outer radius of rolls is 3.5in.

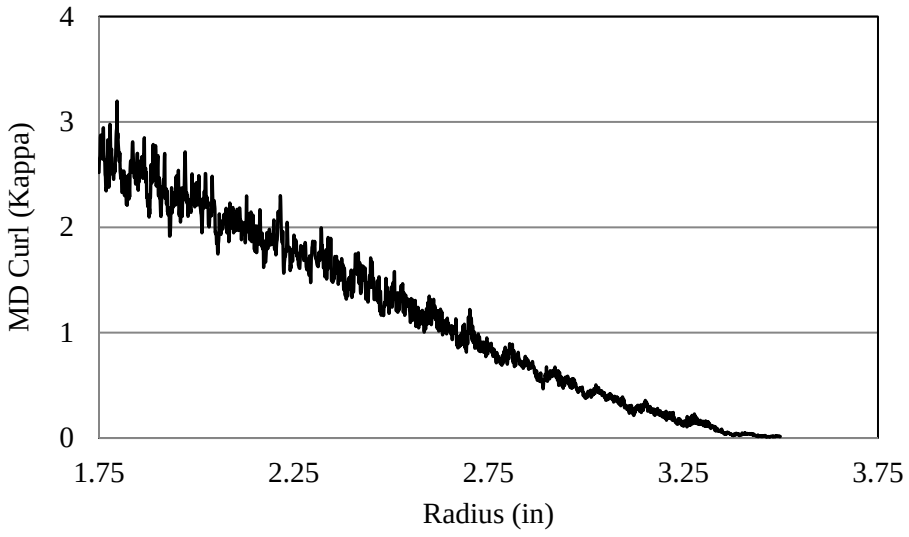

Fig. 6.13 Online MD Curl after Removing Initial Curl

After removing the initial curl several times, online measurement from Fig. 6.13 shows that the initial curl is less than 2 Kappa for most of rolls, which means the whole roll is reasonably flat. Then the roll was stored one day at room temperature and online measurement was conducted again. Fig.6.14 shows that the final online MD radius through the radial direction in Kappa unit, while radius of curl (inch unit) shows in Fig. 6.15.

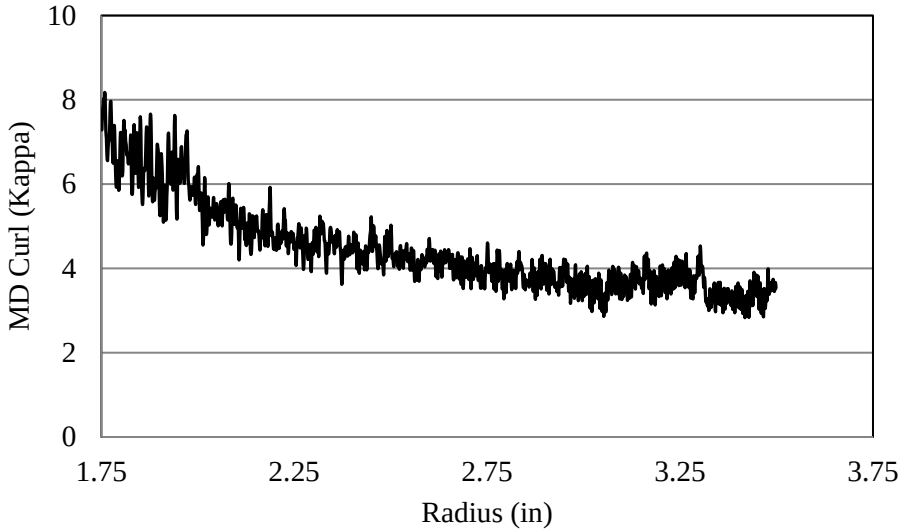

Fig. 6.14 Online MD Curl after 1 Day Storage (Kappa Unit)

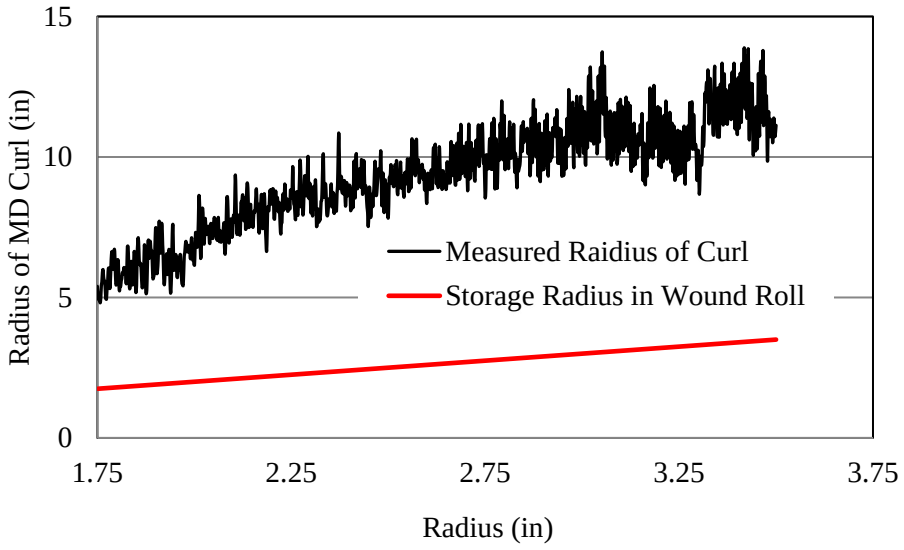

Fig. 6.15 Online MD Curl after 1 Day Storage (Radius of Curl)

The specimens of web were cut from the innermost and outermost layer also to directly measure the MD curl through Kappa Gauge. The results compare quite well with online measurement.

Table 6.8 Kappa Gauge Measurement and Online Measurement

	Direct MD Measurement	Online MD Measurement
Innermost Layer	8.0 Kappa	7.7Kappa
Outermost layer	3.5 Kappa	3.8Kappa

Fig. 6.16 shows a comparison between the online measurement and Winder 6.3. For the outermost layer and innermost layer, the results compare quite well. For the middle part of the web, the error is about 15%. Dissimilar relaxation may happen and thus the Kappa Gauge of middle part will become smaller compared with the Winder 6.3 which did not consider this phenomenon. The influence of friction might be another reason, since the existence of slippage also reduces the Kappa value.

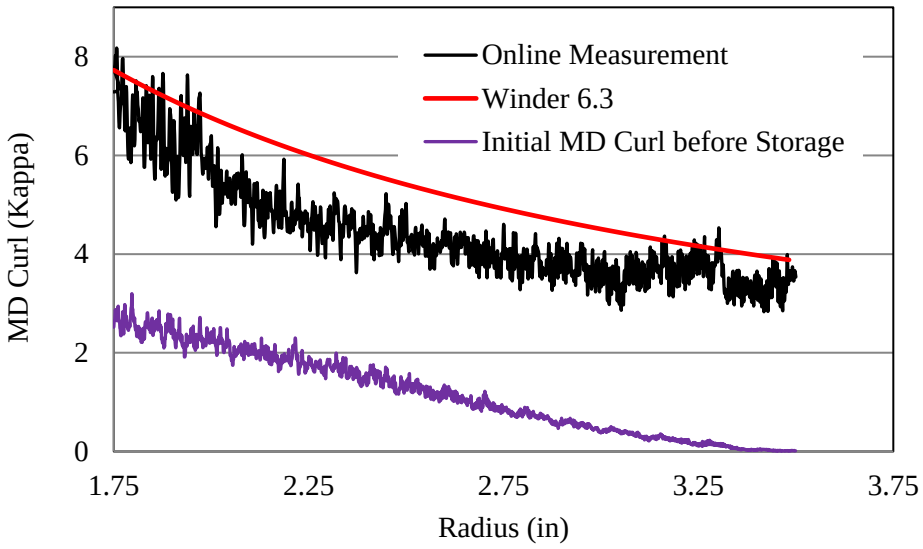

Fig. 6.16 Comparison between Online Measurement and Winder 6.3

Even though the web is flat enough (less than 2Kappa), the final curl is still related to the winding direction according or conversing to the initial curl direction, especially for the high temperature. Several outer layers (at least 10 layers) become quite loose after a certain storage time, since the radial pressure is not large enough for it. The test results always a little less than the values from Winder 6.3. Some possible factor influences the curl, such as the friction or dissimilar relaxation.

So maybe the correlation is not great all radius locations but this is the first attempt to characterize the curl in an entire roll of web.

CHAPTER VII

CONCLUSIONS AND FUTURE WORK

7.1 Findings and Conclusions

1. An orthotropic 1D finite element plane strain winding model with Poisson effects included in all dimensions was developed and verified for a newsprint web. This model was extended for laminate webs. Laminates may or may not be strain matched when laminated. The winding model was validated for both cases where the web strains were matched at the laminator and for cases where the strains were intentionally not matched. This research was published [38].
2. The laminate winding model developed and repeated laminate winding test results demonstrate that there was no difference in the wound roll pressures based on which ply of a laminate faces outward. The combined membrane and bending stresses in the laminate will be affected by which ply faces outward.
3. We explored multiple methods to characterize the viscoelastic properties of web. DMA, creep and relaxation measurements were performed and a master curve for each was compared to standard creep tests at room temperature. DMA method and relaxation (or creep) master curve methods characterized the viscoelastic properties much more quickly than laboratory creep tests. Currently the bending recovery is estimated using the relaxation modulus. Characterization directly in the form of the relaxation modulus is recommended since the conversion errors would be eliminated.

4. MD curl in winding was simulated using commercial finite element software (Abaqus). Such simulations are currently limited to a few wound layers and isotropic material behavior. WINDER 6.3 was extended to model MD curl for rolls that may have several thousand layers and that exhibit non-isotropic viscoelastic behavior. This code was verified for a low density polyethylene web.
5. An online measurement method for MD curl was developed. The method was used to characterize the MD curl of an entire wound roll of LDPE film. This method has potential for commercial application and is a non-destructive in comparison to the destructive Kappa tests.

7.2 Future Work

1. Laminate curl analysis would be an interesting and meaningful topic for future research. Laminate webs may curl for several reasons. This curl can be an elastic response due to the strain mismatch during lamination or due to viscoelastic creep of one or more of the laminate layers. The curl could also be affected by the viscoelastic behavior of the adhesives used to laminate the layers.
2. Methods to characterize the dissimilar relaxation effect for tensile and compressive states in thin webs should be developed.

REFERENCES

[1] Catlow, M.G. and Walls, G.W. *A Study of Stress Distribution in Pirns*. J. of textile Institute part 3, ppT410-429, 1962.

[2] Pfeiffer, J.D. *Internal Pressure in a Wound Roll of Paper*. Tappi Journal, Vol.49, No.8, pp.342-347, August 1966.

[3] Yagoda,H.P. *Resolution of a Core Problem in Wound Rolls*. Transactions of ASME, Journal of Applied Mechanics, Vol.47, pp.847-854,1980.

[4] Hakiel,Z. *Nonlinear Model for Wound Roll Stresses*. Tappi Journal, Vol.70,No.5,pp.113-117, May 1980.

[5] Kandadai B.K. and Good, J.K. *Winding Virtual Rolls.* Tappi Journal, June, 2011, pp. 25-31.

[6] Ren, Y., Kandadai B.K. and Good, J.K. *Center Winding versus Surface Winding: The Effect of Winder Type and Web Material Properties on Wound Roll Stresses*. Transactions of the 15th Fundamental Research Symposium, Cambridge, England, September, 2013.

[7] Good, J.K. and Pfeiffer, J.D. *Tension Losses During Centerwinding*. Proceedings of the 1992 Tappi Finishing and Converting Conference, pp.297-306.

[8] Mollamahmutoglu C. and Good, J.K. *Large Deformation Winding Models*. Proceedings of 10th International Web Handling Conference, pp 55-80, 2009.

[9] Tramposch, H. *Relaxation of Internal Forces in a Wound Reel of Magnetic Tape*. ASME Journal of Applied Mechanics, 32, 1965, pp. 865-873.

[10] Tramposch, H. *Anisotropic Relaxation of Internal Forces in a Wound Reel of Magnetic Tape.* ASME Journal of Applied Mechanics, 34, 1967, pp. 888-894.

[11] Lin, J. Y. and Westmann, R. A. *Viscoelastic Winding Mechanics*. ASME Journal of Applied Mechanics, 56, 1989, pp. 821-827.

[12] Qualls, W.R. and Good, J.K. *An Orthotropic Viscoelastic Winding Model Including a Nonlinear Radial Stiffness*. Journal of Applied Mechanics, 64, 1997, pp. 201-208.

[13] Frye, K.G. *Runnablity in the Press Room and Converters.* 1988 Tappi Finishing and Convertying Conf. Proc., Tappi Press, Atlanta, pp.139-162.

[14] Frye, K.G. *Finishing Defects: Core Bursts and Crepe Wrinkles.* Tappi Journal, 69(7) July 1986, p.67.

[15] Roisum, D.R. *Critical Thinking in Converting*. Tappi Press, 2002.

[16] Roisum, D.R. *Moisture Effects on Webs and Rolls*. Tappi J., 79(10), pp.129-138, June, 1993.

[17] Smith, R.D. *Roll and Web Defect Terminology*. Tappi Press,2006.

[18] Good, J.K. *Winding: Machines, Mechanics and Measurement.* Tappi Press, 2008.

[19] Schrader, W, Carroll and J, F. *Process for Reducing Core-Set Curling Tendency and Core-Set Curl of Polymeric Films*. US41417345A, 1979.

[20] Maier, K. Larry, Moszkowicz, J. M and Laney, M, T. *Process for Controlling Curl in Polyester Film*. US5076977A, 1991.

[21] Takami Onishi and Satoshi Dotani. Process for controlling curl in coated papers. US4853255A, 1989.

[22] J.Greener, A.H. Tsou, K.C, Ng, and W.A. Chen, *The Bending Recovery of Polymer Films*, Journal of Polymer Science, Part B, Polymer Physics,1991.

[23] S. Timoshenko and S. Woinowsky-Kreiger. Theory of Plates and Shells, 2nd ed. McGraw-Hill, New York, 1958.

[24] S. Matsuoka, in Failure of Plastics, W. Brostow and R.D.Corneliussen, Eds. Hanser Pulishers, New York, pp.24,1987.

[25] J.Creener, J.RGillmor*, Long-Term Growth of Core-Set Curl in Poly(ethylene terephthalate) Film*, Journal of Polymer Science, Part B, Polymer Physics, 2001.

[26] Sam, Kidane. *Laminate Theory Based 2D Curl Model.* Proceedings of the Tenth International Conference on Web Handling, Web Handling Research Center, Oklahoma State University, Stillwater, Oklahoma, 2009, pp. 387-401.

[27] Swanson, R.P. *Measurement of Web Curl.* Applied Web Handling Conference, 2006, Charlotte,NC.

[28] Swanson, R.P. *Web Curl and Web Curl Measurement.* Proceedings of the 14th International Conference on Web Handling, Web Handling Research Center, Oklahoma State University, Stillwater, Oklahoma, 2017.

[29] Robert M. Rivello. *Theory and Analysis of Flight Structure*. McGraw-Hill Inc Press,1969.

[30] Qualls,W.R. *Hygrothermomechanical Characterization of Viscoelastic Center wound* Rolls, PhD dissertation, Oklahoma State University,1995.

[31] Mollamahmutoglu, C. and Good, J.K., *Modeling Thermo-Viscoelastic Behavior in Wound Rolls Used in Roll-to-Roll Manufacturing*, In Development, 2019.

[32] M.Baumgaertel and H.H.Winter, "Determination of Discrete Relaxation and Retardation Time Spectral from Dynamic Mechanical Data",Rheologica Acta,1989.

[33] N.W. Tschoegl and I. Emri,"Generating Line Spectra from Experimental Responses.Part II: Storage and Loss Functions", Rheologica Acta,1993.

[34] Arsia Takeh and Sachin Shanbhag, "A Computer Program to Extract the Continuous and Discrete Relaxation Spectral from Dynamic Viscoelastic Measurements, Applied Rheology,2013

[35] Roisum,D.R. *The Mechanics of Rollers.* Tappi Press, 1998.

[36] Roderic S. Lakes *Viscoelastic Solids*. CRC Press, 1998.

[37] Mollamahmutoglu,C.and Good,J.K. *Axisymmetric Wound Roll Models*. Proceedings of 10th International Web Handling Conference, pp 105-130, 2009.

[38] Pan, S.and Good,J.K. *The Winding Mechanics of Laminate*. Proceedings of 14th International Web Handling Conference, 2017.

[39] Kwang Soo Cho. *Viscoelasticity of Polymers.* SSMATERIALS, 2016.

APPENDICES

APPENDIX A

Moduli and Relaxation Times in Chapter V

Table 1 Moduli and Relaxation Time in Fig. 5.18

Moduli(MPa)	113.27	27.27	7.12	5.21	6.33	5.04	102.81
Time(s)	1	10	50	500	5E3	5E4	Equilibrium

Table 2 Moduli and Relaxation Time in Fig. 5.19

Moduli(MPa)	95.25	54.34	37.29	11.49	9.44	10.97	6.91
Time(s)	0.1	1	10	1E2	1E3	1E4	1E5
Moduli(MPa)	7.55	5.47	4.92	4.01	6.01	44.41	
Time(s)	1E6	1E7	1E8	1E9	1E10	Equilibrium	

Table 3 Moduli and Relaxation Time in Fig. 5.20

Moduli(MPa)	87.29	40.14	31.70	21.35	16.15	11.85	9.58
Time(s)	0.01	0.06	0.40	2.51	15.85	10^2	630
Moduli(MPa)	8.05	7.39	7.02	6.91	6.83	6.63	6.33
Time(s)	3.98E3	2.51E4	1.58E5	1E6	6.31E6	3.98E7	2.51E8
Moduli(MPa)	5.76	5.09	4.17	3.32	2.29	1.72	1.05
Time(s)	1.58E9	1E10	6.31E10	3.98E11	2.51E12	1.58E13	1E14
Moduli(MPa)	1.75	1.24	8.17	2.08			
Time(s)	6.31E14	3.98E15	2.51E16	Equilibrium			

Table 4 Moduli and Relaxation Time in Fig. 5.21

Moduli(MPa)	30.98	144.78	88.00	134.45	192.48	200.09	190.64
Time(s)	1E-13	1.25E-12	1.58E-11	2.00E-10	2.51E-9	3.16E-8	3.98E-7
Moduli(MPa)	153.43	134.61	110.60	96.91	75.30	75.47	64.47
Time(s)	5.01E-6	6.31E-5	7.94E-4	6.31E-3	5.01E-2	3.98E-1	3.16
Moduli(MPa)	56.02	46.95	30.94	19.92	10.82	4.71	3.41
Time(s)	3.16E1	3.16E2	3.16E3	3.16E4	2.00E5	1.26E6	Equilibrium

APPENDIX B

Converting Routine

The Web Handling Research Center has developed two winding codes (Winder 6.3 and Maxwinder), which are widely used for winding analysis. In Winder 6.3, tangential and radial creep functions are the direct viscoelastic inputs. The user must input the number of Prony series terms, the creep coefficients and time constants that fit their creep data. In Qualls' creep test [30], he measured the elastic modulus firstly through Instron machine, and then captured the displacement due to the creep using a separate apparatus. The creep function is as in Table 5. The instantaneous Young's modulus for the LDPE is $E_0 = 24{,}000psi$, which means that $J_0 = \frac{1}{24{,}000}/psi$.

In order to simplify the problem, Qualls removed the elastic displacement from creep test, and thus the initial creep at t=0 is also zero. Qualls used the excel solver routine to determine the values of J and through curve fit and thus these are viscoelastic inputs in Table 5.

Table 5 Qualls Creep Function for LDPE at 70°F

J_0(1/psi)	J_1(1/psi)	τ_1(s)	J_2(1/psi)	τ_2(s)
0	1.05E-05	581	1.62E-05	121,900

(J_0 is 0 here since the elastic part has been removed)

More recently, Mollamahmutoglu [31] developed an axisymmetric finite element winding code that allows the user to study how web thickness and length variations affect the residual stresses in a wound roll called Maxwinder. Internally they use the relaxation modulus to predict how time and temperature affect winding residual stresses and deformations. Mollamahmutoglu added a robust semi-analytical method and converts creep functions into relaxation functions, which allows creep

function input in this FEM winding model. The similar form of relaxation function in equation (1) would be derived through Mollamahmutoglu's conversion routine if creep function is Merchant model (5.13).

$$E(t) = E_0 + \sum_{i=1}^{n} E_i \left(1 - \exp\left({}^{-t}/_{\lambda_i}\right)\right) \tag{1}$$

The conversion routine from Mollamahmutoglu's paper is as follows:

The Laplace transform is applied for the convolution and a relation is obtained for creep compliance J(t) from equation (5.13) and the corresponding relaxation modulus E(t):

$$s^2 \bar{J}(s)\bar{E}(s) = 1 \tag{2}$$

The Laplace transform of *J*(t) and *E(t)* can be given as (3) and (4), respectively ($\tau_0 = \lambda_0 = 0$).

$$\bar{J}(s) = \sum\nolimits_{i=0}^{m} \frac{J_i}{s(s\lambda_i + 1)} \tag{3}$$

$$\bar{E}(s) = \sum\nolimits_{i=0}^{m} \frac{E_i}{s(s\tau_i + 1)} \tag{4}$$

If we introduce two functions:

$$\begin{aligned} \mathrm{X}(s) &= \left(\sum\nolimits_{i=0}^{m} J_i \prod\nolimits_{j\neq i}^{m} (s\lambda_j + 1)\right) \\ Y(s) &= \left(\sum\nolimits_{i=0}^{m} E_i \prod\nolimits_{j\neq i}^{m} (s\tau_j + 1)\right) \end{aligned} \tag{5}$$

Equation (2) simplifies to (6):

$$\left(\prod\nolimits_{i=1}^{m} (s\lambda_i + 1)\right)\left(\prod\nolimits_{i=1}^{m} (s\tau_i + 1)\right) = \mathrm{X}(s)Y(s) \tag{6}$$

The relaxation times λ_i will be the roots of a high order equations, and the modulus E_i are expressed in equation (7):

$$E_i = E_0 \frac{\prod_{j=1}^{m} \left(\frac{\tau_i}{\lambda_j} - 1\right)}{\prod_{j \neq i}^{m} \left(\frac{\tau_i}{\tau_j} - 1\right)} \tag{7}$$

The creep input shown in Table 5-1 as the input but the conversion routine would produce the relaxation modulus terms needed by the code as shown in equation (8):

$$E(t) = 24000 + (-4850) * \left(1 - e^{-t/463}\right) + (-4520) * \left(1 - e^{-t/93082}\right) \tag{8}$$

Reorganize equation (8)

$$E(t) = 14630 + 4850 * e^{-t/463} + 4520 * e^{-t/93082} \tag{9}$$

APPENDIX C

Winder 6.3 Input

Table 6 Main Material Properties Input (70°F and 110°F) for Chapter VI

Caliper	0.02 in
Width	4 in
CMD Modulus	22,200 psi
MD Modulus	22,200 psi

Table 7 Main Winding Parameters Input (70°F) for Chapter VI

Core OD	3.5 in
Core ID	3.0 in
Material Modulus	1E8 psi
Calculated Core Stiffness	16,029,593 psi
Poisson's Ratio of Core	0.3
Wound Roll OD (in)	9.5(test1), 9(test2), 8.7(test3), 8.6(tests4,5)
Winding Tension (psi)	112.5(tests1,2,3), 225(test4), 62.5(test5)
K1 (psi)	1E-05
K2	246.5

Table 8 Main Viscoelastic Input (WHRC Creep) for Chapter VI

MD Creep Terms	
J1	-1.467E-05 in/in/psi
J2	-5.376 E-06 in/in/psi
J3	-7.913E-06 in/in/psi
Tau 1	13s
Tau 2	1445s
Tau 3	100,512s
Radial Creep Terms	
J1	-8.869 E-06 in/in/psi
J2	-9.312E-06 in/in/psi
Tau 1	696s
Tau 2	72,810s

Table 9 Main Viscoelastic Input (Relaxation Master Curve 70°F,110°F) for Chapter VI

MD Relaxation Terms (Radial direction is the same as in Table 8)							
Moduli(psi)	12,660	5,821	4,598	3,097	2,342	1,719	1,389
Time(s)	0.01	0.06	0.40	2.51	15.85	10^2	630
Moduli(psi)	1,168	1,071	1,018	1,002	991	962	918
Time(s)	3.98E3	2.51E4	1.58E5	1E6	6.31E6	3.98E7	2.51E8
Moduli(psi)	838	738	605	482	332	250	1.05
Time(s)	1.58E9	1E10	6.31E10	3.98E11	2.51E12	1.58E13	1E14
Moduli(psi)	152	180	1,185	3.02	Storage Time		
Time(s)	6.31E14	3.98E15	2.51E16	Equilibrium	86,400s		

(70°F,110°F have the same input, since the shift factor 5.2 is applied to110°F)

Table 10 Main Winding Parameters Input (110°F) for Chapter VI

Core OD	3.5 in
Core ID	3.0 in
Material Modulus	1E8 psi
Calculated Core Stiffness	16,029,593 psi
Poisson's Ratio of Core	0.3
Wound Roll OD (in)	6(tests6,7), 10(tests8,9)
Winding Tension (psi)	112.5
K1 (psi)	1E-05
K2	246.5

Table 11 Main Viscoelastic Input (WHRC Creep 110°F) for Chapter VI

MD Creep Terms	
J1	-1.40E-05 in/in/psi
J2	-1.19 E-05 in/in/psi
J3	-1.87E-05 in/in/psi
J4	-1.32E-05 in/in/psi
Tau 1	1E03s
Tau 2	1E04s
Tau 3	1E05s
Tau 4	1E06s

VITA

Sheng Pan

Candidate for the Degree of

Doctor of Philosophy

Dissertation: THE MECHANICS OF WINDING LAMINATE WEBS AND THE PREDICTION OF MACHINE DIRECTION CURL

Major Field: Mechanical Engineering

Biographical:

Education:

Completed the requirements for the Doctor of Philosophy in Mechanical Engineering at Oklahoma State University, Stillwater, Oklahoma in May, 2019.

Completed the requirements for the Master of Science in Machinery in Chemical Industry Process at Beijing University of Chemical Technology, Beijing, China in 2013.

Completed the requirements for the Bachelor of Science in Process Equipment and Control at Beijing University of Chemical Technology, Beijing, China in 2010.